Power Adaptive Communication for Wireless Body Area Networks

Abbas Arghavani

a thesis submitted for the degree of

Doctor of Philosophy

at the University of Otago, Dunedin,

New Zealand.

31 January 2019

Abstract

Fast advancement in physiological sensors, low-power circuits, and short-range wireless communications has enabled the development and deployment of ubiquitous wearable networks called Wireless Body Area Networks (WBANs) that consist of a few or tens of miniaturised body-mounted or implanted sensors. WBAN is an appealing technology for a wide range of applications including health monitoring, athlete training, and entertainment. In most applications, the sensor devices need to report the measurements to a body central gateway (e.g., a smartphone) through wireless communication, and the gateway can further send the measurements to a remote monitoring centre through the Internet or cellular networks. As a particular type of wireless sensor networks (WSNs), WBANs inherit many characteristics of traditional WSNs such as restricted energy capacity, limited computation capability, and unreliable wireless communication. Radio links in WBANs commonly experience highly time-varying attenuation due to dynamic network topology and frequent occlusions caused by body movements, making it challenging to design a real-time reliable, energy-efficient, and interference-aware communication protocol for WBANs.

Since communication protocols with fixed transmission power are not able to perform well, this thesis proposes communication protocols to adaptively adjust the transmission power level of the sensor nodes through which they can save energy and reduce potential interference while still guaranteeing high communication reliability. Firstly, a new channel prediction model for power-adaptive communication in WBANs is proposed. To this end, the channel behaviour in WBANs is precisely analysed, which demonstrates that the existing channel models either cannot accurately predict channel burstiness

or have high prediction complexity. Then, a new, accurate lightweight Markov model is presented to allow the dynamic power adjustment at a per-transmission level. Motivated by the accuracy of the proposed channel model in terms of channel estimation, a channel-aware deadline-constrained policy for scheduling packet transmissions is proposed. The experimental results demonstrate that the proposed scheme can self-learn the channel burstiness patterns, and choose the best transmission power to reduce energy consumption and improve communication reliability. With retransmissions, this scheme can achieve almost 100% on communication reliability but significantly reduces the number of packets transmitted using high power levels. Since the proposed channel model requires a continuous channel measurement, it only supports applications with periodic constant packet rate.

Secondly, Chimp, a learning-based power-aware communication protocol is proposed in which each sending node can self-learn the channel quality and choose the best transmission power level to reduce energy consumption and potential interference but achieve good communication reliability. Chimp is designed to support event-driven applications as well as the applications with periodic constant packet rate. It is designed based on learning automata that use only the acknowledgment packets and motion data from a local gyroscope sensor to inform the real-time channel status. A new learning function is developed that can guarantee to select the optimal transmission power level to minimise the cost function for a given channel quality. For highly dynamic postures such as walking and running, Chimp exploits the correlation between channel quality and motion data generated by a gyroscope sensor to quickly estimate channel quality, eliminating the need to use expensive channel sampling procedures. The performance of Chimp is evaluated through experiments using TelosB motes equipped with the MPU-9250 motion sensor chip and compared with the state-of-the-art protocols in different body postures. Experimental results demonstrate that Chimp outperforms existing schemes and can work efficiently in most common body postures. It achieves almost the same performance as the optimal power assignment scheme for high date rate scenarios.

Thirdly, a localisation algorithm is proposed to find the location of the sending node by combining the locally measured orientation information of

the sending node with anatomical constraints of the body parts. The results of the experiments show the channel quality between the sending node and the gateway is highly dependent on the location of the sending node. Motivated by this, Tuatara, a location- and learning-based communication protocol for WBANs is presented to support event-driven applications as well as applications with periodic constant packet rate, even at extremely low packet rate scenarios. Tuatara benefits from the location information provided by the localisation algorithm and prior knowledge about the optimal power level in different locations of the sending node around the body. The experimental results show Tuatara can perform almost as well as the Optimal scheme.

Acknowledgements

First and foremost, I would like to thank the support of my supervisors, Dr. Haibo Zhang, and A/Prof. Zhiyi Huang for the continuous support and cooperation throughout my Ph.D. study. Their guidance helped me in all the time of research and writing of this thesis. I could not have imagined having better supervisors for my Ph.D. study.

Nevertheless, I am also grateful to all my colleagues in the Department of Computer Science who provided a pleasant and cooperative atmosphere. I wish to thank my mother, my brother, and my sisters for their huge patience, understanding, and support during all my life. Without their precious support, it would not be possible to conduct this research. Finally, I would like to express my special love to my wife Maryam for her patience, and support when I was not around her.

Publications

Parts of the work presented in this thesis have already been published in peer-reviewed conference proceedings and international journal:

- **Journal Papers**

  1. Arghavani, A., Zhang, H., Huang, Z. and Chen, Y., Chimp: a Learning-based Power Aware Communication Protocol for Wireless Body Area Networks. In ACM Transactions on Embedded Computing System (TECS), 2019.

- **Conference Papers**

  1. Arghavani, A., Zhang, H., Huang, Z. and Chen, Y., ATPS: Adaptive Transmission Power Selection for Communication in Wireless Body Area Networks. In IEEE 42nd Conference on Local Computer Networks (LCN), pp. 615-618, 2017.
  2. Arghavani, A., Zhang, H. and Huang, Z., LPA: Learning-based power aware communication protocol in WBANs. In IEEE 14th Conference on Pervasive Intelligence and Computing (PiCom), pp. 512-519, 2016.

Contents

List of Tables

List of Figures

Chapter 1

Introduction

Fast advancement in physiological sensors, low-power circuits, and short-range wireless communications has enabled the development and deployment of ubiquitous Wireless Body Area Networks (WBANs). A WBAN is a particular type of Wireless Sensor Networks (WSNs) which consists of a few to tens of miniaturised body-mounted or implanted wireless nodes. A wireless node is a device that integrates several units such as sensors, radio chip, processor, memory storage, battery, etc. Sensors can measure a wide variety of parameters from physiological parameters such as EMG (Electromyography), EEG (Electroencephalography), or ECG (Electrocardiography) signals, heart rate, body temperature, and blood glucose, to environmental parameters (e.g., air quality) and even body motion data (such as acceleration). Wireless nodes based on their role in a WBAN can be classified into three groups, however, a wireless node might be in more than one group:

(1) *Sensor node* is a wireless node that is responsible for measuring body parameters and transmit the measurements to other nodes or to a central point.

(2) *Gateway* is a body central node (e.g., a smartphone) that is in charge of coordinating communications in a WBAN. It collects the measurements from sensor nodes in a WBAN and provides feedback to the user after some preprocessing. The gateway can also send the measurements to the cloud, where massive computational and storage capabilities are available to accurately and quickly analyse the collected data. By connecting to the cloud, the measurements can be analysed at the monitoring centres (e.g., hospital or clinics) to make real-time decisions (Figure 1.1). The gateway is usually a resource-rich device that supports different communication technologies from Bluetooth and WiFi to cellular networks.

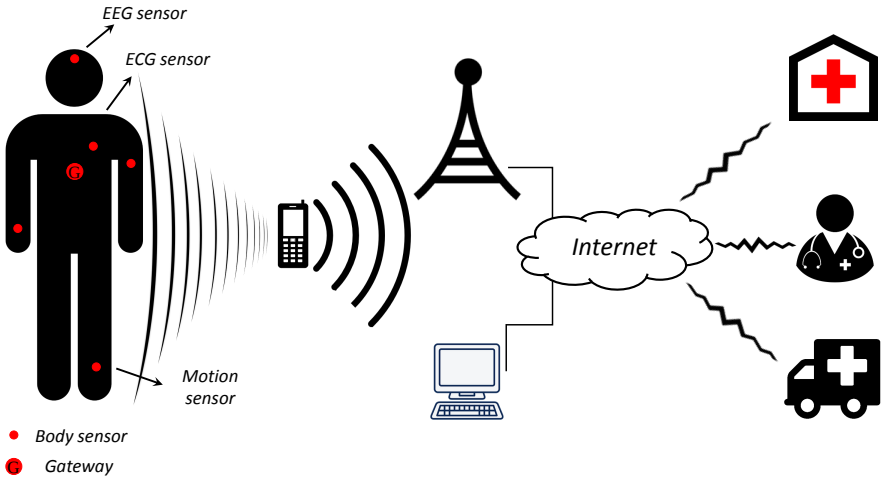

Figure 1.1: Wireless Body Area Network.

(3) An *actuator* is a small component implanted in or attached to body parts and acts on the information from the sensor nodes or gateway based on predetermined instructions. For example, it delivers the proper doses of drugs in drug-delivery systems or provides electrical stimulation in heart attack prevention systems.

1.1 Wireless Body Area Networks

1.2 Applications

WBAN is an appealing technology for a wide range of applications including health monitoring and fall detection (Mahmood, Jafer, Hussain, and Fernando, 2017; Baek, Kim, Bashir, and Pyun, 2013), assisting with visual or aural disabilities (Grimm, Guilmin, Poppen, Vlaming, and Hohmann, 2009), athlete training, fitness, and entertainment (Preuschl, Baca, Novatchkov, Kornfeind, Bichler, and Boecskoer, 2010; Novatchkov and Baca, 2012). In what follows, a more detailed discussion of the various applications of WBANs is presented.

- **Healthcare Applications:** The fast growth in world population which leads to different challenges such as an ageing population and rise in healthcare costs (Milenkovic, Otto, and Jovanov, 2006) has brought the healthcare applications of WBANs into focus. WBANs can be used to monitor and analyse the physiological signals and prevent many diseases by providing real-time health feedback to both users and physicians. They can monitor heartbeat (Luo, Dai, Li,

Zhou, Lu, Poon, Chen, Zhang, and Zhao, 2016), blood glucose (Nelson, Sloan, Jin, Jiang, Chen, Anderson III, and Liamos, 2017), body temperature (Vaz, Ubarretxena, Zalbide, Pardo, Solar, Garcia-Alonso, and Berenguer, 2010), and many more vital signals for early detection of heart attack, diabetes, cancer, etc. WBANs ease the treatment process and reduce the number of times a patient has to visit the doctors (Ciemins, Coon, Peck, Holloway, and Min, 2011) and provide ambulatory rehabilitation services to injured people or people with disabilities (Baek *et al.*, 2013). With the continuous increase in the ageing trend, many studies have shown that substantial benefits can be achieved by encouraging people to participate in physical activities across all age groups (Kosma, Cardinal, and Rintala, 2002; Tudor-Locke, 2002). Wearing GPS and motion sensors enabled WBANs to help monitor and report daily physical activities and encourage people to keep track of their activities and movements throughout the day (Casselman, Onopa, and Khansa, 2017; Yusif, Soar, and Hafeez-Baig, 2016).

- **Sports Applications:** Each match usually brings thousands to tens of thousands of fans to the stadium. Sports clubs can make lots of money through TV deals, player transfer, sponsorship, ticket sales, etc. Accordingly, players earn millions of dollars each year, especially for those skilled players who can improve the performance of their team and the quality of the match, and consequently increase the income of the club. Hence, all professional and amateur sportsmen spend many hours to improve their skills or learn new skills. Recently developed WBANs such as golf swing training aid system (Snyders, 2010), smart soccer shoes (Zhou, Koerger, Wirth, Zwick, Martindale, Cruz, Eskofier, and Lukowicz, 2016), and wearable assistant for swimmers (Bachlin, Forster, and Troster, 2009) can help athletes and athlete trainers by improving the level of their skills.

- **Gaming and Entertainment:** By bringing a large number of innovations into the gaming area, WBANs are changing the future of the games. Combining wireless motion tracking suits with Augmented Reality (AR) and Virtual Reality (VR) headsets, gamers have no need to sit and look at the screen while they can keep playing, even when they are away from the game console (Chan, Leung, Tang, and Komura, 2011). WBANs can provide a Brain to Computer Interface (BCI) communication system using EEG sensors (Chi and Cauwenberghs, 2010). Therefore, the game players can control the game using brain waves (Liao, Chen, Wang, Chen, Li, Chen, Chang, and Lin, 2012). They also have a potential to

combine art, entertainment, and technology such as phone based WBANs which benefit from wearable accelerometers to provide dancing games (Clawson, Patel, and Starner, 2010).

- **Safety:** WBANs have the potential to make life not only easier but also safer through injury and death prevention. Body sensors can monitor the user's stress, brainwaves, body temperature, and many other biometrics as well as toxic gases and the quality of the air he breathes to alert him to potential risks and hazards. WBANs allow locating fire-fighters inside a building (Klann, 2008), detecting the drivers' drowsiness (Li, Lee, and Chung, 2015), and recognising carbon dioxide in underground mines (Takiff and Aiken, 2010). Besides, insurance companies, as well as employers, are keen to use WBANs to reduce the workers' compensation claims (Horton, Cameron, Devaraj, Hanson, and Hajkowicz, 2018).

1.3 Characteristics of WBAN

WBANs inherit some of the characteristics of traditional WSNs such as limited energy budget, limited computation capability, and unreliable wireless communication. WBANs also have their unique features such as frequent topology changes and time-variant channel quality due to body postural movements. In this section, some of the most important specific characteristics of WBANs are discussed.

- **Network topology:** IEEE standards for WBANs support one-hop and two-hop star topology, in which the gateway is placed at the centre of the network and the sensor nodes either directly communicate with the gateway or ask other sensor nodes to forward their data packets. Since a human body may experience different postures even in a short period of time (e.g., sitting, standing, walking, etc.), the network topology in WBANs is usually changed over time and shows a high instability. This instability in the network topology and the position of the sensor nodes can create significant fluctuations in the quality of wireless channels due to frequent blockage and variable absorptions of the radio propagation energy by body parts. On the other side, the network topology in WSNs is relatively stable with limited changes in the distance between the sensor nodes, the orientation of their antenna, and consequently their channel quality.

- **Network mobility:** Since subjects move through different places (e.g., offices, shops, streets, homes, and so on) WBANs experience different environments

resulting in significant variations in the background noise and interference from other wireless systems in the neighbourhood of WBANs that influence the quality of the wireless signals. Compared to WBANs, the environment in WSNs is usually much more stable over time.

(a) (b)

Figure 1.2: (a) Implantable neural dust sensor (Seo *et al.*, 2016), (b) xsens motion tracking module (xsens, 2014)

- **Sensor node design:** Sensor nodes in WBANs generally should be designed to be as small as possible to support wearability and implementability. The size of a sensor node in a WBAN depends on its application and varies from a rice-grain-sized neural dust sensor (Seo *et al.*, 2016) (a sensor with the dimensions of $3 \times 1 \times 0.8\, mm^3$) for monitoring nervous system (Figure 1.2a) to the xsens inertial and magnetic sensor module (xsens, 2014) (a sensor with the dimensions of $47 \times 30 \times 13\, mm^3$) for body motion tracking (Figure 1.2b). Compared to the sensor nodes in WSNs that can use a couple of AA size batteries in most of the applications, the power source for body sensor nodes should be as tiny and light as possible. Depending on the application, sensor nodes in WSNs may benefit from solar energy to recharge their batteries, while there is no room for solar panels in body sensor nodes as they are implanted in body tissues, embedded in clothes, or attached to body parts. However, several energy harvesting mechanisms have been proposed to enable sensor nodes in WBANs to harvest energy from body heat (Leonov, 2013), body movements (Lu, Wang, Chen, Zhang, and Huang, 2014), or radio frequency radiation (Barroca, Saraiva, Gouveia, Tavares, Borges, Velez, Loss, Salvado, Pinho, Goncalves, *et al.*, 2013). Apart from the size, those sensor nodes in WBANs, that are going to be attached to the body skin or implanted in body tissues for long-term continuous health monitoring, are required to be designed using biocompatible materials to provide physical compatibility and

minimum invasion to the body.

- **Resource Constraint:** Although resource constraint is one of the major challenges in WSNs, it is more crucial in WBANs because of the miniaturised size of the sensor nodes. Intensive resource constraints in WBANs can cause some serious challenges in many different aspects of WBANs' operation. For example, the network lifetime is highly influenced especially when replacing or recharging the battery of the sensor nodes is difficult. Security challenges compared to WSNs are more difficult to address in WBANs as running complex security protocols on low-power tiny nodes with highly limited computational power is almost impossible (Saleem, Ullah, and Yoo, 2009). Furthermore, since body sensor nodes can collect personal data, privacy policies need to be considered in WBANs as users may be concerned whether they are being tracked or spied on. Such a concern can threaten users to benefit from all the advantages of WBANs. Another major challenge is to guarantee high Quality of Service (QoS) in resource-constrained WBANs because of the heterogeneous unpredictable traffic pattern. Sensor nodes in the same WBAN may monitor different vital signals, which means different packet rates, priorities, and transmission delay sensitivities need to be considered to guarantee QoS.

- **Antenna design:** One important challenge in designing antennas in WBANs is the adaptation of the antenna topology to the shape of the body (Arriola, Sancho, Brebels, Gonzalez, and De Raedt, 2011). An antenna easily adapting to the dynamic motions of the body needs to be made by stretchable materials to allow flexibility (Huyghe, Rogier, Vanfleteren, and Axisa, 2008; Arriola *et al.*, 2011). Besides, the antenna size should be small enough to fit into the clothes, body tissue, or a wristband. Furthermore, since body tissue is a semiconductor (Movassaghi, Abolhasan, Lipman, Smith, and Jamalipour, 2014), it propagates electromagnetic (EM) waves (Vallejo, Recas, Garca del Valle, and Ayala, 2013) and absorbs some radiation energy that will cause tissue heating when the wireless node is placed close to the body skin or tissue. To avoid tissue heating, the strong electrical field (E-field) at the antenna coils should be avoided with low power, small duty cycle communications.

1.4 Challenges on Communication and Motivations

These unique features and constraints make it challenging to design an efficient communication protocol for WBANs to achieve:

- **High energy efficiency**: Although energy efficiency is an important metric for almost all wireless devices, it is more critical in WBANs. Battery replacement in WBANs is not possible for those implanted sensors which are expected to work for many years. Another constraint is battery size. For many applications, the sensors attached to the body are required to be small, which limits the battery size and its power capacity. The locations of senders and receivers and their distance are unstable due to topology changes. In addition, the Line of Sight (LoS) path between transceivers is frequently blocked by body parts and clothes. Such an instability highly influences the channel quality and increases packet loss rate. Since the lost packets are required to be retransmitted until they are received, especially in medical applications where the measurements are vital to be received at the monitoring centre, retransmission imposes a remarkable energy overhead to WBAN. To maximise the lifetime of the sensor nodes, the transmission power should be as low as possible under the condition of reliable communications.

- **High communication reliability**: The quality of wireless links in WBANs can experience significant fluctuations due to dynamic network topology, frequent occlusions, and variable absorption of the signal propagation energy caused by body movements. Figure 1.3 depicts a 2D view of the topology for a WBAN during five postures in a gait cycle. It can be seen that the distances between body sensors can vary quickly, and the wireless links can be interrupted by body

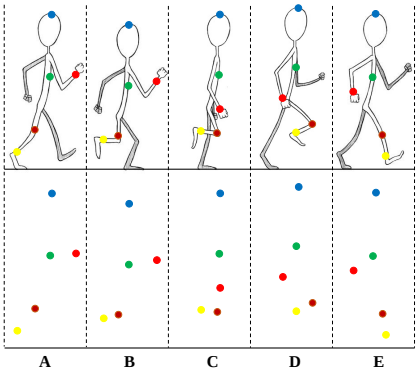

Figure 1.3: Topology instability in WBANs

parts frequently. In such a dynamic scenario, wireless channels are highly subject to both short-term and long-term fading. Hence, it is very challenging to achieve high communication reliability with low energy consumption.

- **Low interference**: WBANs usually operate in dense social environments (e.g., hospitals) in which several WBANs could be co-located together with other WSNs as illustrated in Figure 1.4. Consequently, inter-network interference becomes a serious issue if all sensor nodes always use a high transmission power to achieve high communication reliability. According to the IEEE 802.15 working group document (Yazdandoost and Sayrafian-Pour, 2009), the transmission range of the sensor nodes in a WBAN should be less than 3 meters when there could be up to 10 WBANs in a space of $6\,m^3$.

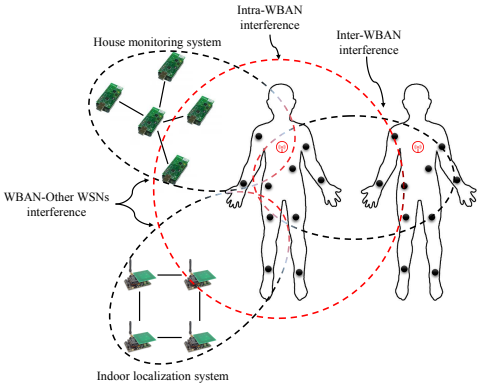

Figure 1.4: Different types of interference in WBANs

Due to the dynamic network topology and the highly time-varying wireless channel, existing communication protocols using fixed transmission power (Yang, Lu, Yang, Kong, Shu, and Wu, 2013) cannot meet all the above three goals because: (1) a fixed low transmission power can reduce interference but may produce very poor communication reliability, which may further increase energy consumption due to retransmissions, and (2) a fixed high transmission power can improve communication reliability at the cost of more energy consumption but may produce more interference.

To achieve high communication reliability with low energy consumption and limited interference, a straightforward approach is to let each sensor node adaptively control its transmission power based on the channel quality, that is, use a low transmission power when the channel is good (e.g., a short-distance LoS communication path is available) and switch to a high transmission power when the channel becomes bad (e.g., the LoS communication path is completely blocked). The **key challenges** in

developing such a power-adaptive communication protocol are: (1) how can each sensor node know its channel status before transmission? (2) how can each sensor node choose the best transmission power if it knows its channel status? Besides these challenges, a comprehensive communication protocol is expected to support a wide range of applications from an extremely low packet rate application (such as an application which reports high blood pressure) to an application with periodic high packet rate transmission mode (such as inertial motion tracking suits).

1.5 Thesis Contributions

Recently, several power-adaptive communication protocols have been proposed for WBANs and remarkable improvements in enhancing energy efficiency and communication reliability have been achieved through efficient power control mechanisms (Kindt, Jing, Peters, and Chakraborty, 2015; Quwaider, Rao, and Biswas, 2010; Kim, Kim, and Eom, 2013). However, these protocols do not take into account the impact of power control on joint inter-network interference, energy consumption, and communication reliability. Moreover, most of these protocols usually work under some special conditions and support particular types of applications, which limits the range of potential applications. For example, the scheme proposed in (Kindt *et al.*, 2015; Zang and Li, 2017) works in postures with periodic movements such as walking, when the packet rate is high and periodic, whereas the scheme proposed in (Quwaider *et al.*, 2010) works more efficiently in static postures such as sitting.

The aim of the thesis is to design reliable communication protocols to jointly reduce energy consumption and interference range for a wide range of applications of WBANs. The **key contributions** are as follows:

- A set of experiments is conducted using the TelosB platform to get insights on communication in WBANs by measuring key parameters such as transmission signal power, usage of current, maximum transmission range, and average packet loss rate at each power level. Experimental results show that with the gateway attached to the chest and the sending node attached to the wrist, using only a small number of transmission power levels (3 power levels in the schemes proposed in this thesis) is enough to achieve energy-efficient interference limited reliable communication. However, the proposed schemes can handle a larger number of power levels and restricting the number of power levels to three levels is just to simplify the problem of finding the optimal power level. Then, a unified

transmission cost function that reflects performance metrics including energy consumption, interference, and communication reliability is introduced to enable the sensor nodes to select the optimal transmission power level and minimise the transmission cost.

- Analysing collected channel samples in different postures shows a strong spatial and temporal dependency between the quality of consecutive channel samples. Motivated by this dependency, a general framework for analysing channel behaviour using existing Markov chain models is designed. Since the existing Markov chain models need a lot of memory for accurate channel behaviour estimation, a new Markov chain model is presented that sustains the advantage of the existing models in terms of prediction accuracy but also overcomes their drawback of memory complexity.

- ATPS, an Adaptive Transmission Power Selection algorithm for applications with constant periodic packet rate is proposed in which each sensor node estimates the channel quality using the designed Markov chain model and adjusts its transmission power at a per-transmission level to cope with channel dynamics. ATPS is then extended to use the channel estimation model for scheduling the packets in deadline-constrained applications. That is, ATPS buffers the packets when the channel is bad and sends them when the channel quality is expected to be good. The performance of ATPS is evaluated through experiments on the TelosB sensor motes under three different data rates in several postures (sitting, standing, walking, and running). The results reveal a significant improvement in interference limitation and energy efficiency.

- Since ATPS needs periodic channel measurement to keep the properties of Markov chain model (i.e., the properties of channel fluctuation pattern) up to date for accurate channel estimation, it only supports applications with periodic high packet rate communication. Chimp, a learning-automata based power-adaptive communication protocol is designed to sustain the advantages of ATPS but partially compensate its drawbacks by supporting low packet rate applications. Chimp exploits the correlation between channel quality and motion data provided by a local gyroscope so it does not need periodic channel measurement. It enables the sensor node to self-learn channel fluctuations and predicts the channel quality by monitoring the locally measured motion data. The performance of Chimp is evaluated through experiments on the TelosB sensor motes under different

scenarios and is compared with the state-of-the-art protocols as well as the optimal power assignment that is calculated off-line. The experimental results reveal that in some postures Chimp performs better than ATPS and existing state-of-the-art protocols.

- Due to the trial and error based learning nature of Chimp, its learning procedure for finding the optimal power level takes a lot of time in extremely low packet rate applications especially in postures with highly dynamic channels. On the other hand, when the subject's movement pattern is changed (e.g., from slow walking to fast walking), Chimp has to relearn the correlation between the motion data and the channel quality. To reduce the learning overhead of Chimp and motivated by the correlation between the location of the sensor node and the channel quality, an IMU-based localisation method is proposed to estimate the real-time location of the sensor nodes by combining the 3D orientation of body segments and the anatomical limitations of the human body movements. Then, Tuatara [1], a location-based communication protocol is introduced to benefit from the locally provided real-time location information of the sensor node for fast channel estimation and quick power adjustment. Although channel quality in a fixed location relative to the gateway is expected to be constant, a previously available LoS path to the gateway in a fixed location might be blocked by other objects (e.g., clothes). Hence, Tuatara is further extended to combine the channel quality prediction using a location estimation algorithm with the learning ability of Chimp, so that the sensor node is able to adjust its transmission power level to the optimal level even if an unexpected channel blockage occurs. The experimental results in different scenarios reveal that Tuatara outperforms Chimp in both static and dynamic postures, especially when the packet rate is extremely low. Tuatara can quickly adjust the transmission power level to the appropriate level even in scenarios with extremely low packet rates. Tuatara is a solution for a wide range of WBANs' applications, from applications with extremely low packet rate to applications with high packet rate periodic communication.

1.6 Thesis Structure

Chapter 2 gives some background on WBANs and reviews the existing communication protocols for WBANs. In Chapter 3, a WBAN testbed that is used for experiments is

[1] Tuatara is a reptile endemic to New Zealand with an excellent energy management

introduced, and a transmission cost function for designing a communication protocol is presented. Chapter 4 analyses the channel behaviour in WBANs and introduces a new channel estimation model whereby the sensor node can predict the channel. Then, ATPS is proposed to benefit from the channel model and enable the sensor node to adjust its transmission power at a per packet level. In Chapter 5 the correlation between channel fluctuation and motion data is examined. This chapter introduces a learning-based communication protocol named Chimp to show how learning this correlation can be used for designing a power-adaptive communication for a wider range of WBANs' applications. Chapter 6 presents a location-based communication protocol named Tuatara and explains how a sensor node can adjust its transmission power level by estimating its real-time location even in extremely low packet rate applications. Finally, Chapter 7 suggests future work and concludes the thesis.

Chapter 2

Literature Review

In this chapter, the IEEE standards for WBANs are briefly introduced. Then, an overview of the existing communication protocols designed for WBANs is presented. Finally, it is explained in which way the work presented in this thesis is different from the existing works.

2.1 IEEE standards for WBANs

The communication architecture of WBANs can be considered in three different scopes: (1) on-body communication among wireless nodes in the same WBAN which is expected to be limited to 2 metres (Movassaghi *et al.*, 2014); (2) body-to-body communication between two WBANs; and (3) off-body communication between a WBAN and a monitoring centre (e.g., a hospital) via an access point or a base station with the coverage area up to 100 metres (Movassaghi *et al.*, 2014). The physical layer and Medium Access Control (MAC) sub-layer of WBANs are defined and standardised by IEEE 802.15 Task Group 4 (TG4) and Task Group 6 (TG6) under the title of IEEE 802.15.4 (IEEE LAN/MAN Standards Committee, 2011) and IEEE 802.15.6 (IEEE LAN/MAN Standards Committee, 2012). These standards are discussed in the following paragraphs.

2.1.1 Frequency Bands

Radio spectrum is a limited resource regulated by governments to avoid interference among different users. The spectrum for wireless communication can be simply categorised in two groups: **licensed** and **license-free** frequency bands:

- A **licensed** band can be used by those users who already have purchased it. These users are known as primary users. There might be other users called secondary users who can use the licensed band at a cheaper price. However, the secondary users have to avoid producing interference for primary users while they may receive interference from primary users. There are some licensed frequency bands available for WBANs. Medical Implant Communication Service (MICS) is a licensed band for ultra-low power and short-range implant communication with a range of 402–405 MHz and a small bandwidth of 300 kHz. The Wireless Medical Telemetry Service (WMTS) is also a licensed band with 13 MHz available bandwidth in three separate sub-ranges (608–614 MHz, 1395–1400 MHz, 1427–1432 MHz). Neither MICS or WMTS bandwidth are enough to support hundreds of patients in large places such as hospitals. Moreover, they both have to accept co-channel interference from primary users (Meteorological Aids for MICS and legal digital TV broadcasters in WMTS). Medical Body Area Network (MBAN) is another licensed band for WBANs which allows operation in the 2360–2400 MHz band with a wide bandwidth of 40 MHz. However, similar to WMTS and MICS, MBAN provides operation on a secondary basis as the frequency band has been already allocated to aeronautical mobile telemetry (AMT) users.

- The **license-free** bands can be used by any certified device if it follows some predefined conditions (e.g., it communicates with a limited signal power). Industrial, Scientific, Medical (ISM) frequency bands are generally licensed-free and have many popular sub-ranges for WBANs. For example, the 433 MHz ISM band with the nominal data rate of 28 kbps (Ghamari, Janko, Sherratt, Harwin, Piechockic, and Soltanpur, 2016) and good signal propagation characteristics is a good choice for low-power low data rate WBANs. However, the wavelength at 433 MHz frequency band is about 70 cm which means communication at this band requires a large antenna at the size of about 17 cm. IEEE 802.15.4 offers operation in 868 MHz, 915 MHz, and 2.4 GHz ISM bands for WBANs. All the offered bands not only require relatively small antennas for communication but also have good signal propagation characteristics. However, 868 MHz band is a licensed band in the US, similar to 915 MHz band in Europe. The 2.4 GHz band is probably the most popular (and consequently the most congested) ISM band as it is available worldwide. It provides 80 MHz contiguous bandwidth which is much more than that of 868 MHz and 915 MHz. IEEE 802.15.6 provides three different physical layers including Ultra Wide Band (UWB), Narrow Band (NB),

and Human Body Communication (HBC) for WBANs as shown in Figure 2.1. Communication in UWB (which is license-free in the frequency range of 3.1 to 10.6 GHz) achieves higher data rate relative to the communication in other bands. Because of the larger bandwidth, communication in UWB is more robust to multipath fading. Besides, the antenna can be designed much smaller though, the path loss of communication in UWB is higher and also it cannot penetrate the human body. Considering the pros and cons of the available bands, the proper selection of physical layer and frequency band depends on the application of WBAN much more so than anything else.

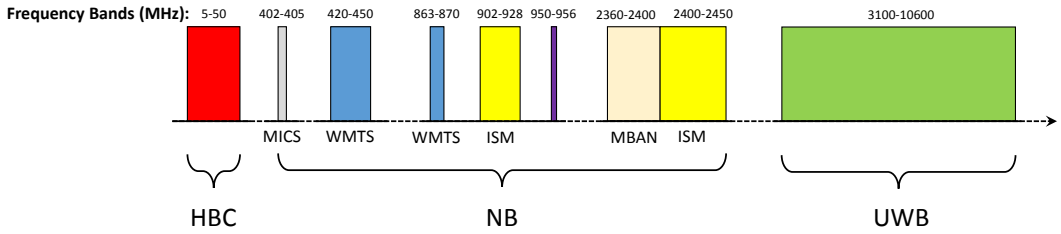

Figure 2.1: Frequency bands in WBANs.

2.1.2 WBANs' Channel Characteristics

Wireless channels in WBANs are highly subject to attenuation because of many reasons such as the mobility of the network and the movements of the sensor nodes during physical activities. The channels between moving sensor nodes are prone to an intensive dynamic path-loss. Please note that although the changes in the distance between two sensor nodes on the same body are probably limited to a few dozens of centimetres, its impact on the path-loss of the link is relatively large. To make an analogy with other wireless networks, it has been shown that changing the distance between two sensor nodes in the same body from 20 centimetres to 50 centimetres (that may happen because of body movement) can result an increase of 12 dBm in the path-loss, comparable with the increase in the path-loss of a link between a mobile user and the base station in a cellular network when the distance is changed from 20 metres to 50 metres (Hauer, 2014b). Additionally, body motion may cause changes in the direction of the antenna that further increase the path-loss. On the other hand, because of network mobility WBANs experience different environments even in a short period which leads to a different absorption rate, scattering, and reflection from the objects and environments. Therefore, wireless channels are likely to suffer from different interferers such as other

WBANs or even other wireless technologies operating in the same frequency band. These unique features of WBANs result in a time-variant channel quality fluctuation, requiring new channel models different from the existing models for typical wireless networks.

For the sake of unique characteristics of channels in WBANs, modelling of the channels is very difficult (Cotton, Conway, and Scanlon, 2009). Some of the existing channel models for typical wireless networks commonly investigate the statistical distribution of channel properties (such as signal amplitude) (Rappaport *et al.*, 1996). Similar models have been proposed for WBANs which focus on differences of the channels in specific scenarios such as the communication type (e.g., on-body communication versus off-body communication), environment (e.g., indoor versus outdoor), body posture and physical activity (e.g., dynamic versus static), the location of the sensor nodes (e.g., implanted versus on-body), and frequency range (e.g., 2.4 GHz versus UWB). Many of the models assume on-body channels are wide-sense stationary processes (Rozanov, 1967; Kim, Park, Cha, and Kim, 2010), however, this is neither the case in dynamic postures (e.g., walking) nor in static postures (e.g., standing) (Chaganti, Hanlen, and Smith, 2014) as the channel quality may show fluctuation up to 3 dBm in 2.45 GHz band just because of breathing (Hall, Ricci, and Hee, 2002).

Although the channel quality represents highly unstable fluctuations, some empirical studies have been conducted to show the spatio-temporal dependency between channel quality samples in different postures. In (Smith, Zhang, Hanlen, Miniutti, Rodda, and Gilbert, 2009), it is discussed that the average coherence time (the period the channel is expected to be stable) in walking and running is about 48 ms and 31 ms, respectively. Many of the channel models do not consider the spatio-temporal locality of the channel quality in their models. Some studies have tried to model the channel fluctuation pattern in cyclic activities (e.g., in walking). For example, the on-body propagation channel in periodic movements is analysed by applying autoregressive (AR) transfer functions over the collected channel samples from different on-body links in (Cotton *et al.*, 2009). Markov chain models have been extensively used to model the channel fluctuation, with a particular focus on dynamic postures with cyclic motion patterns. In (Tselishchev, Libman, and Boulis, 2011) a simple two-states Gilbert-Elliot (GE) Markov chain model is used to monitor the channel fluctuations. This model partitions the channel quality according to the Bit Error Rate (BER) in two states, good and bad. It then extracts a fixed state transition matrix (showing the transition probability among channel states) from a large number of collected channel samples for allocating

slots to different sensor nodes. As it is discussed in Chapter 4, simple Markov chain models cannot give an accurate estimation of the long-term channel status in WBANs when the distribution of the length of stay in a state is not exponential.

2.1.3 MAC Protocols

A MAC protocol in resource-constrained WBANs is expected to manage access to the channel to reduce energy consumption, avoid interference and collision, and provide reliable communication. Over the last decades, a big effort has been made to design MAC protocols for WSNs. Since these protocols do not address the specific challenges in WBANs, such as highly unstable topology, heterogeneous traffic rate, and strict delay sensitivity (as in medical applications), they usually cannot achieve high performance in WBANs. Accordingly, the IEEE 802.15.4 and IEEE 802.15.6 task groups released MAC protocols (which are actually a combination of basic channel access methods such as TDMA and CSMA) to enable efficient communication in WBANs.

The MAC protocol in IEEE 802.15.4 has two operational modes: beacon mode which uses slotted CSMA/CA and non-beacon mode which uses unslotted CSMA/CA. In beacon mode, the transmissions are organised by the gateway so that, the gateway periodically broadcasts a beacon packet to both synchronise the sending nodes and notify the beginning and the end of the superframes. In the non-beacon mode, there is no beacon, superframe, and synchronisation. The sending nodes do not need a coordinator and can sense the channel and transmit the packets once it is required. IEEE 802.15.6 MAC layer supports three operational modes: beacon mode with beacon period superframe boundaries and non-beacon mode without superframe boundaries, similar to IEEE 802.15.4, and non-beacon mode with superframe boundaries. Different from other modes, the non-beacon mode with superframe boundaries is more like polling mechanism in which, the gateway grants allocation to a sending node first, then, the sending node performs CSMA/CA procedure and transmits its packet once the channel is expected to be available.

2.2 Power-adaptive Communications in Wireless Networks

The idea of using power-adaptive communication to reduce energy consumption and interference range has been extensively studied in typical wireless networks since the

1980s. COMPOW (Narayanaswamy, Kawadia, Sreenivas, and Kumar, 2002) is a distributed power control mechanism for WSNs which operates in the network layer and tries to adjust the transmission signal power of all sensor nodes in the network to an optimal level. Using the optimal transmission signal power through the entire network, COMPOW keeps the topology connected but at the same time minimises the network energy consumption and maximises the network capacity. Finding the optimal power level in COMPOW imposes a significant message passing overhead since each sensor node has to exchange its link state with other sensor nodes by performing a separate routing protocol for each single transmission signal power provided by the radio chip. Furthermore, COMPOW suggests only a single fixed transmission power level for all communications in the whole network, therefore, it wastes energy in some scenarios with a short distance between the sender and the receiver.

ConeBased (Wattenhofer, Li, Bahl, and Wang, 2001) is a distributed topology control algorithm which adapts the idea of power control for energy-efficient communication in multi-hop wireless networks. ConeBased assumes the sensor nodes can detect the direction of a received signal. In the mechanism suggested by ConeBased, each sensor node increases its transmission signal power step by step until it finds a neighbour in every cone of α degrees, centred on the node. Using such a simple mechanism, the network connectivity is guaranteed while different sensor nodes can use a separate transmission signal power. However, the signal power used by each sensor node is constant for communications with all its neighbours.

Similar to COMPOW, ConeBased assumes that the channel quality between the sensor nodes in a WSN is constant over time. However, the experimental results presented in (Lin, Zhang, Zhou, Gu, Stankovic, and He, 2006) reveal the channel quality between sensor nodes shows some variations due to the changes in the surrounding environment (e.g., weather conditions). Therefore, the assumption of constant channel quality is not held even in those WSNs with no changes in the location of the sensor nodes and the gateway. Motivated by this, ATPC (Lin *et al.*, 2006), a power-aware communication protocol was designed for WSNs. ATPC adjusts the transmission signal power based on the linear relationship between the signal power and the Received Signal Strength Indicator (RSSI). In ATPC, each sensor node keeps a table for each neighbour so that it can remember the relation between the transmission signal power and the channel quality to the neighbours. Using this table and a feedback loop, the sensor node can gradually increase or decrease its transmission signal power until it finds the appropriate power which results in a RSSI in a predefined optimal range.

ATPC assumes the channel conditions are not changing quickly and the sensor node has enough time to adjust its transmission signal power.

In addition to WSNs, adaptive power control has many applications in both uplink and downlink of cellular networks. For example, the Foschini-Miljanic algorithm (Foschini and Miljanic, 1993) which is a very simple yet powerful method tries to iteratively adjust the transmission signal power of users in a cellular network to satisfy a predefined fixed Signal-to-Interference-Ratio (SIR) in a distributed manner. This algorithm assumes each user can measure its SIR after each transmission so that, if the SIR is below the target SIR, the user increases its transmission signal power, otherwise, it decreases the transmission signal power until the target SIR is observed. Although the fixed SIR assumed in Foschini and Miljanic algorithm is feasible in voice networks, it is quite a challenging assumption in wireless data networks (Chiang, Hande, Lan, Tan, *et al.*, 2008). A game-theory-based solution to cope with variable SIR has been presented in (Alpcan, Başar, Srikant, and Altman, 2002) which suggests the mobile users selfishly maximise their SIR regardless of the network throughput. This solution is then formulated as an N-person non-cooperative game with a unique Nash equilibrium.

Power control strategies have also applications in cognitive radio systems (Chen, Yu, Zhang, Chen, and Qiu, 2008), mesh networks (Luo, Rosenberg, and Girard, 2010), WLAN (Qiao, Choi, Jain, and Shin, 2003), etc. In (Chen *et al.*, 2008), for example, a power control strategy has been proposed for cognitive radio systems. In this strategy, the users opportunistically adjust their transmission power to maximise their transmission rate without sacrificing the outage probability of primary users due to interference from the secondary users. In (Qiao *et al.*, 2003) an energy-efficient adaptive power-control mechanism is proposed to enforce an RTS/CTS message passing before a data packet transmission to enable the transmitter to select the appropriate transmission signal power. Since the design of these protocols does not take into account the special features of WBANs, such as highly unstable network topology, they cannot work efficiently in WBANs to achieve high energy efficiency, low interference range, and acceptable communication reliability.

2.3 Power-adaptive Communication in WBANs

Several experiments have been conducted to study the effects of body postural movements on channel quality. These experiments show that body postural movements, depending on the physical activity, can result in small-scale and large-scale fading

with path-loss of up to 46.8 dB (Miniutti, Hanlen, Smith, Zhang, Lewis, Rodda, and Gilbert, 2008). Motivated by such a time-variant channel quality, several communication protocols have been designed to adaptively adjust transmission signal power of sensor nodes to an appropriate level so that, the sensor nodes can save energy and avoid interference while achieving acceptable communication reliability. Existing power-adaptive communication protocols can be simply categorised into two types: communication protocols which benefit from *channel estimation* for properly adjusting the transmission signal power and communication protocols that exploit *body motion patterns* to opportunistically transmit the packets with a low level of signal power.

2.3.1 Communication Protocols Based on Channel Estimation

Channel estimation as a tool for understanding the channel quality and selecting the proper transmission signal power has been discussed to a large extent in the literature. A channel estimator monitors the channel history to exploit the channel variation pattern and predicts its behaviour in the near or distant future. A practical channel estimator for WBANs should meet the requirements below (Smith *et al.*, 2009):

- It should have memory to track the behaviour of the channel quality and analyse its statistical behaviour to estimate the next value of the variable.
- It should be able to quickly adapt its estimations with the sharp channel fluctuations.
- It should be lightweight so that the resource-constrained sensor nodes can perform it and estimate the channel in a real-time manner.

The rest of this section gives an overview over the simple and the more complex channel estimators.

Linear Channel Estimators

Lightweight regression-based and linear estimators such as linear least square have been widely used to estimate the channel quality in wireless networks (Zahid, Sodhro, Zafar, Zahid, Khan, and Akhter, 2019; Tong and Zhao, 1999; Song, Lim, Baek, and Sung, 2002; Lin, 2008). However, in WBANs, they cannot predict the rapid channel dynamics as they essentially behave like a filter which generates a delayed version of the channel waveform (Smith, Lamahewa, Hanlen, and Miniutti, 2011), and therefore they cannot predict sharp changes.

Dynamic Postural Position Inference (DPPI)(Quwaider *et al.*, 2010) adapts the idea of ATPC (Lin *et al.*, 2006) for WBANs based on the assumption of a linear relationship between transmission power level and RSSI. In DPPI, the gateway compares the measured RSSI of each received packet with the empirically measured optimal RSSI threshold range $[RT_L, RT_H]$. If the RSSI falls in the optimal range, the selected power level is considered optimal; otherwise, an appropriate power level is selected with the expectation that the RSSI of the next packet will fall in the optimal range. DPPI is simple and extremely lightweight, which is ideal for resource-constrained body sensors. However, it does not perform well in dynamic postures because the assumption on the linear relationship between power level and RSSI does not hold due to the frequent topology changes. For example, assume the sending node communicates with a power level j at time t_i and a higher power level $j+1$ at time t_{i+1}. Based on the linear relationship, $RSSI(t_i) < RSSI(t_{i+1})$. In dynamic postures, it might happen that the LoS communication path is available at t_i but completely blocked at t_{i+1}, and it turns out that $RSSI(t_i) > RSSI(t_{i+1})$. In these experiments, it is also observed that DPPI suffers from a ping-pong effect in which the sending node frequently switches between two adjacent power levels, which is explained as follows: since transmitting using level i has a poor RSSI lower than RT_L, the sending node chooses a higher power level $i+1$. However, transmitting with power level $i+1$ has a very good RSSI higher than RT_H. Hence, the sending node will switch back to power level i. This ping-pong effect will have a big impact on communication reliability when transmitting with power level i experiences high packet loss. However, the ping-pong effect would be less problematic if the transmission signal power range is quantised with a finer granuality and thus, more power levels would be available.

A roughly similar work named Hybrid TPC is introduced in (Lee, Lee, and Kim, 2014). Hybrid TPC defines a target RSSI margin first. Then, using an aggressive power control mechanism and a conservative power control mechanism, Hybrid TPC enables the sensor node to adjust its transmission signal power to a level which results in the target RSSI margin. To this end, whenever the channel is fluctuating frequently (e.g., in dynamic postures), the conservative mechanism is used to smoothly adjust the transmission signal power to a proper level. Using a conservative mechanism (e.g., a mechanism that adjusts the transmission signal power linearly) the sensor node spends more time on power adjustment to avoid overreacting and oscillating the transmission signal power. On the other side, when the body posture is transformed between two static postures with a different channel quality (e.g., transition from sitting to standing),

since the channel quality in the new static posture is stable, the aggressive mechanism (for example, a mechanism that adjusts the transmission signal power exponentially) is used to quickly adjust the transmission signal power. Because of using a conservative mechanism in dynamic postures, the sensor node cannot quickly adjust its transmission signal power for opportunistic communication. Instead, it converges its transmission signal power to a fixed level which is optimal for the average RSSI during the posture.

RSSI/LQI Transmission Power Control (RL-TPC) (Kim *et al.*, 2013) is another communication protocol for WBANs that assumes a linear relationship between RSSI and transmission signal power. Different from DPPI, it uses both the channel RSSI and the Link Quality Indication (LQI) to adjust the transmission signal power, since the interference from an illegitimate transmitter can increase the RSSI value of a receiving packet at the legitimate receiver. For each transmission, RL-TPC considers the average LQI first. If it is higher than a threshold, the channel quality is good with no remarkable interference, and the optimal power level can be estimated using RSSI. If the RSSI is high, but the LQI is low, it indicates strong interference. In this case, RL-TPC suggests changing channel frequency to avoid interference.

A regression-based self-predictive power control (SPPC) solution has been proposed to enable decentralised efficient per packet power control in WBANs (Zahid *et al.*, 2019). To choose the proper power level for next transmission, SPPC considers the recent communication history and variation rate of channel RSSI under the use of the current transmission power level. To do so, the gateway feedback the sending node with an ACK packet including the measured RSSI of the received packet. Besides, the sending node records the last three RSSIs corresponding to each transmission power level. Similar to DPPI, low and high RSSI thresholds are predefined at the sending nodes based on which, the sending node compares the received RSSI to evaluate the efficiency of the selected power level.

Markov Chain-based Channel Estimators

To compensate the drawbacks of the linear channel estimators while keeping their advantages (e.g., low complexity overhead), a prediction-based power-adaptive communication protocol for WBAN is proposed (Smith *et al.*, 2011) which combines the ability of Finite State Markov Chain models (FSMC) in describing the behaviour of a complex system with the simplicity of linear estimators. This method benefits from reciprocity of WBAN wireless channels (Hanlen, Chaganti, Gilbert, Rodda, Lamahewa, and Smith, 2010) and assumes the on-body channels are relatively stable for a short

period and the channel prediction is valid up to 1 second. In this protocol, the sending node estimates the channel according to the measured RSSI of the last received packet from the gateway and selects the lowest transmission signal power that is higher than the measured RSSI for all communications until the next packet is received from the gateway. If the selected transmission signal power is lower than the minimum received power sensitivity of the radio of the gateway, the sending node selects the maximum transmission signal power and communicates with the gateway. In this method it is assumed that the sending node can increase the transmission signal power from -30 dBm to 0 dBm in 0.5 dBm step which is supported neither by CC2420 (Texas Instruments, 2007) nor other off the shelf WBAN consistence radio chips. Moreover, it does not propose any solution for a long-term channel prediction.

Similarly, a lightweight channel prediction algorithm is presented in (Zhang, Smith, and Chen, 2012) to enable the sensor nodes to track the channel quality variation, however, its accuracy in dynamic postures or generally in situations with a noisy channel RSSI is unacceptable. Therefore, its channel prediction algorithm is combined with finite state Markov chain model so that the sending node can monitor the channel history and extract the channel properties (i.e., the statistics of the channel behaviour). In this model, the states in the Markov chain represent the channel RSSI sub-ranges and the transition probabilities between different states are maintained using a large-size Transition Matrix (TM). Although this method has a very low computational complexity, its memory complexity is extremely large, in the order of $O(M^{L+1})$, where M is the number of RSSI sub-ranges and L is the length of the history of channel observations. Moreover, this model only predicts the next channel state and does not give a long-term channel estimation. Therefore, the sending node cannot save more energy and reduce interference range by scheduling the packets for late transmissions in delay-tolerant applications.

Unlike the discussed methods that directly monitor the channel, posture based data transmission (PBDT) (Maitra and Roy, 2019) benefits from Markov chain models to predict the body posture through which it can estimate the channel quality. PBDT has two phases: (1) scanning phase, and (2) packet transmission phase. PBDT considers a periodic physical activity (which is the main reason for channel fluctuation) as a repeated finite sequence of body postures. In the scanning phase, each sending node monitors the variation of channel RSSI from neighbour nodes over time to detect the sequence of body postures. If the current activity is periodic and the sequence of body postures is detected, the second phase is run. In this phase, the sending node exploits

the best posture (i.e., the posture with the best channel quality among all the other postures) for packet transmission from the sequence of postures. Finally, the upcoming posture is predicted using a Markov chain model. If the predicted posture is the best, the sending node transmits the packet. PBDT does not require extra hardware but it relies on the measured RSSI from neighbour nodes around the sending node and thus, the accuracy of posture detection algorithm is highly dependent on the number of neighbours. On the other hand, since listening to the channel is an energy consuming task (Texas Instruments, 2007), the scanning phase imposes a considerable amount of energy overhead to the sending node.

Deep Learning-based Channel estimator

Based on the idea of short-long term memory (LSTM), a centralised long-term channel prediction solution for WBANs is proposed in (Yang, Smith, and Seneviratne, 2019). LSTM is a deep learning recurrent neural network (RNN) architecture. LSTM-based channel prediction algorithm aims to estimate the channel fluctuation using the past channel RSSIs recorded in the gateway, making efficient transmit power control possible. In practice, it is less likely a trained LSTM network can maintain a low prediction error for a long time. Thus, an online training scheme is proposed by which the initially trained LSTM network is iteratively fine-tuned with the new training data set consisting of a couple of seconds of recently received channel samples.

2.3.2 Exploitation of Body Motion Patterns for Opportunistic Communication

DPPI, RL-TPC, and Hybrid TPC are roughly similar in their nature, that is, they assume a linear relationship between the transmission signal power and channel RSSI and accordingly adjust the transmission signal power level based on the recently measured channel RSSI. Hence, they all require a very high packet rate communication to follow quick channel changes in dynamic postures. Moreover, the conducted measurements that are discussed in the next chapter reveal that the assumption of the linear relationship between transmission signal power and channel RSSI does not hold when the channel is changing quickly during dynamic postures such as walking and running. Hence, these protocols are just suitable for static postures, where the link is stable for a while. Similarly, Markov chain-based models require very high packet rate communication to measure the channel to the gateway and exploit the channel behaviour so, they are

appropriate for the applications which require a high packet rate communication.

The channel quality fluctuation in many postures such as walking and running follows a periodic pattern when the channel link alternates between available and blocked LoS path (Miniutti *et al.*, 2008; Kindt *et al.*, 2015; Zang and Li, 2017; Hauer, 2014a). Such a periodic pattern indicates a potential gain from power-adaptive communication which can be achieved by low-power communication when the LoS path between the sensor node and the gateway is available and the distance is short, and high-power communication when the LoS path is blocked. Some of the existing communication protocols try to exploit the connectivity pattern of the links to estimate the channel and opportunistically transmit the packets when the link is expected to be connected.

In ExPerio (Kindt *et al.*, 2015), the sending node monitors the acceleration signal of the body part to find a periodic pattern. Once a periodic pattern is observed, it monitors the channel RSSI fluctuation for 10 seconds and calculates the time-offset between each acceleration peak and its corresponding RSSI peak. Once the average time-offset is calculated, ExPerio schedules the packets to be transmitted in a bursty fashion using the minimum power level according to the computed time-offset. However, ExPerio does not work efficiently when there is not a periodic motion (e.g., in sitting and standing), and also it has a remarkable computation overhead for periodicity detection. In ExPerio, finding the time-offset requires 10 seconds of communication at the packet rate of at least 17 packets per second, regardless of the requirement of the application (Kindt *et al.*, 2015) which means ExPerio does not support low packet rate applications. The accuracy of the periodicity detection algorithm is another challenge because many of the body movements are not purely periodic. Above all, the 10-second learning phase in ExPerio takes about 100000 arithmetic operations (Kindt *et al.*, 2015) which is unaffordable for resource-constrained body sensors.

Similar to ExPerio, G-TPC (Zang and Li, 2017) monitors the fluctuations in acceleration signal and channel RSSI to find the channel peak during a gait cycle. G-TPC is a centralised communication protocol which performs the acceleration and RSSI analysis at the gateway. In static postures, it benefits from the idea of RL-TPC to find the proper transmission power level. In dynamic postures, it collects the acceleration data for 1.6 seconds as the template of the acceleration pattern of the current posture and uses a template matching algorithm over the real-time acceleration signal to find the similar pattern. Through analysing the channel RSSI, the gateway finds the best time for communication and schedules the packet to be transmitted at the expected channel peak.

M-TPC (Zang and Li, 2015) is another centralised power-adaptive communication protocol which tries to find the optimal transmission power level by monitoring the acceleration signal and measuring channel RSSI in a closed feedback loop. M-TPC assumes the real-time physical activity is perfectly detected using the existing activity detection algorithms. Hence, whenever a packet is transmitted, the gateway measures its RSSI. If the measured RSSI is not in a predefined optimal RSSI margin, the gateway calculates the optimal transmission signal power and sends a control packet back to the sensor node to inform the optimal signal power. M-TPC assumes a linear relationship between the transmission signal power and the channel RSSI. Similar to ExPerio, G-TPC and M-TPC require a very high packet rate communication to detect the channel peak. Moreover, they do not support event-driven applications.

In BANMAC (Prabh, Royo, Tennina, and Olivares, 2012), the gateway periodically broadcasts the probing packets so that the sending nodes measure the RSSI of the packets to find the channel fluctuation pattern. BANMC filters the RSSI signal and applies Fast-Fourier Transform (FFT) to exploit the channel peak frequency. Then, BANMAC opportunistically transmits the packets at the Opportune Transmission Windows (OTWs) which are the time periods with a high channel RSSI. BANMAC is a communication protocol for fully periodic postures so, its performance is dramatically degraded in postures with aperiodic channel fluctuations and static postures. Calculating OTWs suffers from drift due to the noisy channels and unexpected variations in the movement pattern. To compensate for the drift, BANMAC uses probing packets which impose extra energy overhead. Since estimating a channel peak for a packet transmission requires several channel measurements and calculations, BANMAC is not a good solution for event-driven applications as well as applications with low-packet rate.

As discussed, power-adaptive communication suggests increasing the transmission signal power in situations with a bad channel quality because of blocked LoS or a long distance to the gateway. Instead of adjusting the transmission signal power, some research suggests building a path from the sensor node to the gateway including a couple of sensor nodes to break a one-hop communication into a multi-hop communication using a low transmission signal power to further reduce energy consumption and potential interference. The next section gives a brief discussion on power-aware routing protocols and clarifies the limitations of this type of communication protocol in WBANs.

2.4 Multi-hop Communication and Routing Protocols in WBANs

Routing protocols in WBANs with the purpose of reducing transmission signal power have been extensively investigated. In (Watteyne, Augé-Blum, Dohler, and Barthel, 2007) a cluster-based routing protocol named Anybody based on the LEACH protocol (Heinzelman, Chandrakasan, and Balakrishnan, 2000) is proposed. Set up phase (including cluster formation, cluster-head selection, and building the rout) in Anybody is a five-step procedure in which, the sensor nodes exchange some hello packets to find the cluster heads. Once cluster-heads are identified, a backbone including cluster-heads are constructed after some message passing among cluster-heads. Then, a routing path is set up that guarantees a multi-hop path from each sensor node to the gateway. Although Anybody can effectively replace a long distance one-hop communication with a multi-hop communication, its set up phase imposes a lot of message passing overhead to the WBAN. Additionally, Anybody does not discuss how the clusters and the routes to the gateway are maintained while the distance between the sensor nodes is changed over time due to topology changes.

WASP (Braem, Latre, Moerman, Blondia, and Demeester, 2006) is a tree-based routing protocol in WBANs. It sets up a gateway-rooted spanning tree in a distributed manner for energy efficient routing and presents a slotted multi-hop channel access mechanism using the same spanning tree. In this routing protocol, each parent node controls the channel access among its children through sending a message called WASP-scheme. WASP-scheme is a node-unique message constructed in each parent node and includes information for the children. By broadcasting WASP-scheme, a sensor node not only informs its children about their access time to the channel but also informs its parent regarding the resources it needs. WASP routing protocol is started by transmitting a WASP-scheme from the gateway. Then, the children of the gateway which are in its one-hop distance will find the time slots they are allowed to communicate with the gateway. In the same way, the one-hop neighbours of the gateway broadcast WASP-scheme to let their children know about the time slots they can access the channel. Because of the time-slotted channel access method and the tree structure of the communication between sensor nodes and the gateway, WASP provides a constant end-to-end delay and a high Packet Delivery Rate (PDR). Similar to Anybody, WASP imposes a lot of message passing overhead to construct the spanning-tree and does not provide a mechanism for topology control to avoid network partitioning.

RLOFC (Quwaider and Biswas, 2009a) is an opportunistic routing protocol in WBANs that cancels the extra communication overhead required in WASP and Anybody because it neither presents a fixed structure (e.g., tree or cluster) nor sets a path until a packet needs to be forwarded. RLOFC assumes the location of the sensor nodes and therefore, their distance to the gateways is known a priori. Whenever a packet is generated but the LoS path to the gateway is blocked, the sensor node selects another sensor node as a relay node so that: (1) the LoS path between the sensor node and the relay node is available; (2) the relay node is closer to the gateway rather than the sensor node; (3) the relay node is the closest node among other candidates that pass the first two conditions. Using this method, if the LoS path to the gateway is blocked and the sensor node cannot find any relay node which passes the mentioned conditions, it buffers the packets until a relay node is found or the LoS path to the gateway becomes available. Since there are situations in which the LoS path from the sensor node to other sensor nodes as well as the gateway is blocked for a long time, there is a high possibility that the packets suffer from a long delay. On the other hand, RLOFC assumes the shorter distance between the sensor node and the gateway guarantees a better channel quality. So, regardless of the LoS path between the relay nodes and the gateway, RLOFC tries to forward its packet to a relay node closer to the gateway. However, there are examples in which a sensor node near the gateway is completely blocked by body parts (for example in scenarios with the gateway attached to the chest and the sensor node attached to the back). Furthermore, knowing the initial distance between a sensor node and the gateway does not help as body postural movement changes the distances over time.

To cope with the problem of topology changes and network partitioning, a probabilistic store-and-forward routing protocol named PRPLC is presented in (Quwaider and Biswas, 2009b). PRPLC shows that although the channel quality fluctuates quickly in WBANs, it is relatively stable for a very short period. Therefore, PRPLC defines a factor named LLF (Link Likelihood Factor) which represents the probability of connectivity of the link from each sensor node to the gateway. To calculate and maintain the link likelihood factor, the sensor nodes exchange hello messages periodically. Whenever a sensor node has a packet to transmit to the gateway, it checks to see whether any of its neighbours has a higher LLF to the gateway. In case such a neighbour is available, the sensor node forwards its packet to that neighbour expecting that the neighbour with a better LLF to the gateway can deliver the packet to the gateway more reliably. Although using LLF helps the sensor node to better manage the network topology

changes, updating it requires a high message passing with other sensor nodes which is highly energy consuming. On the other hand, the packet forwarding scheme in PRPLC assumes there is always a neighbour with available LoS to both the sensor node and the gateway. However, this assumption does not hold in many scenarios. PRPLC is a greedy algorithm which only considers the LLF of the next hop. Hence, it does not guarantee the selected path has the best end-to-end quality. To solve this problem, the extension of PRPLC is presented in (Quwaider and Biswas, 2010) under the title of DVRPLC which considers the end-to-end path cost for choosing the forwarding path.

Behaviour-Aware Probabilistic Routing (BAPR) (Yang *et al.*, 2013) improves the performance of PRPLC and DVRPLC by taking into account the current body motion (i.e., trend) in the process of selecting the forwarding link. BAPR incorporates inertial motion information captured by low-cost accelerometer into the routing logic. To do so, each sensor node maintains a routing table. Each entry in the routing table includes the ID of the destination, the relay node, and the connectivity factor. Therefore, whenever a packet is generated or received from a neighbour, the sensor node considers the destination and selects the next hop with the highest connectivity factor. To calculate the connectivity factor, BAPR formulates the expected link status by combining the short-term and the long-term channel records using a simple weighted averaging method in the following way: if the acceleration data shows a high fluctuation, short-term channel history gets more weight on calculating the expected link status; otherwise, the long-term channel history has a higher impact. BAPR needs to keep a large routing table with N^2 entries where N is the number of the sensor nodes.

Energy-aware link-efficient routing approach for WBANs (ELR-W) is proposed in (Anwar, Abdullah, Altameem, Qureshi, Masud, Faheem, Cao, and Kharel, 2018) to provide a green communication framework for on-body communications. ELR-W is a three-step protocol: the first step proposes a metric namely link-efficiency to represent the quality of the links by considering the RSSI, LQI, and PDR of the link. The second step derives a path cost function by considering the link quality, the hop counts, residual energy, and the distance to the gateway. Finally, the path cost function is used in the third step to select the next-hop when a packet is ready to be sent. Similarly, a reliable, energy-efficient multi-hop communication packet forwarding scheme is presented in (Abidi, Jilbab, and Mohamed, 2018). Apart from implanted sending nodes which are in charge of measuring vital body parameters, a set of forwarder nodes are used to deliver the collected vital measurements from the sending nodes to the gateway. A cost function is utilised by the sending nodes through which they can choose the

proper forwarder nodes. The cost function considers two metrics: the distance from the forwarder node to the gateway and its residual energy. Therefore, the forwarder node with the higher residual energy and the shorter distance to the gateway has a lower communication cost. Finally, a greedy strategy is used to select the forwarder node with minimum transmission cost.

Although routing protocols in wireless networks have achieved groundbreaking results in different aspects, there are major concerns regarding their performance and feasibility in WBANs as listed below:

- **Low energy-efficiency:** Most of the routing protocols assume the energy consumption in receiving mode is negligible while this is not the case in some IEEE standard compatible radio chips (e.g., in CC2420 radio chip). Therefore, multi-hop communication has a potential to impose a significant energy overhead to the network.

- **High heterogeneity in sensor nodes' applications:** The existing routing protocols usually do not consider a WBAN including sensor nodes with different sizes, resources, capabilities, various applications, heterogeneous traffics, and dissimilar duty cycles. For example, a sensor node in a WBAN which monitors the patient's blood glucose probably needs a very low packet rate communication when the blood glucose goes higher than a threshold while EEG sensors have to report the measured signals continuously at a very high sampling rate.

- **High end-to-end delay:** Many power-aware routing protocols do not incorporate the end-to-end delay in their routing logic while health-related applications of WBANs are highly delay-sensitive and the end-to-end delay higher than a threshold is not acceptable.

- **Low performance in small WBANs:** The performance of a majority of routing protocols is highly dependent on the size of the network so that, finding a multi-hop path with a better performance than direct communication in a smaller WBAN with a few sensor nodes is usually less likely.

- **No limitation on packet hop count:** Only one-hop and two-hop communications are supported by IEEE standards for WBANs while most of the routing protocols do not consider this limitation.

2.5 Dynamic Slot Scheduling for Opportunistic Communication

The idea of dynamic slot scheduling (DSS) methods is estimating the channel condition and then, scheduling the sending nodes so that the network performance is maximised. It is worth noting that DSS methods are centralised. That is, the scheduling decisions are made at the gateway, and there is no increase in the sending nodes' complexity. Using a simple two-state (good and bad) GE Markov chain model a DSS method named flipping (Tselishchev, Boulis, and Libman, 2012) is proposed to maximise the average successful transmission rate in a superframe. Markov chain model is used to exploit the on-body channel behaviour in WBANs. Based on the link quality in the previous superframe, flipping method divides the links into two groups, bad and good. Bad links are scheduled last in the current superframe right in the same order they were scheduled in the previous superframe. But, the good links are scheduled first, however, in the reverse order that they were observed. The idea of flipping scheme is to postpone the communication over the bad links to give them time to recover. However, using only good and bad states for describing the channel behaviour is highly insufficient and affects network performance in complex daily activities.

A novel DSS method namely DSS-TA (Zhang, Safaei, *et al.*, 2018) is proposed to schedule the sending nodes to minimise the average packet loss rate of the network. Using experimental investigation, it is shown the temporal autocorrelation is high within a time lag of about 500 ms. DSS-TA is a centralised method which relies on the temporal autocorrelation of the on-body channels. In DSS-TA the gateway periodically broadcasts control packets. Then, the sending nodes feedback the measured RSSI value of the control packets to the gateway. By monitoring the latest 2 seconds of channel feedback, the gateway tries to estimate the temporal autocorrelation in channel samples through which, it can predict the packet loss rate of communication with different sending nodes in different time slots. Once the packet loss rate in different slots is predicted, the sending nodes are scheduled for packet transmission. The scheduling problem in DSS-TA is converted into a minimum cost bipartite graph matching problem, where the sending nodes and time slots are two separate sets of vertices and the edges are weighted by predicted average packet loss rate. Although the experimental results show DSS-TA reduces the average packet loss rate, it does not consider the effect of transmission signal power on the results. Moreover, transmitting a high number of RSSI feedback from the sending nodes to the gateway imposes a considerable energy

overhead as mentioned before.

A priority-based time slot allocation technique is presented in (Sun, Wang, Yu, Du, and Guizani, 2019). This method defines a utility function to prioritise the data packet of the sending nodes. To do so, the utility function considers the remaining energy of the sending node, its packet rate, the importance of its data, and its time-out conditions. Once the utilities of the packets are calculated and the channel is estimated, a greedy strategy is used to maximise the network utility within a superframe. That is, the slot with the highest channel quality is allocated to the packets with the highest priority.

2.6 Relay Networks and Topology Design

Instead of applying routing protocols for cooperatively forwarding the packets toward the gateway, some studies have considered employing a separate relay network in parallel with the WBAN. The relay network includes several relay nodes. Relay nodes do not measure body parameters and are only in charge of collecting data from sensor nodes in their neighbourhood and forwarding the collected data toward the gateway. Relay nodes should be designed to be simple, cheap, light, and small. Using such a relay network distributed through the whole body, the sensor nodes can simply transmit their packets to a relay node in their LoS path. Therefore, a long distance one-hop communication in WBAN is replaced by a short distance one-hop communication in WBAN as well as a multi-hop communication in the relay network.

In (Ehyaie, Hashemi, and Khadivi, 2009), in conjunction with WBAN, an on-body relay network is developed to play the role of a backbone in WBANs. To construct the relay network, this scheme suggests placing the relay nodes on the body until all sensor nodes in the WBAN, as well as relay nodes, have at least one relay node with LoS path. It then suggests that the multi-hop communication in the relay network is organised by the existing dynamic routing protocols to support topology changes. That is, whenever a previously available path from the sensor node to the gateway through relay network is blocked, the dynamic routing protocol replaces it with a new path. This scheme does not discuss the maximum number of the relay nodes. On the other hand, since the human body experiences different postures over time, there are situations in which the sensor nodes are completely blocked by other body parts. So, it is difficult if not impossible to design a topology for the relay network to guarantee the availability of LoS path between each sensor node and at least one relay node. Instead of designing a relay network with a separate topology, the relay nodes can be simply

placed right beside the sensor nodes to forward their packets (Reusens, Joseph, Latré, Braem, Vermeeren, Tanghe, Martens, Moerman, and Blondia, 2009). Therefore, the relay nodes play the role of a spare battery for resource-constrained sensor nodes.

A roughly similar idea is proposed in (Elias and Mehaoua, 2012) and (Elias, 2014) to limit the number of relay nodes in the relay network. This idea introduces a new optimisation framework for energy-efficient topology design to reduce the transmission energy cost of WBANs. Assuming the location of the sensor nodes is predetermined, this method tries to add extra relay nodes into the WBAN so that, a one-hop communication to the gateway which possibly requires a high transmission signal power is split into a multi-hop communication with a minimised total transmission energy cost. The problem of finding the optimal number and the optimal locations of the relay nodes is then formulated and solved by linear integer programming.

Relay-aided Transmission Power Control (RA-TPC) (Zhang and Zhang, 2017) is a centralised power adaptive communication protocol which combines the idea of power control and two-hop communication to extend the overall network lifetime and guarantee communication reliability. RA-TPC enables the sending node to decide between one-hop communication and two-hop relay-assisted communication at a per packet-level depending on the real-time channel status. RA-TPC has three modules: (1) RSSI-based channel estimation module which utilises a simple weighted averaging method; (2) a module which selects the transmission strategy (to be one-hop or two-hop); (3) a transmission power selection module.

Apart from an extra cost for installing new relay nodes, adding extra sensor nodes or relay nodes is neither easy nor convenient as the area of a WBAN is limited to the human body. On the other hand, because of rapid topology changes due to different physical activities, the location of the sensor nodes is highly unstable. Therefore, even adding relay nodes does not guarantee that the communication links in WBANs remain stable.

The idea of optimal node placement for energy efficient communication has been extensively studied in WSNs. As it mentioned, a major challenge in WBANs is the time-variant channel quality due to the network topology instability. Thus, the optimal topology design and efficient node placement can effectively improve the performance of a WBAN in those applications which allow some flexibility on the changes in the places the sensor nodes can be attached or implanted. However, this is not the case in most of the applications in WBANs because the locations of the sensor nodes are predetermined according to the physiological features of the body parts. For example,

EEG sensors should be placed on top of the sculpt, and the ECG sensors are needed to be installed on the chest.

Although the physiological aspects of the human body somewhat determine the location of the sensor nodes, the gateway, which is normally the user's mobile phone, can sometimes be placed in different locations such as waist, side pockets, chest pockets, etc. Motivated by this, some research has been conducted to address the effect of different locations for the gateway on the performance of WBANs. The propagation properties (e.g., fade depth and path gain) of the channel between four sensor nodes (attached to the upper arms, chest, and back) and the gateway are measured and discussed in (Sipal, Gaetano, McEvoy, and Ammann, 2015). The measurements are repeated for three different locations of the gateway including head, foot, and waist. The analysis of the measured channel samples reveals that the worst scenario is attaching the gateway on the waist, which is also confirmed in (Gaetano, Sipal, McEvoy, Ammann, Brannigan, Keating, and Horgan, 2013; Sipal, Gaetano, McEvoy, and Ammann, 2014).

2.7 Interference Mitigation in WBANs

Interference is commonly defined as an addition of interfering signal from an illegitimate transmitter at a legitimate receiver (McWhinney, 1971) so that the stronger signal from the interferer leads to a higher disruption at the receiver. Interference increases packet loss and causes throughput reduction, thereby leading to energy waste because of retransmission. As previously mentioned, channel links in WBANs are prone to both inter-WBAN interference from coexistence WBANs or other wireless technologies and intra-WBAN interference from the sensor nodes in the same WBANs. Hence, it is considered necessary to avoid interference to improve the network performance. The existing solutions for mitigating interference in WBANs can be generally discussed in three groups: *power control* based solutions, *MAC protocol* based solutions, and *cognitive radio* based solutions.

2.7.1 Power Control Based Solutions

Power control mechanisms for interference mitigation have been studied extensively in typical wireless networks (Pantazis and Vergados, 2007; Chiang *et al.*, 2008), however, the existing methods usually do not support the unique specifications of WBANs. A WBAN specific fuzzy system named Fuzzy Power Controller (FPC) is presented in (Kazemi, Vesilo, and Dutkiewicz, 2011) to jointly minimise the transmission signal power and

maximise the communication throughput. To find the transmission signal power for communication in the current time slot, FPC applies the Genetic Algorithm (GA) to a set of inputs including the Signal-to-Interference-Noise-Ratio (SINR), interference power, and the selected transmission power level at the previous time slot (which is actually the output in the previous time slot) in a closed feedback loop. FPC focuses on reducing the inter-WBAN interference and assumes the sensor nodes in a WBAN adjust the same power level for all inter- and intra-WBAN communications.

A game theory-based approach named proactive power update (PAPU) (Fang, Dutkiewicz, Yu, Vesilo, and Yu, 2010) is proposed to optimise the balance between energy consumption and throughput while reducing the interference among coexistence WBANs. Using a game theory model, PAPU first defines a payoff function representing the tradeoff between the network throughput and a cost function. The cost function combines the transmission power level and power price where power price is the tradeoff between the transmission rate and power efficiency. Then, WBANs try to maximise their payoff selfishly by adaptively adjusting their transmission power level, measuring the SINR of their neighbours, and exchanging messages with them for knowing the transmission power level of the neighbours. Although PAPU converges the transmission power level of all WBANs so that each WBAN maximises its payoff, its convergence in highly mobile WBANs is not discussed. Moreover, converging to the optimal power level requires a lot of message passing between WBANs which imposes extra energy and interference overhead. Last but not least, similar to FPC, PAPU assumes all sensor nodes in a WBAN communicate with the same power level which is not efficient. Although previously discussed power-adaptive protocols have not specifically focused on interference mitigation, they may implicitly reduce the interference range as they try to adjust the transmission signal power to its minimum reliable level. In order to avoid repetition, these protocols were discussed only in Section 2.2.

2.7.2 MAC Protocol Based Solutions

Some solutions in MAC layer suggest the sensor nodes switch their operating frequency band to mitigate the interference. For example, Interference aware Channel Switching (InterACS) (Mahapatro, Misra, Manjunatha, and Islam, 2012) is a centralised algorithm that enables the gateway to switch the frequency channel of the sensor nodes with the purpose of reducing the interference when different WBANs meet each other. In InterACS, the gateway measures the SIR of the received signal from the sensor node and decides to change the frequency channel if the measured SIR is below a predefined

threshold. The change in the frequency channel suggested by InterACS depends on the difference between the measured SIR and the threshold so that if the difference is low, the channel is changed to the next 2-hop channel while if the difference is high, the channel is changed to the next 4-hop channel. Although changing the operating channel to a less congested channel may reduce interference, the sensor nodes need a more complex hardware to support this function which is not available in many tiny sensor nodes.

Some other interference mitigation solutions suggest the gateway to re-schedule the transmission slots of the sensor nodes in the superframe upon detecting an unwanted signal from an interferer. In (Movassaghi, Abolhasan, and Smith, 2014) a cooperative scheduling scheme for reducing inter-WBAN interference is introduced. This method partitions the area (where WBANs are coexisting) into several clusters each of which includes two WBANs. Then, the gateways in the same cluster start negotiating on using orthogonal channels. Assuming each WBAN has N sensor nodes, at the first step the shared channel between two WBANs is divided into $2 \times N$ slots which form a superframe. Hence, there is a separate time slot for each sensor node in the cluster to freely communicate with its gateway. During the communication, each gateway measures the potential interference from the transmitting sensor nodes on the other WBAN as well as the signal power of its sensor nodes. In the next step, each gateway finds the sensor node with the lowest signal power in its network and lists the ID of the sensor nodes in other WBAN that produce interference higher than a threshold. This threshold is defined based on the measured minimum signal power. Then, two gateways share the list of the interferers. In the last step, the gateways do not change the allocated time slots to the sensor nodes in the list of interferers but the rest of the time slots are allocated to all sensor nodes in each WBANs, leading to a higher spatial reuse. For example, if N is 5, and the list of interferers includes 2 sensor nodes (one interferer from each WBAN), then each interferer takes one time slot as before, but the other 4 sensor nodes in each WBAN can take 2 time slots without generating interference for other WBAN. Although this method has been designed for WBANs, it does not take the network mobility and body postural movements into account for scheduling which leads the scheduling to be valid only for a short period. Therefore, by any major changes in the location or the topology of a WBAN, the clusters need to be rearranged, the set-up phase needs to be repeated, and the gateways need to negotiate again, which is a very expensive procedure.

2.7.3 Cognitive Radio Based Solutions

Cognitive Radio (CR) systems have a great potential to enhance the performance of WBANs by addressing the spectrum scarcity (Chávez-Santiago, Nolan, Holland, De Nardis, Ferro, Barroca, Borges, Velez, Goncalves, and Balasingham, 2012; Syed and Yau, 2013). CR systems can monitor the channel for spectrum estimation and access the channel when it is expected to be idle. They enable the sensor nodes to efficiently use the spectrum and manage interference problems by adjusting the transmission and reception parameters of communication (e.g., transmission signal power and frequency band) (Shen, Liu, Yu, Ma, Li, Shen, and Chen, 2013). In (Shen *et al.*, 2013) an IEEE 802.15.6 compatible Adaptive Cognitive Enhanced Platform (ACEP) is developed. ACEP incorporates three subsystems including a WiFi interferer as the interference subsystem, two sensor nodes for monitoring the system workflow as the observation subsystem, and a gateway node for sensing the spectrum and estimating the channel interference as the WBAN subsystem. Then, Fast Dynamic Cognitive Radio (FDCR) (Shen *et al.*, 2013) algorithm is proposed to be implemented on ACEP for opportunistic interference avoidance and enhancing the coexistence of WBANs. Following the FDCR algorithm, the gateway senses the channel and measures the background noise and interference to check whether the channel is idle or busy. If the gateway detects the channel is idle, it broadcasts some information (e.g., the channel access-time) to allow the sensor nodes to communicate. By monitoring the collision rate in a feedback loop FDCR adjusts the channel sense-time and the channel-access time for the next round of communication. Although this solution can mitigate interference, it cannot avoid collision in many scenarios. For example, it does not consider the hidden terminal problem as the channel sensing is entirely done in the gateway without any cooperation with other gateways or sensor nodes.

2.8 Novelty of This Thesis Work

In this thesis, three communication protocols for WBANs are introduced in three separate episodes (i.e., chapters) so that each protocol not only supports a wider range of applications of WBANs but also performs better than the state-of-the-art protocols in several scenarios. The novelties and advantages of the works in this thesis can be summarised as follows:

(1) Instead of directly exploiting body motion patterns for opportunistic communica-

tion, the proposed protocols benefit from *on-line learning* algorithms to implicitly learn the channel pattern so they can adjust the transmission signal power to a proper level. Because of the learning nature of the algorithms, they can achieve excellent performance not only in dynamic postures, but also in static postures.

(2) The proposed protocols are *decentralised*, therefore, a sensor node can locally adjust its transmission signal power to reduce its transmission cost without imposing extra message passing or a considerable computation overhead to the network.

(3) The communication protocols are designed based on the idea of *one-hop communication* with the gateway being in a fixed location to support the star topology suggested in (IEEE LAN/MAN Standards Committee, 2012). Because of one-hop communication architecture of the protocols, their performance in WBANs does not depend on the network size (i.e., the number of the sensor nodes in the WBANs). On the other hand, according to the properties of IEEE 802.15.4 compatible radio chips (e.g., CC2420, CC2430, CC2520, etc.), energy consumption for receiving a packet is extremely high and comparable with energy consumption for transmitting a packet using a high transmission signal power. That is, one-hop communication in WBANs is usually more energy efficient than a multi-hop communication.

(4) Unlike many of the existing schemes which generally consider a single performance metric, the proposed protocols try to reduce the *energy consumption* and *potential interference*, while providing a *reliable communication*.

Chapter 3

System Description and Performance Metrics

3.1 WBAN Testbed and Hardware Platform

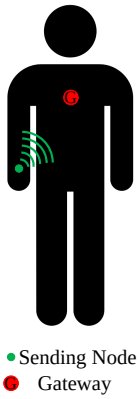

Figure 3.1: Test WBAN consisting of a sending node on the wrist and a gateway on the chest.

All experiments in this thesis were done using a test WBAN including a sending node and a gateway (Figure 3.1). The sending node is attached to the wrist. This is a reasonable design as most of the wearables tend to be embedded into the user's wristwatch. Additionally, the shoulder joint is the most mobile joint (Dodson and Cordasco, 2008) and provides the widest range of movements for the wrist (in combination with the elbow joint). Therefore, assuming the sending node is attached to the wrist is not only a realistic assumption for many applications, but also makes the experiment scenarios more challenging. On the other hand, the gateway is usually the user's mobile phone, which can be placed in his shirt pocket or side pocket, but, in this setup, it is

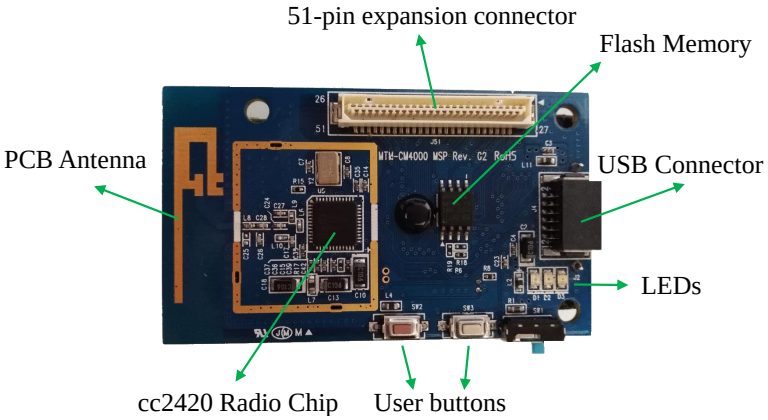

Figure 3.2: TelosB platform.

attached to the chest as it is quite common in body motion tracking systems.

The IEEE 802.15.4 compatible TelosB mote (UC Berkeley, 2004) (presented in Figure 3.2) that integrates a 16-bit RISC architecture MSP430F1611 Micro Controller Unit (MCU) (Texas Instrument, 2006), a CC2420 radio chip, a PCB antenna, and a flash memory is used for WBAN hardware platform in this work to play the role of the sending node and the gateway. The MSP430F1611 MCU with the current consumption of $330\mu A$ in active mode (at 1MHz) and only $1.1\mu A$ in standby mode is a good choice for ultra-low power applications. The CC2420 radio chip is compatible with the IEEE 802.15.4 standard for WBANs and is designed for low power and low voltage short-range wireless communication. It operates in the 2.4 GHz unlicensed ISM band and provides a programmable output power with 32 different levels of signal power and an effective data rate of 250 kbps.

3.2 Experimental Measurements on CC2420 Radio Chip Properties

In this section, the properties of CC2420 radio chip are examined.Then, the necessity of designing a power-adaptive communication protocol for WBANs is justified. For all experiments in this thesis, the described TelosB sensor motes are used. The measurements are summarised in Table 3.1. Since the CC2420 datasheet provides the transmission signal power and usage of current for only a few power levels, the values for other power levels are estimated through linear interpolation. To validate the accuracy of the calculated values for transmission signal power, the receiving power is measured by placing the receiver very close to the sending node with the distance

Power (Level)	Transmission range (m)	Signal power (μW)	Usage of current (mA)	PDR (1)	(2)	(3)	(4)	(5)	(6)
1	1.2	0.5	7.6	0%	0%	0%	63.6 %	84.3%	94.54%
2	1.5	1.35	8.1	0%	7.1%	17.3 %	88.29 %	96.09%	98.08%
3	35	3.16	8.5	92%	96.8%	95%	99.5 %	99.3%	≈100%
4	40	6.61	8.85	96.3%	99.2%	97.4%	≈100 %	≈100%	≈100%
5	44	12.02	9.2	96.6%	99.4%	97.4%	≈100 %	≈100%	≈100%
6	50	20.42	9.55	96.7%	99.4%	97.4%	≈100 %	≈100%	≈100%
7	> 50	31.62	9.9	99.15%	99.4%	98.7%	≈100 %	≈100%	≈100%
⋮	⋮	⋮	⋮	⋮	⋮	⋮	⋮	⋮	≈100%
15	> 75	199.5	12.5	≈100%	≈100%	≈100%	≈100 %	≈100%	≈100%
⋮	⋮	⋮	⋮	⋮	⋮	⋮	⋮	⋮	≈100%
32	> 100	1000	17.4	≈100%	≈100%	≈100%	≈100 %	≈100%	≈100%

Table 3.1: Transmission range, signal power, current, and PDR under different power levels and postures

between their antennas less than a couple of millimetres. In such a way the path loss effect is almost negligible. For each power level, the receiving signal strength for 1000 transmissions is measured and averaged. It is observed that the calculated values using interpolation match with the experimentally measured signal strength with a maximum difference of $1.1\mu W$. To validate the accuracy of the calculated values for usage of current, the current of the radio chip is measured using a digital oscilloscope connected to the ferrite bead in series between the switcher and the radio Voltage Drain Drain (VDD). Although the measurements obtained through such an approach are not very accurate, the changes in usage of current for different power can be well characterised. It is observed that the variation trend of the measured values is consistent with that of the interpolated values.

Some other experiments are also carried out to measure the maximum transmission range at each power level, considering the maximum transmission range of a power level is the maximum range within which the SINR is high enough to ensure at least 90% PDR. In these experiments (which is carried out in a free-space grassfield), a transmitter and a receiver are placed on the top of two wooden poles with the height of 1.7 m, by which the transmission distance can be increased step by step. At each distance, the transmitter sent 1000 packets with each power level. Table 3.1 shows the measured maximum transmission range for several power levels. It is worth noting that only the two lowest levels have the maximum transmission range within 3 metres (the maximum range suggested by the IEEE 802.15 working group (Yazdandoost and Sayrafian-Pour, 2009)), where the others significantly exceed this limit.

Despite the fact that low-power communications may consume less energy and produce less interference to other surrounding devices, it might not always be feasible

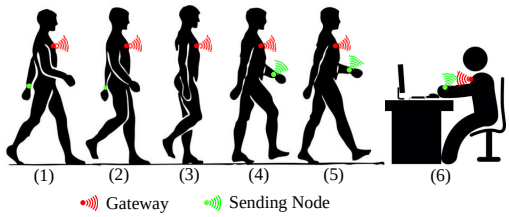

Figure 3.3: Postures (1)-(5): the LoS path is interrupted by body parts during walking. Posture (6): the LoS path is available and stable during sitting.

to use low-power communication due to the low channel quality. To investigate the communication reliability under different transmission power levels, another set of experiments is carried out, in which a subject was asked to stay in five common postures of walking plus a posture of sitting at the desk as depicted in Figure 3.3. For each posture, the sending node attached to the wrist transmits 1000 packets to the gateway, with a 30 ms interval between two consecutive transmissions. Table 3.1 shows the PDR of different transmission power levels for each posture. There are the following **two key observations**: (1) *power levels 1 and 2 are suitable for communication in postures (4), (5), and (6) where a LoS path with short distance is available.* For example, the PDRs achieved by power level 1 and power level 2 in posture (6) are 94.54% and 98.08%, respectively. In many postures such as studying, eating, and driving, the sensor attached to the wrist has a LoS path to the gateway with very short distances. Communicating using power levels 1 and 2 can consume less energy and produce less interference (transmission ranges are smaller than 2 metres), but still provide very good communication reliability. (2) *power level 3 already achieves excellent communication reliability for most postures, and level 7 ensures above 99% communication reliability almost in all postures.* Hence, in the given setup, it is not necessary to use power levels even higher than level 7 as it would just result in wasting of energy and increasing potential interference range. In comparison with power levels 1 and 2, power levels 3 and 7 consume more energy and have a much larger transmission range. Therefore, they should be used as little as possible.

The above discussion based on the experimental measurements justifies the feasibility to achieve reliable communication with low energy consumption and interference by using only a small number of transmission power levels. For example, in the configuration with only power levels 1, 3, and 7, a sending node uses power level 1 when there is a LoS short-distance path, switches to power level 3 when the LoS communication is partially blocked, and uses power level 7 for the case where LoS communication

is completely blocked, and ultra-reliable communication is required to deliver a vital measurement. In static postures such as sleeping, sitting, standing, and lying down, where the location of the sending node is not changing for minutes or even hours, the power-adaptive scheme should quickly adjust its transmission power level to the optimal level for communication to save energy and reduce interference. For dynamic postures such as walking and running, the channel quality generally exhibits a cyclic pattern, i.e., alternates between availability and unavailability of LoS path. Hence, there is still a remarkable potential gain for opportunistic low-power communication when the LoS path is available.

3.3 Transmission Cost Function

Since the goal of the thesis is proposing a power-adaptive communication protocol that selects the best transmission power to reduce energy consumption and interference, without sacrificing the communication reliability, a unified cost function that reflects all performance metrics is needed so that each sending node can choose the optimal transmission power to minimise this cost function. In this section, a new energy-, interference-, and reliability-aware cost function is presented, that will be used throughout the thesis.

To give the insights on the best power level for packet transmission, the effect of transmission power on interference and energy consumption is first explained. The scenario presented in Figure 3.4 is used to describe how intra-WBAN communications can produce interference to other WBANs or devices operating at the same frequency. In this example, it is assumed that the transmissions from S_3 can produce interference

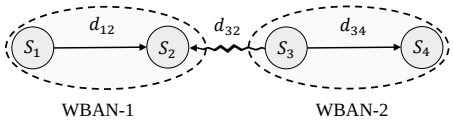

Figure 3.4: Coexisting WBANs where S_3's transmission can interfere packet reception at S_2

to packet reception at S_2. Let $P_{rx}^{j}(d_{ij})$ be the signal power perceived at a receiver S_j for the signal from S_i over a distance of d_{ij}. According to (Yazdandoost, 2007), the SINR perceived by S_2 for the signal received from S_1, denoted by $SINR_2$, can be estimated:

$$SINR_2 = \frac{P_{rx}^{2}(d_{12})}{N + P_{rx}^{2}(d_{32})}, \tag{3.1}$$

where N is background noise. It can be seen that $SINR_2$ is inversely proportional to the received interfering signal $P^2_{rx}(d_{32})$. Since the antenna is omnidirectional, the power of a transmitted signal drops as a function of distance (Stutzman and Thiele, 2012). The perceived signal power $P^2_{rx}(d_{32})$ can be modelled as:

$$P^2_{rx}(d_{32}) = \frac{P^3_{tx}}{d^{\gamma}_{32}} \tag{3.2}$$

where P^3_{tx} is the signal power emitted at the transmitter S_3, γ is the path loss exponent, and d_{32} is the distance from S_3 to S_2. Since the propagation environment, the distance, the antenna characteristics, and the frequency band are all the same for different transmission power levels, the perceived signal at the receiver is linearly proportional to the signal power emitted at the transmitter, that is, $P^2_{rx}(d_{32}) \propto P^3_{tx}$. From both Eqn. (3.1) and Eqn. (3.2), it is easy to see that the interference produced by a packet transmission to any nearby receiving device is proportional to the transmission power.

The energy consumption for sending L bits using power level i can be modelled as (Quwaider *et al.*, 2010):

$$E^i_{tx} = V.\frac{L}{B}e^i_{tx}, \tag{3.3}$$

where B is bandwidth, e^i_{tx} is the usage of current of the radio circuit for transmission with power level i, and V is the supply voltage. It can be seen that the energy consumption for transmitting a single packet is linearly proportional to its usage of current ($E^i_{tx} \propto e^i_{tx}$) as B, L, and V are constant for a given transmission power. Since the usage of current of the radio circuit is also proportional to the transmission power, that is, $e^i_{tx} \propto P^i_{tx}$ (Texas Instruments, 2007), it can be concluded that the energy consumption for transmission is also proportional to the transmission signal power ($E^i_{tx} \propto P^i_{tx}$).

Let P^i_{tx} be the transmission power of power level i, and r_i be the communication reliability achieved using power level i. r_i is defined as the probability that a packet is successfully delivered to the gateway with power level i. Motivated by the above discussion, the following cost function is proposed that reflects energy consumption, interference, and communication reliability:

$$cost_i = \frac{P^i_{tx}}{r_i}, \tag{3.4}$$

The feasibility of this cost function can be explained as follows: for a single transmission, a smaller P^i_{tx} can consume less energy and produce less potential interference according to the above analysis. However, a smaller P^i_{tx} may have lower communication

reliability r_i, leading to even more energy consumption and interference for successful packet delivery due to retransmissions. On the other hand, a larger P_{tx}^i will increase the energy consumption and interference for a single transmission, but might still be the best as the channel reliability with a high transmission power can be high as well. Accordingly, the next three chapters present novel solutions to enable the sending node to select the power level with the smallest cost as the best transmission power level aiming to reduce the energy consumption and interference range while guaranteeing the communication reliability.

Chapter 4

ATPS: Adaptive Transmission Power Selection for Communication in Wireless Body Area Networks

4.1 Introduction

As discussed before, a desirable communication protocol for WBANs should be able to adaptively choose a proper signal power at each transmission to achieve an acceptable communication reliability with low channel interference and energy consumption. The relatively large channel coherence time in WBANs (which is up to 70 ms (Smith *et al.*, 2009)) has brought the channel estimation for power-adaptive communication into focus. However, the existing methods described in Chapter 2 are highly memory inefficient (Zhang *et al.*, 2012), inaccurate (Quwaider *et al.*, 2010), or support only some special postures (Kindt *et al.*, 2015). Considering channel quality (i.e., channel gain) over time as a random process (Zhang *et al.*, 2012), the idea of channel estimation is to predict the behaviour of this process by knowing its previous values and the coherence between them. In channel prediction for power-adaptive communication, the sending node adjusts its transmission power level according to the expected channel quality. Motivated by the temporal correlation in on-body channels, a new Markov chain based channel estimation model is proposed to predict the quality of the channel through monitoring the communication history of the links. Then, using the information provided by the channel estimator, a power-adaptive communication protocol for WBANs is proposed, in which each sending node can self-learn its channel behaviour and dynamically adjust its transmission power to achieve high communication reliability,

low energy consumption, and low interference. In comparison with the existing schemes, the major contributions of this work are summarised as follows:

- A general framework for analysing channel behaviour is proposed, through which it is demonstrated that: (1) the GE Markov chain model is not accurate enough to capture the channel behaviour; (2) the Extended GE (EGE) Markov chain model can achieve high prediction accuracy at the cost of high memory complexity, thus not suitable for WBANs.

- A new channel prediction model called the Improved GE Markov chain model (IGE) is designed by sustaining the advantage of the EGE model in terms of prediction accuracy but also overcomes its drawback on memory complexity.

- A power-adaptive communication protocol named Adaptive Transmission Power Selection (ATPS) protocol is designed to use channel prediction models and enable the sending node to adjust its transmission power level at a per-transmission level.

- A channel-aware deadline-constrained policy for scheduling packet transmissions is proposed to improve ATPS. Based on the designed IGE model, each sending node locally makes optimal decisions on packet transmissions to minimise the transmission cost, i.e., to transmit immediately or to postpone the transmission and wait for the best channel quality.

- The performance of the proposed channel model and communication protocol is evaluated through experiments on the TelosB sensor motes under different packet rates and body postures. The results reveal a significant reduction in energy consumption and interference range.

The rest of this chapter is organised as follows: Section 4.2 presents the background. Section 4.3 presents the analysis on channel behaviour, discusses the channel behaviour using well-known Markov chain models, and introduces the proposed channel model. The power-adaptive communication protocol is presented in Section 4.4. Section 4.5 discusses the optimal deadline-constrained scheduling policy and Section 4.6 evaluates the proposed channel model and the communication protocol. Section 4.7 concludes this chapter.

4.2 Background

A practical channel estimator for WBANs should meet the requirements below (Smith *et al.*, 2009):

- It should have memory to track the behaviour of the random process (i.e., channel quality) and analyse its statistical behaviour to estimate the next value of the variable.
- It should be able to quickly adapt its estimations with the sharp channel fluctuations.
- It should be lightweight so that the resource-constrained sending nodes can perform it and estimate the channel in a real-time manner.

Lightweight linear estimators such as linear least square have been widely used to estimate the channel quality in wireless networks (Tong and Zhao, 1999; Song *et al.*, 2002; Lin, 2008). However, in WBANs, they cannot predict the rapid channel dynamics as they essentially behave like a filter which generates a delayed version of the channel waveform (Smith *et al.*, 2011).

To compensate the drawbacks of the linear channel estimators while keeping their advantages (e.g., low complexity overhead), a linear prediction-based power-adaptive communication protocol for WBAN is proposed (Smith *et al.*, 2011) which combines the ability of finite state Markov chain models in describing the behaviour of a complex system with the simplicity of linear estimators. This method benefits from reciprocity of WBAN wireless channels (Hanlen *et al.*, 2010) and assumes the on-body channels are relatively stable for a short period and the channel prediction is valid up to 1 second. In this protocol, the sending node estimates the channel according to the measured RSSI of the last received packet from the gateway and selects the lowest transmission signal power that is higher than the measured RSSI for all communications until the next packet is received from the gateway. If the selected transmission signal power is lower than the minimum received power sensitivity of the radio of the gateway, the sending node selects the maximum transmission signal power and communicates with the gateway. In this method it is assumed that the sending node can increase the transmission signal power from -30 dBm to 0 dBm in 0.5 dBm steps which is supported neither by CC2420 nor other off the shelf radio chips. Moreover, it does not propose any solution for a long-term channel prediction.

Similarly, a lightweight linear channel prediction algorithm is presented in (Zhang *et al.*, 2012) to enable the sending node to track the channel quality variation, however, its accuracy in dynamic postures or generally in situations with a noisy channel RSSI is unacceptable. Therefore, the linear channel prediction algorithm is combined with Finite State Markov Chain (FSMC) model so that the sending node can monitor the channel history and extract the channel properties (i.e., the statistics of the channel behaviour). In this model, the states in Markov chain represent the channel RSSI sub-ranges and the transition probabilities between different states is maintained using a large-size Transition Matrix (TM). Although this method has a very low computational complexity, its memory complexity is extremely large in the order of $O(M^{L+1})$, where M is the number of RSSI sub-ranges and L is the length of history of the latest channel observations. Moreover, this model only predicts the next channel state and does not give a long-run channel estimation. Therefore, the sending node cannot save more energy and reduce interference range by scheduling the packets for late transmissions in delay-tolerant applications.

Beside the existing models, GE (Gilbert, 1960; Elliott, 1963) and EGE (Sanneck and Carle, 1999) model have been extensively used to predict the behaviour of computer networks with a special focus on burst error patterns modelling of communication links. For example, in (Liu, Yan, and Chen, 2017) a centralised communication protocol is proposed which benefits from the GE model to provide a reliable and energy efficient TDMA-based MAC protocol. In this method, the gateway monitors the behaviour of the links to the sending nodes to estimate the channel fluctuations and adjust the transmission order of the sending nodes to minimise the energy consumption of the network subject to the network communication reliability and throughput constraints. This method assumes some channel parameters such as the transition probability between different channel states is constant as long as the body posture has not been changed. Moreover, it assumes the body posture is known by the gateway.

In contrast, the proposed channel prediction model is self-organised and neither needs information about the current body posture nor the location of the sending node. It can self-learn the channel quality in both static and dynamic postures even when the motion patterns (and consequently the channel properties) of the subject are changed during a single posture (e.g., when the subject who was walking, starts walking faster/slower). The proposed model is highly memory efficient and extremely lightweight, so, it can be used by the sending node for power-adaptive communication without imposing a problematic overhead.

4.3 Channel Characterising and Modelling

Assume that time is slotted and one channel sample is generated in each time slot. The channel samples are considered as a discrete-time time series $X = \{x_t\}_{t=1}^{n}$ where n is the number of samples and the lower index t is the slot number. Each sample has a value in $\Omega = \{1, 2, 3, \dots\}$ representing the channel state or the channel quality level. The samples are grouped in the form of *i-run-lengths* $\{i_r^c\}_{r=1}^{n}$, where i_r^c represents the r^{th} *run-length* with length of c ($c \in \{1, 2, 3, \dots, n\}$) consecutive samples in state i. For example, the sample set $\{11113311331133777\dots\}$ can be represented by a set of run-lengths:

$$\{1_1^4, 3_1^2, 1_1^2, 3_2^2, 1_2^2, 3_3^2, 7_1^3, \dots\}$$

This classification of channel samples helps show the high-level view of channel behaviour (i.e., channel state transition). To analyse the long-term channel state transition more accurately, the following metric is proposed:

- $P_{ij}^c(t)$: assuming the channel moves to state i at slot t, $P_{ij}^c(t)$ is defined as the probability of observing $c-1$ consecutive channel samples in the current state i after t and observing the c^{th} sample in the state j at time $t+c$, that is,

$$P_{ij}^c(t) = P\big(x_{t+1} = x_{t+2} = \dots = x_{t+c-1} = i, \wedge x_{t+c} = j \mid x_t = i, \wedge x_{t-1} \neq i\big) \quad (4.1)$$

where $i, j \in \Omega$ and c stands for *consecutive*. Experiments are carried out to collect channel samples in both static postures including standing, sitting, and driving, and dynamic postures including walking and running. In these experiments, the same setup as presented in Chapter 3 is adapted with the sending node attached to the wrist and the gateway mounted on the chest. The sending node transmits packets at the rate of 20 pkt/s to the gateway using power level 1. For the sake of simplicity, only two channel states G and B are considered (i.e., $\Omega = \{G, B\}$), which represents good and bad channel quality, respectively. In these experiments, the sending node transmits packets to the gateway at the rate of 20 pkt/s. If the transmitted packet x_t is received by the gateway, the channel is considered in good state in slot t; otherwise, the channel is recorded in bad state. Once all samples are collected, $P_{ij}^c(t)$ ($i, j \in \{G, B\}$) is calculated using Eqn. (4.1). For scenarios with static body postures such as standing and sitting, it is observed that the channel quality remains stable. $P_{GG}^c(t)$ is close to 1 when LoS communication is available, and $P_{BB}^c(t)$ is close to 1 when LoS communication is blocked by the human body. However, the channel quality during dynamic postures is quite unstable. Figure 4.1 shows $P_{ij}^c(t)$ during walking and running. As it can be seen, $P_{ij}^c(t)$

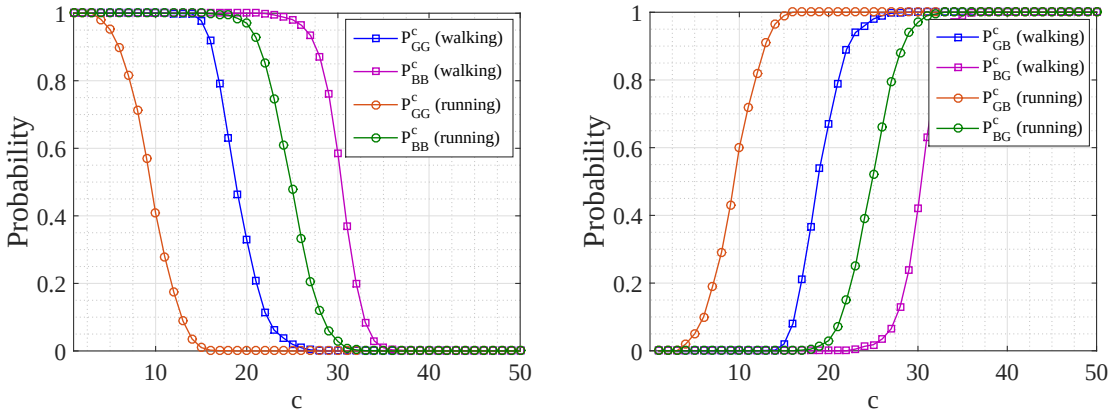

(a) (b)

Figure 4.1: (a) P^c_{ij} for $j = i$ and (b) P^c_{ij} for $j \neq i$ during walking and running.

for the case $j \neq i$ (Figure 4.1b) has the reverse trend to that $P^c_{ij}(t)$ with $j = i$ (Figure 4.1a), however, this is the case only for Markov models with two states. $P^c_{ij}(t)$ looks like *S-shaped* logistic functions, which indicates the existence of spatio-temporal locality among channel samples (that is called channel burstiness). That is, if the channel moves to state i, the probability the channel moves to other state j is low at the beginning but will gradually increase. This metric also shows the length of burst errors in the channel and thus is very useful to characterise channel behaviour. If each sending node has the knowledge of $P^c_{ij}(t)$, it can predict the long-term channel state transitions and adjust transmission power to save energy and reduce interference. Since this knowledge is not available (because calculating $P^c_{ij}(t)$ requires all channel samples which are not available before transmissions), two well-known channel models have been investigated in terms of accuracy of estimating $P^c_{ij}(t)$. Then, a new model for accurately estimating $P^c_{ij}(t)$ is presented.

4.3.1 Gilbert-Elliott (GE) Model

The GE model has been widely used for modelling burst error patterns of communication links. As illustrated in Figure 4.2a, it is a simple Markov chain with two states G (for good) and B (for bad). According to this model, the link transits between two states with probability P_{GB} from G to B and P_{BG} from B to G, and remains in G state with probability P_{GG} and in B state with probability P_{BB}. These probabilities are commonly represented using a matrix called the Transition Matrix (TM). Based

on the collected channel samples, the TMs for walking and running are calculated, as shown in Figure 4.2a. It can be seen that for both walking and running, P_{BB} and P_{GG} are close to 1, indicating the existence of high-degree channel burstiness. To estimate $P_{ij}^{c}(t)$ using GE model, the equation below is used:

$$P_{ij}^{c} = \underbrace{P_{ii} \times P_{ii} \times P_{ii} \times \ldots P_{ii}}_{\text{c-1 times}} \times P_{ij} \tag{4.2}$$

where P_{ii} is obtained from TM. Figure 4.2b shows $P_{ij}^{c}(t)$ for walking and running for the case $j = i$ (i.e., $P_{ii}^{c}(t)$). $P_{ij}^{c}(t)$ for $j \neq i$ has not been shown as it has the reverse trend to that $P_{ii}^{c}(t)$, as demonstrated in Figure 4.1b. By comparing with Figure 4.1a, it can be seen that although the GE model can predict the channel state for the first next channel samples, there is a big difference between the P_{ii}^{c} predicted by the GE model and that calculated based on the real channel measurements. The key reason is that the length of the burst-length does not match an exponential distribution. In other words, in the GE model, the state of the channel at the next time slot depends only on the state at the current slot and the transit probabilities, and not on the channel history. For example, the transition matrix of the following two sample block 'GGBBBBGGGGGGBBBB' and 'GGGGBBGGGGBBBBBB' are the same, but the channel bursty behaviours (i.e., the run-lengths) are different. Due to this memoryless property, the estimated $P_{ij}^{c}(t)$ by GE model does not match with the one presented in Figure 4.1a. Since a closer match between the estimated and the calculated $P_{ij}^{c}(t)$ enables the sending node to more accurately predict the long-term channel state transition, the GE model is not a good choice.

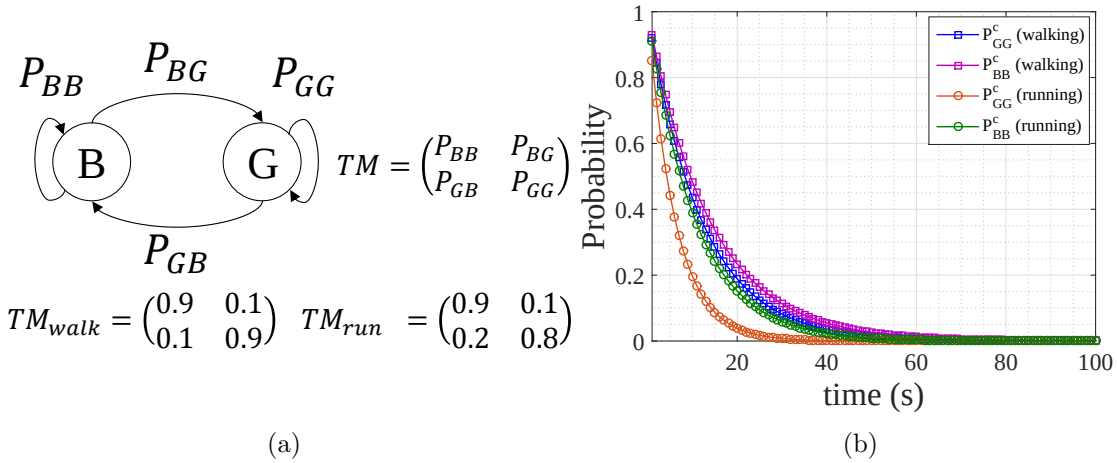

(a) (b)

Figure 4.2: GE model (a) state diagram and transition matrices during walking and running (b) estimated P_{GG}^{c} and P_{BB}^{c} by GE model.

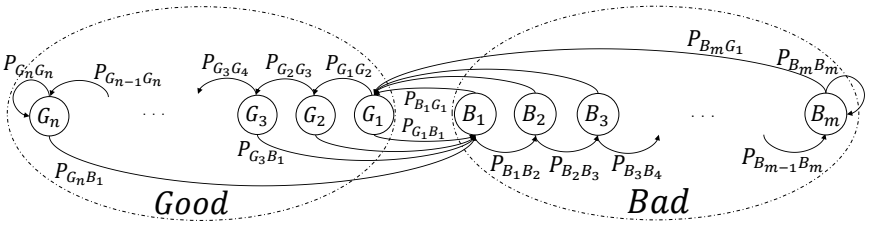

Figure 4.3: Extended GE model.

4.3.2 Extended Gilbert-Elliott (EGE) Model

The Extended GE model (EGE) was proposed in (Sanneck and Carle, 1999) to remember the channel history. As illustrated in Figure 4.3, in a simplified model, the EGE has two general states: GOOD and BAD, and each general state also has some internal sub-states. Therefore, EGE has two types of transitions: intra-transition and inter-transition. An intra-transition at time t occurs if $x_{t-1} = x_t$ otherwise an inter-transition happens. For example, if the channel transits to GOOD state from BAD state, it transits to the first sub-state in GOOD state. If the next channel sample is good, an intra-transition occurs and the channel transits to the second sub-state in GOOD state. After observing n consecutive good samples, if a bad channel sample is observed, the channel transits from the n$^{\text{th}}$ sub-state in GOOD state to the first sub-state in BAD state. In other words, assuming each state i has m internal sub-states, the sub-state i_r represents the r^{th} successive samples in state i. Hence, EGE is able to represent different run-lengths given a sufficient number of internal sub-states. Since the channel fluctuation in the periodic dynamic postures (e.g., in the walking) is like a periodic random process, the sufficient number of sub-states in EGE depends on the fluctuation period (in terms of number of samples). In other words, if the number of sub-states in EGE model is equal or higher than the number of samples in the fluctuation period, EGE can model the behaviour of the periodic random process. A gait cycle (fluctuation period) usually takes about 1 second because the average number of steps in the walking is about 116 steps per minute (Blessey, Hislop, Waters, and Antonelli, 1976). Thus, at the sampling rate of 20 samples per second, EGE requires at least 20 sub-states.

To show the effect of the number of sub-states on the performance of EGE, the channel behaviour in walking and running has been modelled by EGE under two different number of sub-states: (a) 10 sub-states that is fewer than the minimum number of required sub-states; (b) 50 sub-states which is high enough to guarantee the number of sub-states is sufficient. Figure 4.4 shows the P^c_{GG} and P^c_{BB} estimated by EGE with 10 and 50 internal states. To estimate $P^c_{ij}(t)$ using EGE model, the equation below is used:

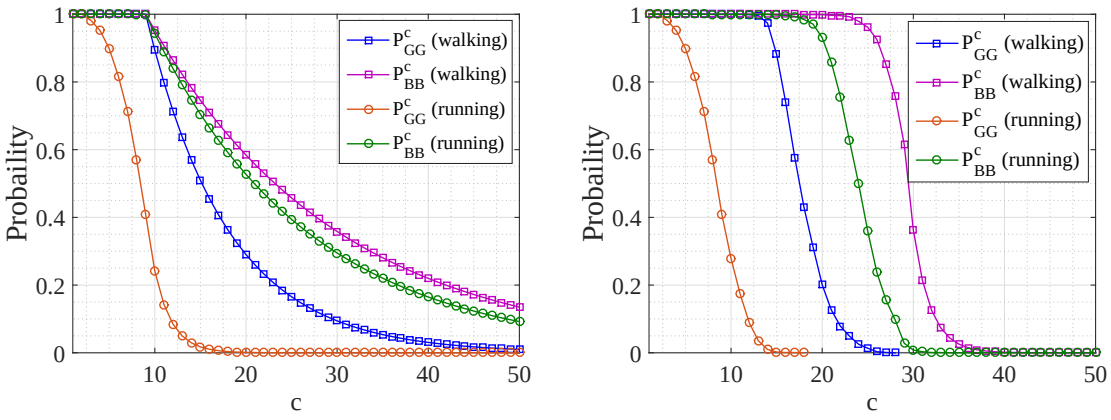

(a) (b)

Figure 4.4: P^c_{GG} and P^c_{BB} estimated by EGE: (a) $m = 10$ and (b) $m = 50$.

$$P^c_{ij} = P_{i_1 i_2} \times P_{i_2 i_3} \times P_{i_3 i_4} \times \ldots P_{i_{c-1} i_c} \times P_{i_c j_1} \tag{4.3}$$

As was expected, the accuracy of EGE is highly dependent on the number of internal sub-states. The more internal states, the higher the estimation accuracy. Its major drawback is the high memory complexity, $O(|\Omega|^2 m^2)$, where $|\Omega|$ is the number of general states, and m is the number of sub-states per general states.

4.3.3 Improved GE (IGE) Model

To sustain the advantage of the EGE model on prediction accuracy but overcome its drawback on complexity, a new channel model is proposed that takes into account the run-length distribution for better channel prediction. Figure 4.5 shows the distribution of the length of good and bad run-lengths for 5 minutes of walking and running. According to the three-sigma-rule of thumb (also called the 68–95–99.7 rule), if at least 65%, 95%, and 99.7% of the samples (run-lengths) lie in the first, second, and third standard deviations of the sample set, respectively, the distribution is normal with high certainty. By analysing the channel samples, it has been observed that the distribution of the length of the run-lengths follows the three-sigma-rule of thumb and thus, it has a normal distribution.

Based on this observation, the GE model is extended by associating the following three parameters with each state: $counter_i$, μ_i, and σ_i, where $counter_i$ represents the length of the current run-length in state i, which is similar to the internal states in EGE and is reset to zero after each inter-transition. For example, if the channel moves to

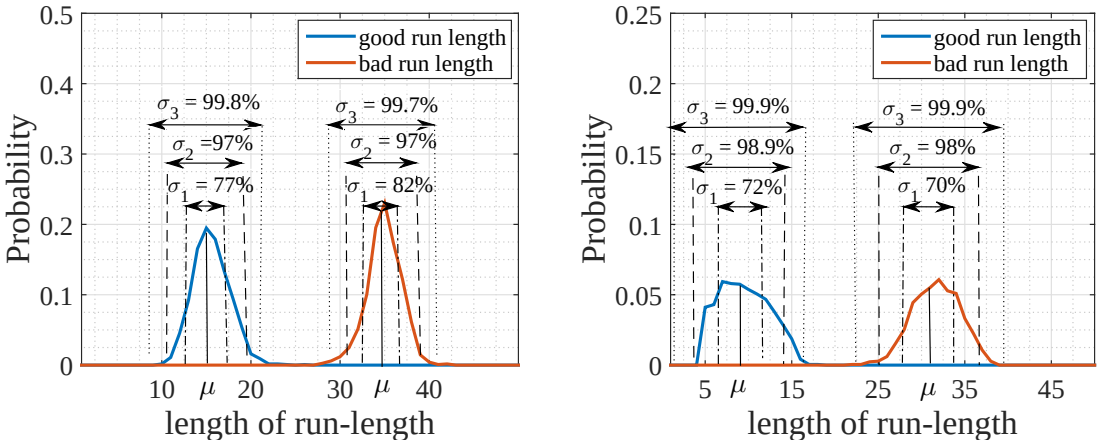

(a) (b)

Figure 4.5: Distribution of run-lengths: (a) walking, (b) running.

state i, from state j, $couter_j$ is reset to zero but $counter_i$ is set to 1. If the next channel state is i, $counter_i$ is increased by 1 (now it is 2). μ_i is the mean value of $counter_i$ that represents the mean length of run-lengths in state i, and σ_i is the standard deviation of run-lengths. μ_i and σ_i are updated as follows for each inter-transition:

$$\mu_i = \omega \times counter_i + (1 - \omega) \times \mu_i, \tag{4.4}$$

$$\sigma_i = \omega \times |counter_i - \mu_i| + (1 - \omega) \times \sigma_i, \tag{4.5}$$

where ω is the weighting factor. Please note since these variables are not included in the transition matrix, do not add memory to the process and thus, do not make the random process non-Markovian. Figure 4.6a gives an example IGE with 3 states (for 3 power levels). Compared to EGE, its memory complexity has been reduced to $O(|\Omega|^2 + 3 \times |\Omega|)$, which is on the same order of magnitude as the GE model ($O(|\Omega|^2)$). In the following, a function to estimate $P_{ij}^c(t)$ as accurate as the estimations made by the EGE is presented.

A Function to Model $P_{ij}^c(t)$ for the Case $j = i$ (i.e., $P_{ii}^c(t)$)

As previously shown, $P_{ii}^c(t)$ function has an *S-shaped* diagram. Figure 4.6b, illustrates the function is divided into three parts based on μ_i and σ_i. $P_{ii}^c(t)$ is approximately 1 in Part I and almost 0 in Part III. The transition occurs in Part II, in which $P_{ii}^c(t)$ is decreased exponentially before μ_i and logarithmically after μ_i. Based on these properties,

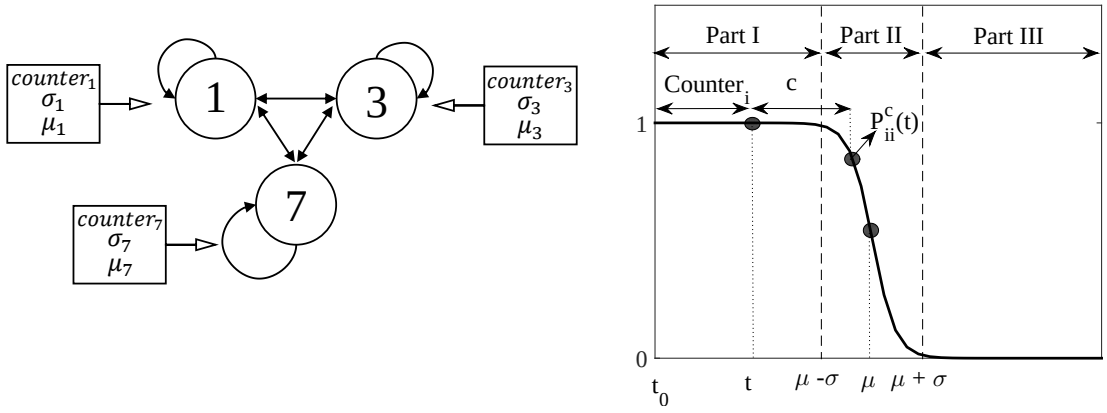

(a) (b)

Figure 4.6: IGE model (a) IGE diagram (b) P_{ii}^{c} variation trend.

the following function is designed to approximate $P_{ii}^{c}(t)$:

$$P_{ii}^{c}(t) = f(c + counter_i) = \frac{1}{1 + e^{\frac{(c+counter_i-\mu_i)}{\sigma_i}}}. \tag{4.6}$$

Suppose t_0 is the time that the channel transits to state i. As illustrated in Figure 4.6b, in the time period $[t_0, t]$, the channel has observed $counter_i$ consecutive samples in state i. Hence, $P_{ii}^{c}(t)$ should be mapped to $f(c + counter_i)$. To evaluate the accuracy of the proposed function, IGE is fed with the measured channel samples for walking and running, and compared to the $P_{ii}^{c}(t)$ estimated by IGE with that calculated using the real channel samples (i.e., Figure 4.1). It can be seen from Figure 4.7 that the proposed model has a very close estimation of $P_{ii}^{c}(t)$. That is, the proposed model can estimate the long-term channel transition accurately.

A Function to Model $P_{ij}^{c}(t)$ for the Case $j \neq i$

According to Eqn. (4.1), $P_{ij}^{c}(t)$ with $j \neq i$ can be rewritten based on the chain rule of conditional probability as below:

$$P_{ij}^{c}(t) = \underbrace{P_{ii}^{c-1}(t)}_{\text{A}} \times \underbrace{P(x_{t+c} = j | x_t = \cdots = x_{t+c-1} = i \wedge x_{t-1} \neq i)}_{\text{B}} \tag{4.7}$$

Eqn. (4.7) defines $P_{ij}^{c}(t)$ as the multiplication of two parts. Part A is the probability of observing state i within time t to $t + c - 1$ and part B is the transition probability from state i to state j at time $t + c$. Part A can be calculated using Eqn. (4.6) but a separate equation needs to be developed to estimate part B. Similar to P_{ij}^{c}, P_{ii}^{c} can be rewritten based on the chain rule of conditional probability as below:

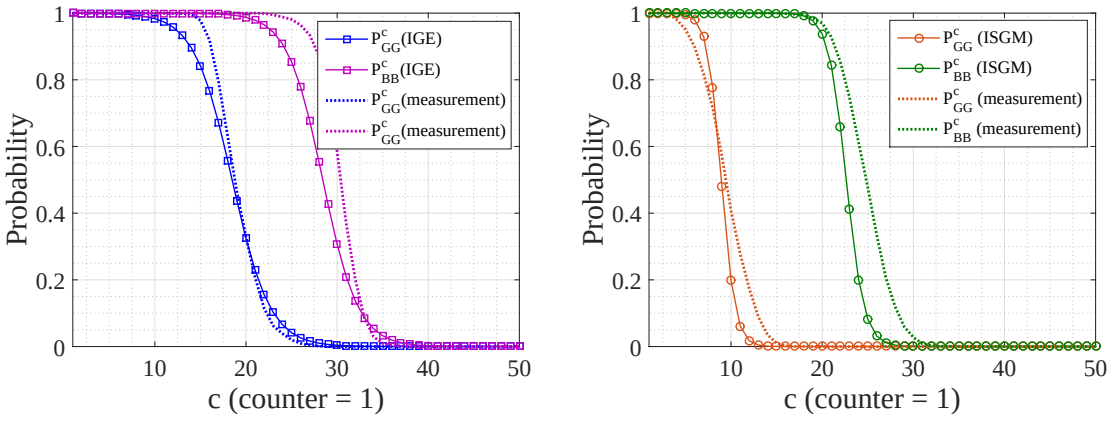

(a) (b)

Figure 4.7: Estimated P^c_{GG} and P^c_{BB} by IGE model compared with real measurements (a) walking (b) running.

$$P^c_{ii}(t) = P^{c-1}_{ii}(t) \times P(x_{t+c} = i | x_t = \cdots = x_{t+c-1} = i \wedge x_{t-1} \neq i) \tag{4.8}$$

Therefore, it can be concluded that:

$$P(x_{t+c} = i | x_t = \cdots = x_{t+c-1} = i \wedge x_{t-1} \neq i) = \frac{P^c_{ii}(t)}{P^{c-1}_{ii}(t)} \tag{4.9}$$

On the other side, the probability of transition to any new state j different from state i ($j \in \Omega$ and $j \neq i$) at time $t+c$ given that the state i has been observed since time t to $t+c-1$ can be calculated as below:

$$\sum_{\substack{j \in \Omega \\ j \neq i}} P(x_{t+c} = j | x_t = \cdots = x_{t+c-1} = i \wedge x_{t-1} \neq i) =$$

$$1 - P(x_{t+c} = i | x_t = \cdots = x_{t+c-1} = i \wedge x_{t-1} \neq i) = 1 - \frac{P^c_{ii}(t)}{P^{c-1}_{ii}(t)} \tag{4.10}$$

In other words, $\left(1 - \frac{P^c_{ii}(t)}{P^{c-1}_{ii}(t)}\right)$ represents the probability of leaving state i at time $t+c$ given that this state has been observed since time t to $t+c-1$. Therefore, the probability of transition to a *specific* new state j ($j \neq i$) can be approximated as follows:

$$P(x_{t+c} = j | x_t = \cdots = x_{t+c-1} = i \wedge x_{t-1} \neq i) = \left(1 - \frac{P^c_{ii}(t)}{P^{c-1}_{ii}(t)}\right) \times \frac{P_{ij}}{1 - P_{ii}} \tag{4.11}$$

where both $P^c_{ij}(t)$ and $P^c_{ii}(t)$ are derived from the transition matrix and represent the transition probability from state i to the state j, and the probability of a self transition

at state i, respectively. Hence, $\frac{P_{ij}}{1-P_{ii}}$ represents the probability of transition to a specific state j given that the channel leaves state i. Considering Eqn. (4.11), Eqn. (4.7) can be rewritten as below:

$$P_{ij}^{c}(t) = P_{ii}^{c-1}(t) \times \big(1 - \frac{P_{ii}^{c}(t)}{P_{ii}^{c-1}(t)}\big) \times \frac{P_{ij}}{1-P_{ii}} = \big(P_{ii}^{c-1} - P_{ii}^{c}\big) \times \frac{P_{ij}}{1-P_{ii}} \tag{4.12}$$

Please note, although long-term channel estimation using the transition matrix is not accurate, it is accurate enough when it comes to predicting only the next channel state.

4.4 Power-aware Communication Protocol

The proposed method is to dynamically control the transmission power at a per-transmission level based on channel prediction. The challenges are how to estimate the channel and how to decide which power level is the best. The key idea is to explore channel symmetry and RSSI-based thresholding.

4.4.1 Validation on Channel Symmetry

A set of experiments is carried out to justify the symmetry of the wireless channels in WBANs. In this set of experiments, the gateway and the sending node exchanges packets periodically. The sending node measures the RSSI for each packet transmitted by the gateway and immediately replies to the gateway by including the measured RSSI in its packet. On the other side, the gateway measures the RSSI for each packet transmitted by the sending node. Hence, the gateway can get the RSSIs for the link in both directions. The experiment was repeated for five different daily postures including sitting, driving, standing, walking, and running, with each one lasting for five minutes.

Figure 4.8a shows the probability distribution of the difference between the measured RSSIs at the sending node and the gateway for power level 7. It can be seen that the difference in RSSIs from and to the gateway has a normal distribution in all postures. The mean differences on RSSIs between measured samples are depicted in Figure 4.8b, as well as their standard deviation. Since the mean and the standard deviation of each distribution is close to 0, it can be concluded that the channel under power level 7 is symmetric. The experiment is repeated for other power levels, and the same conclusion has been achieved.

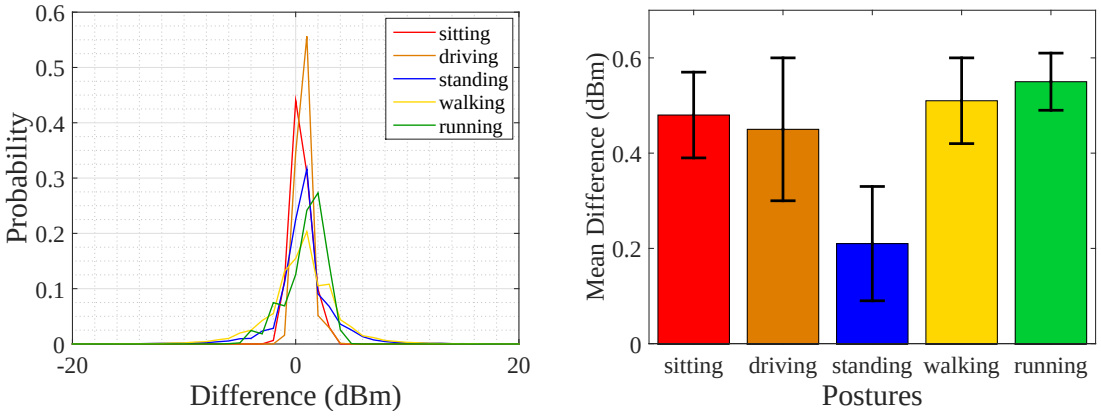

(a) (b)

Figure 4.8: (a) Probability distribution of difference of RSSI at sending node and gateway (b) Mean and standard deviation of differences.

4.4.2 Channel State Modelling

As previously discussed, power level 1, 3, and 7 of CC2420 radio chip are enough for short-range reliable communication in WBANs. Therefore, the channel quality can be partitioned into three states 1, 3, and 7 so that each state i ($i \in \{1, 3, 7\}$) represents a channel quality for which power level i is the best power level for communication. Since the channel quality variation in WBANs can be represented by channel RSSI (Quwaider *et al.*, 2010), each channel state i is defined as a sub-range of RSSI range in which power level i achieves the lowest transmission cost. Figure 4.9a shows the RSSI variation during running. As it can be seen, the RSSI range is partitioned into 3 sub-ranges, each of which represents a channel state. Someone may argue that since the RSSI is noisy, its irregular fluctuations may influence the channel state transition pattern. Due to the very limited RSSI fluctuation, a coarse grain classifying of RSSI range into a few channel states, limits the effects of noise. Figure 4.9b shows joint RSSI (which has been smoothed using a simple weighted averaging filter) and state transition of the same period during running.

To find the boundaries of the corresponding RSSI range per each channel state i, three rounds (called round-1, round-3, and round-7) of experiments in different postures have been carried out. Assuming time is slotted, in each slot of each round-i, the sending node transmits a packet using power level i. Afterward, the gateway sends back an ACK or NACK packet with power level 7 depending on the delivery status of the packet transmitted by the sending node. When the sending node receives the

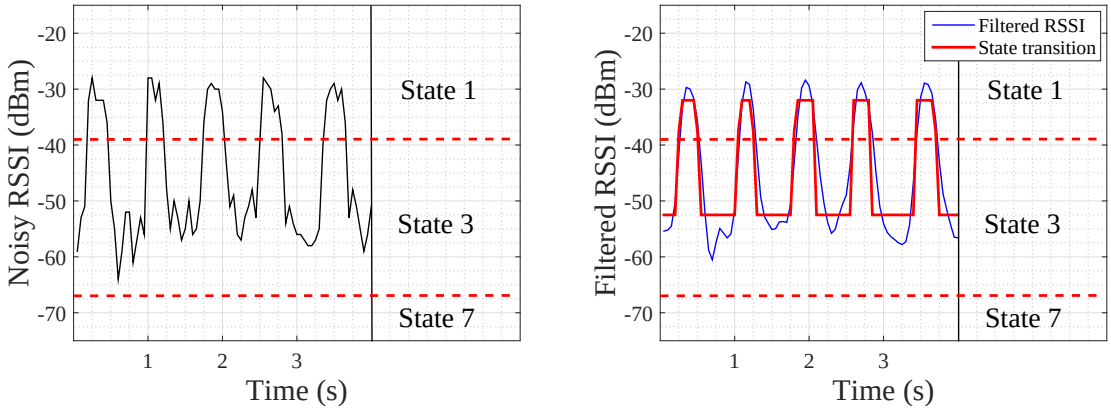

(a) Noisy RSSI

(b) Filtered RSSI

Figure 4.9: Partitioning RSSI range into a few channel states

ACK/NACK packet, its RSSI is measured. By counting the number of ACK packets, the reliability of communication with power level i per each level of RSSI can be calculated. Figure 4.10a shows the communication reliability of different power levels. As is expected, the communication reliability of all power levels is increased as the channel RSSI is increased. By knowing the communication reliability of each power level i at each level of channel RSSI, the transmission cost of all power levels is calculated according to Eqn. (3.4). Figure 4.10b shows how the transmission cost of different power levels is changed with the increase in channel RSSI (i.e., with the increase of communication reliability). By comparing the transmission cost of each power level, the RSSI boundaries for a state i are defined. The RSSI boundaries for a state i are a range of RSSIs within which the transmission cost using power level i is lower than that of other power levels. For example, as can be seen in the Figure 4.10b, the transmission cost of power level 3 in the RSSI range of -67 dBm to -39 dBm is lower than the transmission cost of other power levels. Figure 4.10c shows the state transition machine with RSSI boundaries (i.e., the optimal RSSI range). Each link is labelled with the channel state transition criteria. Hence, a transition from any state to the state i occurs if the measured RSSI falls in the RSSI boundaries of state i.

4.4.3 Adaptive Transmission Power Selection (ATPS)

Algorithm 1 shows the procedure of the proposed ATPS at each sending node. When a packet is generated, the sending node estimates the current channel state using the information provided by previously explained channel models (GE, EGE, or IGE). Since

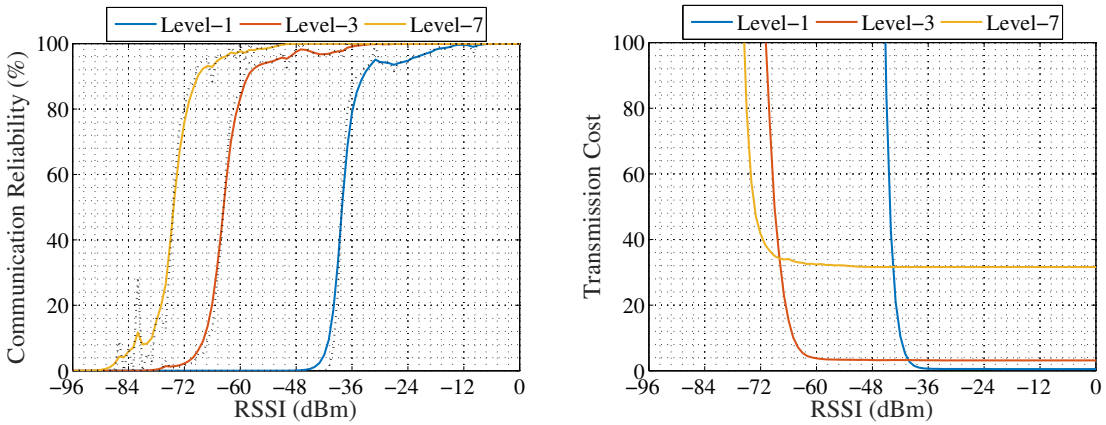

(a) (b)

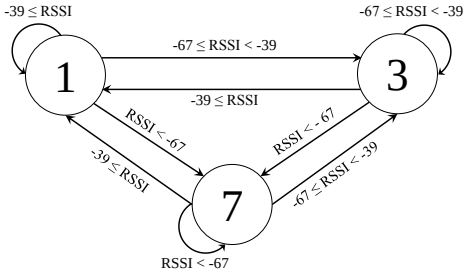

(c)

Figure 4.10: (a) Reliability of different power levels under different channel quality, (b) transmission cost of different power levels under different channel quality, and (c) state transition according to the RSSI range.

each state i ($i \in \{1, 3, 7\}$) represents a channel quality for which power level i is the best power level for communication, the sending node can select the corresponding power level based on the channel estimation (line 3). Once the channel state is estimated and the power level is selected, the packet is transmitted using the selected power level (line 6). Since the time difference between sending a packet and receiving its ACK packet is short, it is reasonable to assume that the channel does not change during a time slot. Hence, due to the channel symmetry, the sending node finds the real current channel state using the measured RSSI of the received ACK which is always transmitted by power level 7. Therefore, according to the Markov models described in Section 4.3, the transition probabilities are updated for future channel estimation.

In case the ACK packet is not received, the sending node finds the channel quality is lower than its estimation. Thus, it makes another estimation among the states related to the lower channel quality. If retransmission is enabled, the sending node repeats all steps mentioned above.

Please note that instead of relying on channel symmetry and measuring RSSI of the ACK packets from the gateway for detecting the channel state, the sending node can ask the gateway to measure the RSSI of its transmitted data packet and send it back to the sending node. Although this method is technically possible, it increases the complexity of detecting the real channel state. In other words, since the sending node uses different power levels, the channel quality cannot be estimated only by the measured RSSI of its transmitted data packet and the transmission power level needs to be considered as well. It means, unlike the proposed method, a separate set of RSSI boundaries for each single power level used by the sending node should be defined.

Algorithm 1: Proposed ATPS

Input : channel model properties at time t_0 ($I(t_0)$)

$p \leftarrow$ packet generated at t_0;
$retrans\_count \leftarrow 0$;
do
    $i \leftarrow channel(t_0)$;/* select power based on the estimated channel */
    $send(p, i)$;/* send packet p using power level i */
    if *ACK is received* **then**
        $rssi \leftarrow RSSI(ACK)$;
        find the real channel state based on the measured rssi;
        update channel model properties;
        break;
    end
    $retrans\_count = retrans\_count + 1$
    update channel model properties;
while $retrans\_count < retrans\_threshold$;

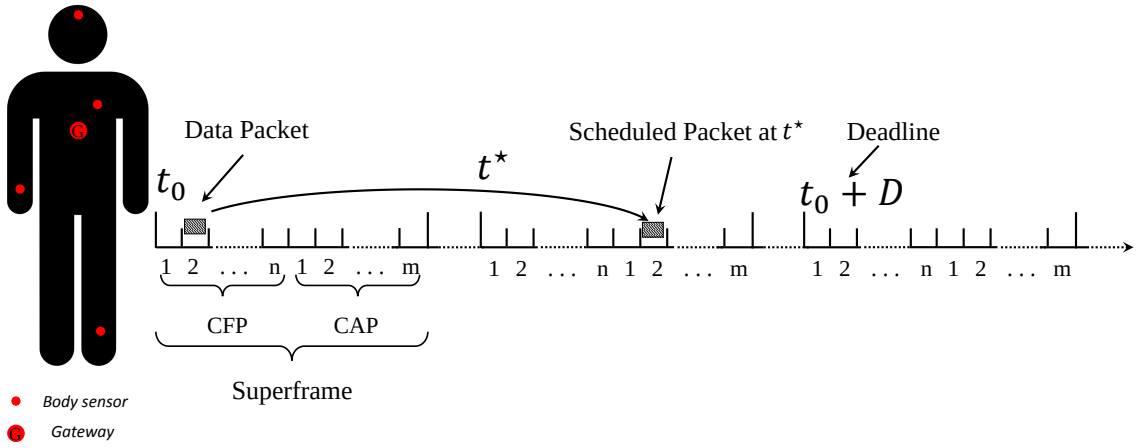

Figure 4.11: Packet scheduling in a TDMA-based MAC protocol (a) a WBAN with 4 sensors; (b) scheduling policy.

4.5 Channel-aware Deadline-Constrained Transmission Scheduling

Since the quality of channels in WBANs changes over time due to body movements, it just wastes energy to transmit packets when the channel quality is poor. In many applications of WBANs, the packet transmission can tolerate some delay. Hence, energy can be saved by postponing the packet transmission until the channel becomes good. Assuming bursty transmission is allowed (which means the sending node can transmit a couple of packets, all at once), this section presents a packet transmission scheduling policy to enable the proposed ATPS to balance energy consumption, interference range, and communication reliability.

Figure 4.11a shows a WBAN including four sending nodes and a gateway where the sending nodes communicate with the gateway directly in a one-hop star topology. As depicted in Figure 4.11b, the designed TDMA based MAC setup is adapted in which the time is divided into superframes. The superframe is started with a beacon packet transmitted by the gateway. Each superframe includes contention free period (CFP) and contention access period (CAP). The CFP includes n time slots (where n is the number of nodes) and each time slot is allocated to a specific sending node in WBAN through which, it avoids intra-WBAN collisions. The CAP consists of several time slots so that, sending nodes that have buffered packets compete with each other to access the channel using a slotted CSMA/CA algorithm. Each time slot is long enough to allow transmitting a 41-byte data packet and receiving its corresponding 13-byte

Algorithm 2: Scheduling enabled ATPS

Input : channel model properties at time t_0 ($I(t_0)$)

$p \leftarrow$ packet generated at t_0;
$retrans\_count \leftarrow 0$;
$t^\star = t_0 + 1$;
for $t = 1, \ldots, D$ **do**
    $C(t_0 + t, I(t_0)) = 0$;
    for $j = 1, \ldots, |\Omega|$ **do**
        $C(t_0 + t, I(t_0)) += P(t_0, i, t_0 + t, j, c) \times cost_j$;
    end
    if $C(t_0 + t, I(t_0)) < C(t^\star, I(t_0))$ **then**
        $t^\star = t_0 + t$;
    end
end
schedule p to be sent at $t^\star$;
$channel(t_0) \leftarrow$ estimated channel state at current time t_0;
if *packet is available to be sent at* t_0 **then**
    $p \leftarrow$ packet scheduled to be sent at t_0;
    do
        $i \leftarrow channel(t_0)$;`/* select power level */`
        $send(p, i)$;`/* send with power level` i `*/`
        if *ACK is received* **then**
            $R_i = \omega \times R_i + (1 - \omega)$;
            $rssi \leftarrow RSSI(ACK)$;
            $channel(t_0) \leftarrow$ real channel state at t_0 that is determined based on rssi;
            break;
        end
        $R_i = \omega \times R_i$;
        $retrans\_count = retrans\_count + 1$
        update model properties;
        $channel(t_0) \leftarrow$ estimated channel state at time t_0;
    while $retrans\_count < retrans\_threshold$;
end

ACK packet. Since the CC2420 radio chip allows the effective data rate of 250 kbps, the duration of each time slot is below 2 ms. Thus, at the packet rate of 20 pkt/s (where the time offset between two transmissions is 50 ms), the superframe can include up to 25 time slots, where n of which belongs to CFP and $25-n$ of which belongs to CAP. To learn the channel variation pattern, the sending nodes benefit from the discussed channel prediction models (GE, EGE, or IGE) so that, for each transmission, the RSSI of the ACK packet is analysed to discover the channel state at transmission time. Since the channel does not vary during a few tens of milliseconds (even when the user is running) and the transmission time is as small as a few milliseconds (because of the wide bandwidth provided by the CC2420 radio chip), it is assumed that the channel quality is stable during a time frame. Algorithm 2 shows the pseudo code of the proposed scheduling enabled ATPS. Consider a newly generated packet at time t_0 which should be transmitted within the next D time frames (Figure 4.11b). The idea of scheduling is to find a time frame $t^\star$ ($t_0 \leq t^\star \leq t_0 + D$) with the minimum transmission cost (line 3-12). To this end, the following function is defined to explore the average transmission cost at time $t_0 + t$ (where $0 < t \leq D$) according to the proposed cost function in Chapter 3:

$$C(t_0 + t, I(t_0)) = \sum_{j \in \Omega} P(t_0, i, t_0 + t, j, c) \times cost_j \tag{4.13}$$

where $cost_j$ represents the transmission cost using power level j and $I(t_0)$ is the information about the channel variation pattern at time t_0, including the mean and the variance of run-length of each state i (i.e., μ_i and σ_i). c represents the length of current run-length in current channel state i. $P(t_0, i, t_0 + t, j, c)$ shows the probability of being in state j at time $t_0 + t$, given that the channel state at time t_0 is i and c consecutive samples in this state has been observed. Please note that to calculate the transmission cost at each channel state j, the reliability of communication at this channel state is needed. R_j is defined as the average communication reliability at channel state j. In the beginning, since there is no idea about the communication reliability of different power levels, R_j is set to 1. Then, R_j is updated after each transmission in state j as below (line 21 and 26):

$$R_j = \omega \times R_j + (1 - \omega) \times ACK \tag{4.14}$$

where $0 \leq \omega \leq 1$ is the weighting factor and ACK is 1 if the packet is delivered and is 0 if the packet is lost. Once the transmission cost at each time frame is calculated,

the packet is scheduled to be sent at the best time frame ($t^\star$) which is the frame with the minimum expected transmission cost. The expected cost of transmission at $t^\star$ is defined as below:

$$C(t^\star, I(t_0)) = \min_{t=0}^{D} C(t_0 + t, I(t_0)) \tag{4.15}$$

To calculate Eqn. (4.13) at each frame t, $P(t_0, i, t_0 + t, j, c)$ needs to be calculated using the equation below:

$$P(t_0, i, t_0 + t, j, c) = \sum_{k \in \Omega} P(t_0, i, t_0 + 1, k, c) \times P(t_0 + 1, k, t_0 + t, j, c') \tag{4.16}$$

where $P(t_0, i, t_0 + 1, k, c)$ is equal to P_{ik}^c and is calculated using Eqn. (4.6) or (4.12). c' is the length of run-length in the channel state at the next frame. Therefore, it is 1 if the next channel state is a new state ($i \neq k$); otherwise, it is $c + 1$. As soon as $t^\star$ is calculated, the packet is buffered until its scheduled release time.

In each time frame, the sending node checks the buffer for any scheduled packet to be sent (line 15). If there is a packet, the sending node transmits the packet and listens to the channel for the ACK packet. If the ACK packet is received, its RSSI is measured, the reliability of communication using the selected power level is updated, and the real channel state is determined (line 20-25). Otherwise, if the packet(s) is lost, the sending node finds it has overestimated the channel quality and thus, it updates the current channel state into a new higher level. In other words, the sending node assumes the channel quality is lower than its estimation and a higher power level is needed. In case there is no packet to be sent (as the packet(s) might be scheduled to be transmitted later), the sending node evaluates its internal channel model to make predictions. Therefore, it updates the channel states according to its estimation as there is no way (no ACK packet) to find about the real channel state.

As can be seen from Eqn. (4.16), $P(t_0, i, t_0 + t, j, c)$ is calculated on a recursive basis. At the first step, $P(t_0, i, t_0 + t, j, c)$ is decomposed into $|\Omega|$ pairs of components. The first component of each pair of the components is directly calculated by Eqn. (4.6) or (4.12), depending on the value of j. In the second step, each component of the $|\Omega|$ remaining components from the first step is decomposed into new $|\Omega|$ pairs of components and thus, there are $2 \times |\Omega|^2$ components in total, $|\Omega|^2$ of them are calculated directly using Eqn. (4.6) or (4.12). Similarly, in the third step, there will be $2 \times |\Omega|^3$ components in which, half of them are directly calculated but $|\Omega|^3$ of them are decomposed into $2 \times |\Omega|^4$ new components. Therefore, in each step t' (where $0 < t' < t$) there are $2 \times |\Omega|^{t'}$

new components, half of which are calculated directly using the Eqn. (4.6) or (4.12) and the other half are decomposed into $2 \times |\Omega|^{t'+1}$ new components to be calculated in the next step. This is continued until $t' = t - 1$ where all components can be directly calculated using Eqn. (4.6) or (4.12). From this step, the recursion is started and each component at step $t' - 1$ can be calculated using the components at step t'. Calculating $P(t_0, i, t_0 + t, j, c)$ on a recursive basis requires $t - 1$ steps. At each step t', $|\Omega|^{t'}$ new components are generated. The total number of components to be calculated is:

$$|\Omega| + |\Omega|^2 + |\Omega|^3 + \cdots + |\Omega|^{t-2} + |\Omega|^{t-1} = \frac{|\Omega|^t - 1}{|\Omega| - 1} - 1 \tag{4.17}$$

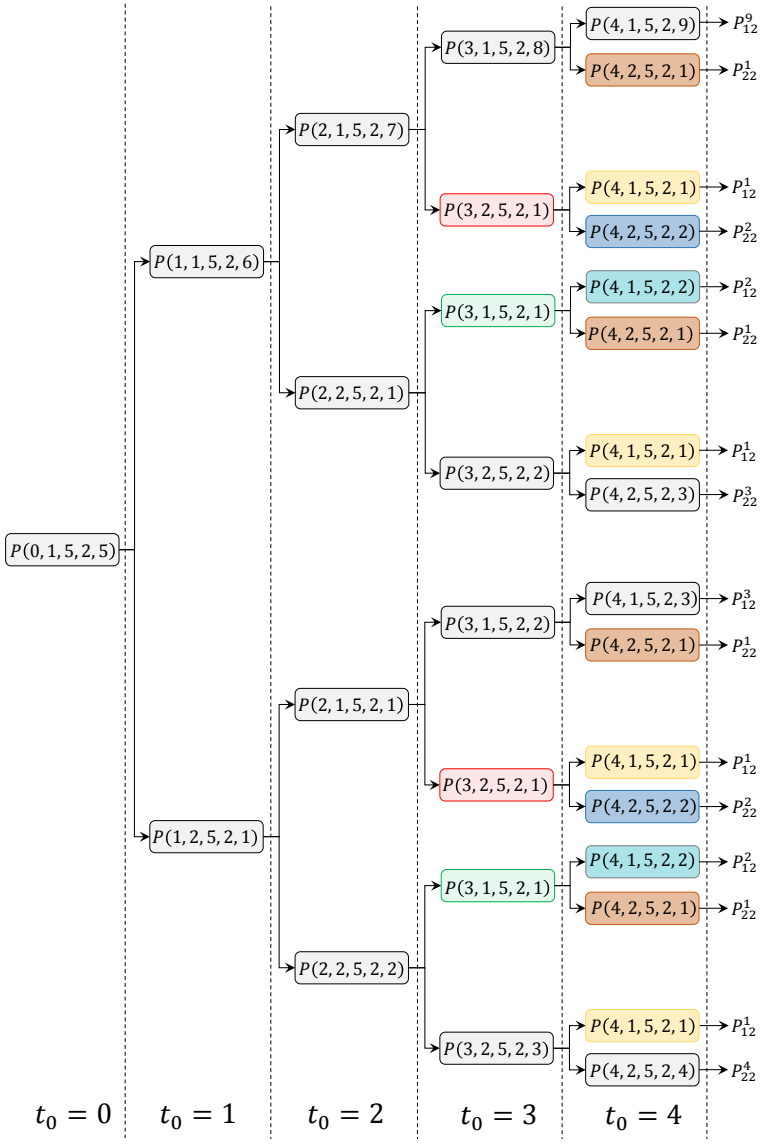

Figure 4.12: Recursive calculation of $P(0, 1, 5, 2, 5)$ in five stages

Let's consider an example to better understand how $P(t_0, i, t_0 + t, j, c)$ is calculated recursively. In this example, i, t_0, j, and c are assumed to be 1, 0, 2, and 5 and the goal is to calculate $P(0, 1, t, 2, 5)$ where $t = 5$. For the sake of simplicity of explanation, a simple IGE model with only two channel states are considered (i.e., $|\Omega| = 2$). Figure 4.12 shows that $P(0, 1, 5, 2, 5)$ can be calculated recursively in five steps. To calculate $P(0, 1, t, 2, 5)$, two (generally $|\Omega|$) pairs of new components, $\big(P(0, 1, 1, 1, 5), P(1, 1, 5, 2, 5)\big)$ and $\big(P(0, 1, 1, 2, 5), P(1, 2, 5, 2, 1)\big)$, need to be calculated at step $t_0 = 1$. Since the first component in each pair is directly calculated, they are ignored in the figure. In other words, $P(0, 1, 1, 1, 5)$ and $P(0, 1, 1, 2, 5)$ are equal to P^5_{11} and P^5_{12}, respectively, and can be calculated using the Eqns. (4.6) and (4.12), accordingly. The second component in each pair needs two (generally $|\Omega|$) other components to be calculated at the step $t_0 = 2$ (totally four components at this step). At the last step, where $t_0 = 4$, totally 16 components need to be calculated. As the figure shows, all components can be directly calculated by Eqns. (4.6) and (4.12) when $t_0 = 4$. This is where the recursion comes in and the components in the previous steps can be calculated.

According to Eqn. (4.17), the time complexity of recursively calculating $P(t_0, i, t_0 + t, j, c)$ is $O(|\Omega|^t)$. Many of the recursive components have the same results. These components have been shown in the same colour and are just repeated which indicates a potential to calculate each component only once and then reuse the results. Motivated by this, instead of using a recursive approach, a dynamic programming solution is used to remember intermediate results and reuse them through which, the time complexity of calculating $P(t_0, i, t_0 + t, j, c)$ is extremely reduced. Considering the example above, it can be seen that in each step only half of the components (generally, only $|\Omega| \times t_0$ components) need to be calculated. Therefore, generally, the total number of the required components to be calculated to find $P(t_0, i, t_0 + t, j, c)$ in dynamic programming is:

$$|\Omega| + 2 \times |\Omega| + 3 \times |\Omega| + \cdots + (t-2) \times |\Omega| + (t-1) \times |\Omega| = \frac{t \times (t-1) \times |\Omega|}{2} \quad (4.18)$$

Thus, the time complexity of calculating $P(t_0, i, t_0 + t, j, c)$ using the dynamic programming solution is reduced to $O(|\Omega| \times t^2)$. Algorithm 3 is the pseudo code of calculating $P(t_0, i, t_0+t, j, c)$ using dynamic programming. As can be seen, the first loop (line 2-32) calculates the components from the last step $(t-1)$ where the components can be directly calculated by Eqns. (4.6) and (4.12). Using this loop, the components in the higher step are available at the beginning of each step. In each step represented

by τ, there is another loop (line 3-31) where the probability of transition from each channel state $k \in \{1, \ldots, |\Omega|\}$ to the state j within the next $t - \tau$ slots is considered. In this loop, different transition probabilities are calculated depending on the current and the next channel state and the length of run-length (line 6-8, 10-12, 16-21, and 23-28) and are stored for further reuse (line 19 and 26). Please note that since D and $|\Omega|$ are usually very small, finding $t^\star$ will not incur a large overhead to the sensor node.

4.6 Experimental Evaluation of ATPS

This section evaluates the behaviour of ATPS under the use of the discussed channel models first. Then, it compares the performance of the proposed IGE enabled ATPS with the state-of-the-art protocols through several experiments based on the following three metrics:

- **Power level usage**: the number of transmissions under each power level is measured, by which the distribution of power level used for all implemented schemes can be compared. Since it is impossible to perform quantitative measurement of the real interference produced by the packet transmissions, this metric allows a comparison between the produced interference of different schemes in a relative way since the more the number of transmissions using a high transmission power, the larger the probability to produce more interference.
- **Energy consumption**: the total energy spent on packet transmission is measured at the sending node side since the gateway is generally a mobile device such as a smartphone that is commonly recharged regularly.
- **Packet loss rate**: it is defined as the ratio of the number of lost packets to the total number of transmitted packets.

4.6.1 Experiment Setup

The same setup as presented in Chapter 3 with the sending node attached to the wrist and the gateway mounted on the chest is adapted. Although this setup is not general enough to support all types of WBANs, the location of the sending node and consequently the channel to the gateway is highly unstable to make the channel estimation challenging. All experiments in this thesis are carried out in an area of about 10 m$\times$10 m at the presence of a wireless access point and an indoor localisation system,

Algorithm 3: Calculation of $P(t_0, i, t_0 + t, j, c)$ using dynamic programming

```
Function: P(t_0, i, t_0 + t, j, c)
for τ = t − 1, ..., 0 do
    for k = 1, ..., |Ω| do
        if τ == t − 1 then
            if k == i then
                for c' = 1, ..., τ − 1, c + τ do
                    P(t_0 + τ, k, t_0 + t, j, c') = P^{c'}_{kj};
                end
            else
                for c' = 1, ..., τ do
                    P(t_0 + τ, k, t_0 + t, j, c') = P^{c'}_{kj};
                end
            end
        else
            if k == i then
                for c' = 1, ..., τ − 1, c + τ do
                    P(t_0 + τ, k, t_0 + t, j, c') = P(t_0 + τ + 1, k, t_0 + t, j, c' + 1);
                    for kk = 1, ..., k − 1, k + 1, ..., |Ω| do
                        P(t_0 + τ, k, t_0 + t, j, c') += P(t_0 + τ + 1, kk, t_0 + t, j, 1);
                    end
                end
            else
                for c' = 1, ..., τ do
                    P(t_0 + τ, k, t_0 + t, j, c') = P(t_0 + τ + 1, k, t_0 + t, j, c' + 1);
                    for kk = 1, ..., k − 1, k + 1, ..., |Ω| do
                        P(t_0 + τ, k, t_0 + t, j, c') += P(t_0 + τ + 1, kk, t_0 + t, j, 1);
                    end
                end
            end
        end
    end
end
```

all working at 2.4 GHz band. However, CC2420 radio chip uses Direct Sequence Spread Spectrum (DSSS) to spread the output power, thereby making the communication link more robust even in a noisy environment. Power levels 1, 3 and 7 are chosen for packet transmission. As illustrated in Chapter 3, both power level 1 and 2 are suitable to scenarios where a short distance LoS path is available. With the gateway attached to the chest and the sending node attached to the wrist, the two power levels achieve similar communication reliability in many daily postures such as studying, driving, and eating, but, power level 1 is chosen as it is more energy efficient. Each packet transmitted by the sending node has a size of 41 bytes. The received packets at the gateway are forwarded to a laptop where the results of the experiments are recorded, and the behaviour of the communication protocols are monitored. For the sake of simplicity for comparison, this setup assumes the packets are generated at a constant rate and transmitted to the gateway according to a predefined TDMA schedule. Since different applications may have different requirements for data rate, the experiments have been carried out under three different packet rates including 0.1 pkt/s and 1 pkt/s for low data rate applications such as monitoring blood pressure as well as 20 pkt/s for high packet rate applications like EMG monitoring or motion tracking systems (Movassaghi *et al.*, 2014). The experiments are performed on three subjects (two males and one female) and averaged the performance metrics among four trials. In each experiment, the subjects were asked to stay in the following four daily postures in the same indoor environment, with each posture lasting for 30 minutes.

- **Sitting with folded hand**: in this scenario, the distance between the sending node and the gateway is only a few centimetres. It is chosen to cover all those postures where the hand is very close to the chest, e.g., eating, drinking, brushing teeth, etc.

- **Standing upright**: in this posture, the thumb is parallel to the trousers so that the sending node is very close to the side pocket and the LoS path to the gateway is blocked.

- **Walking**: in this posture, the LoS path between transceivers is regularly connected/disconnected. It is a good scenario to consider how different channel models can predict quick channel fluctuations.

- **Running**: in this scenario, the channel quality varies very fast. It can be used to test the performance limits of different models.

In the first set of experiments, the performance of the proposed IGE channel model is compared with the GE and EGE model. To this end, three separate versions of the ATPS protocol are developed, each of which uses one of the discussed channel models. For the sake of simplicity, each version of the ATPS protocol is named based on the channel model it uses. All models (GE, EGE, and IGE) have 3 channel states. Each state in the EGE model contains 20 internal states. Hence, the size of the transition matrix in GE, IGE, and EGE model is limited to 64 bytes, 112 bytes, and 6.4 kilo bytes, respectively. In the second set of experiments, the performance of ATPS protocol which uses the IGE model is compared with the following related schemes:

(1) Experio (Kindt *et al.*, 2015): It explores the correlation between acceleration data and RSSI in periodic movements to predict the positions with low data loss rate for data transmission. Once exploitable periodicity is detected, it opportunistically schedules transmissions at positions with low packet loss rate using a low transmission power level; otherwise, packets are transmitted using a high transmission power level.

(2) DPPI (Quwaider *et al.*, 2010): It assumes a linear relationship between the measured RSSI at the receiver and the transmission power. For each transmission, it measures the channel RSSI at the gateway. If the measured RSSI falls out of the empirically measured optimal RSSI range, the gateway communicates with the sending node to adjusts its transmission power level. Through such a feedback loop, DPPI adaptively adjusts the transmission power level until the measured RSSI of the next packet falls into the optimal range. The optimal RSSI thresholds suggested in (Quwaider *et al.*, 2010) (which are also confirmed by empirical investigations) are used.

(3) Fixed Low Power (FLP) and Fixed High Power (FHP) are two baseline schemes which are implemented for comparisons. FLP always uses the lowest power level (level 1), whereas FHP always uses the highest power level (level 7) since it already can achieve very high communication reliability in all postures.

To fairly compare all protocols and channel models, it is necessary to repeat the same experiments for them under the same conditions, which is almost impossible in practice especially for dynamic postures. To address this problem, a two-phase RSSI sample collection is carried out. In the first phase, the three subjects are asked to follow a predefined set of postures including sitting, standing, walking, and running,

RSSI of the Maximum Power Level (dBm)	0	-1	-2	-3	...	-92	-93	-94
RSSI of Power Level i (dBm)	-43	-44	-45.5	-47	...	$-\infty$	$-\infty$	$-\infty$
Communication Reliability of Power Level i	99.9%	99.9%	99.9%	99.8%	...	0%	0%	0%

Table 4.1: Mapping the RSSI of transmission with the maximum power level to the RSSI of a power level $i \in \{1, 3, 7\}$

each of which lasts for 30 minutes. The sending node communicates with the gateway using the maximum power (power level 32), and the gateway measures the RSSI of the packets and collects the RSSI samples to generate the RSSI trace for evaluating the implemented protocols. Since the maximum power level is used for collecting the RSSI traces, the RSSI and the communication reliability of other power levels remains unknown. In the second phase, the mapping between the RSSI of transmission with the maximum power level and the RSSI of transmission with other levels is generated. In this phase, the sending node transmits thousands of pairs of packets in a way that it first transmits the first packet with the maximum power level and then immediately sends the second packet with power level i. Since the time difference between two adjacent transmissions is limited to a few milliseconds, the channel quality for each pair of transmissions is relatively constant. Therefore, by analysing the collected RSSI traces, a mapping between the RSSI of each transmission using the maximum power level and the RSSI of communication using power level i can be created, as illustrated in Table 4.1. Moreover, by counting the number of received packets under a specific channel RSSI, the communication reliability of power level i at each channel RSSI can be calculated. The RSSI traces for low data rates are created by downsampling the above trace generated with 20 pkt/s.

4.6.2 Experimental Evaluation of ATPS Under the Use of Different Channel Models

In this section, the performance of ATPS under the use of three channel prediction models (GE, EGE, and IGE) is evaluated through many experiments based on the discussed performance metrics. Channel models learn the state transition probabilities (i.e., probabilities in the transition matrix) from the run time observations of the channel behaviour (i.e., the collected RSSI traces) based on the ageing method presented in (Rafiq, 2015). In static postures such as sitting and standing, the channel quality is constant over time and postponing the transmission has no impact on communication performance. But in dynamic postures (e.g., walking and running) it is assumed that

a newly generated packet has to be transmitted within 1 second (i.e., the deadline is 1 second) whereby, the sending node has a chance to reduce the transmission cost by postponing the transmissions. Please note, the LoS is blocked during part of a gait cycle and is available for the rest of the cycle. The idea of ATPS is to buffer the packet when the LoS is blocked and send it when the LoS becomes available. Since the average number of steps in walking is about 116 steps per minute (Blessey *et al.*, 1976), a gait cycle usually takes about 1 second. Thus, taking the deadline equal to 1 second guarantees the LoS will become available before the deadline. On the other hand, since the channel is changing periodically, taking the deadline more than 1 second does not significantly influence the performance of ATPS. Please note that since bursty transmission is allowed, the sending node can transmit a couple of buffered packets in a single time slot, however, this does not happen in low packet rate scenarios as the time interval between generating two adjacent packets is not smaller than the deadline.

Experiments with MAC Sub-layer Retransmission Disabled

For all experiments in this section, retransmission at the MAC sub-layer is disabled. Hence, for a given packet rate, the number of transmissions in all implementations of ATPS (i.e., ATPS implementations with three different channel models) are the same. Figure 4.13 illustrates the results of the experiments and shows the performance of ATPS under three packet rates and four body postures in terms of power-level usage, energy consumption, and packet loss rate.

In static postures, all models (GE, EGE, and IGE) achieve excellent performance. In sitting, where the LoS path to the gateway is available, the performance of all models is almost the same. Regardless of the packet rate, they almost consume the same amount of energy, only $30\mu J$ per packet on average. They also drop the same percentage of packets (below 6%) and use power level 1 for more than 95% of transmissions. This is the same for standing. In this posture, the LoS path to the gateway is blocked by body trunk and thus the channel models suggest a higher transmission power level (level 3) and consumes more energy (about $33.5\mu J$ per packet on average), but all protocols still behave almost the same. They drop about 8% of the packets when the packet rate is 0.1 pkt/s. But, the packet loss rate is reduced to about 3.5% when the packet rate is high and the models get more feedback to learn the channel. A common feature of channel quality in both sitting and standing is its stability. In other words, the channel quality in sitting and standing is relatively fixed and thus, postponing a transmission does not increase the chance of communication with a lower transmission cost. When

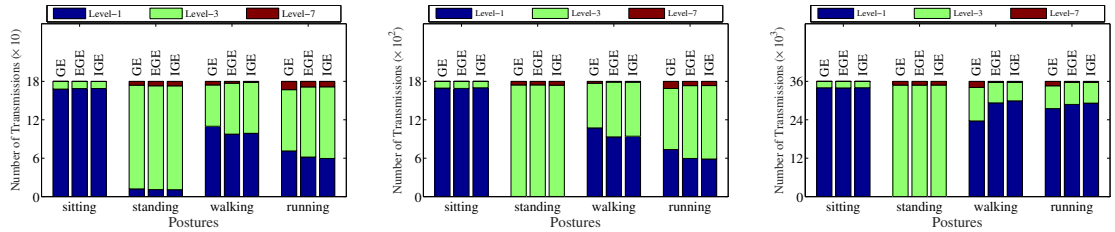

(a) packet rate = 0.1 pkt/s (b) packet rate = 1 pkt/s (c) packet rate = 20 pkt/s

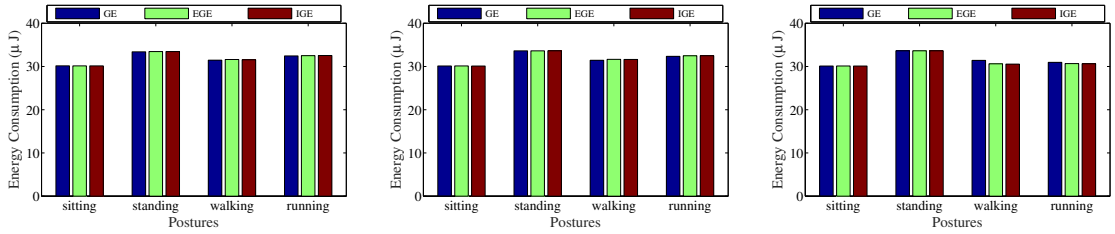

(d) packet rate = 0.1 pkt/s (e) packet rate = 1 pkt/s (f) packet rate = 20 pkt/s

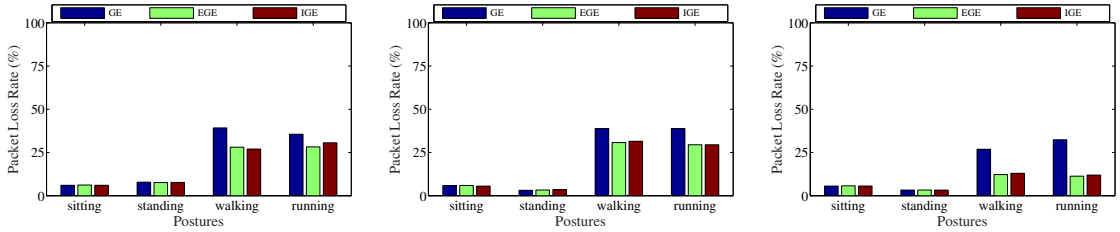

(g) packet rate = 0.1 pkt/s (h) packet rate = 1 pkt/s (i) packet rate = 20 pkt/s

Figure 4.13: Experiments with disabled MAC sub-layer retransmission under different data rates: (a), (b) and (c) show the distribution of power level usage; (d), (e) and (f) show the energy consumption; (g), (h) and (i) show the packet loss rate.

the channel quality is constant over time, there is not a big challenge in predicting the channel behaviour and both GE and IGE model can predict the channel quality as effectively as EGE model.

Unlike the static postures, GE does not perform as well as EGE and IGE models in walking and running. The packet loss rate of all models is increased significantly during dynamic postures because the rapid channel fluctuation makes the channel prediction difficult. This is more critical in the GE model while IGE and EGE show relatively similar behaviour. For example, in walking (and similarly in the running), GE model drops about 39% of the packets at the packet rate of 0.1 pkt/s and 1 pkt/s that is about 10% more than that of EGE and IGE models. Increasing the packet rate to 1 pkt/s does not change the packet loss rate of ATPS significantly, but at the packet rate of 20 pkt/s,

where the models get enough feedback to precisely predict the channel pattern, EGE and IGE models sufficiently decrease the packet loss rate to below 15%. This is not the case for GE model as it still drops about 26% and 32% of the packets in walking and running, respectively. The reason for such a huge packet loss rate in the GE model is its low accuracy of channel prediction. In the walking and the running, the channel mostly and alternatively stays in state 1 and state 3 for tens of milliseconds. As discussed earlier, the GE model is memoryless and cannot remember how long (i.e., for how many transmissions) the channel stays in state 1 or state 3. Therefore, it cannot accurately estimate the state transition and thus, it cannot adjust the transmission signal power of the sending node on time. On the other hand, IGE model learns the channel pattern almost as effectively as EGE model, buffers the packets, and transmits them in a bursty fashion when the channel is expected to be at its peak. In terms of distribution of usage of power levels, GE is not as effective as EGE and IGE, though, they all consume almost the same amount of energy in all scenarios. The distribution of usage of power levels at the packet rate of 20 pkt/s presented in Figure 4.13c clearly reveals that both EGE and IGE models choose power level 1 for most of their transmissions and thus, efficiently reduce the potential interference.

Experiments with MAC Sub-layer Retransmission Enabled

To increase the communication reliability, a lost packet is retransmitted. To this end, once a packet is lost, ATPS makes a new channel estimation according to the channel model it is using and adjusts its transmission signal power based on the new estimation. For a fair comparison among discussed channel estimation models, the previous experiments are repeated with enabled MAC sub-layer retransmission. The maximum number of retransmission is set to 15 for the scenarios with the packet rate of 0.1 pkt/s and 1 pkt/s so that, the time interval between two adjacent retransmissions is increased based on the binary exponential backoff algorithm. In high packet rate scenarios, since the time interval between two adjacent transmissions is too short and the channel is probably not changed significantly, the maximum number of retransmission is set to 3. Figure 4.14 shows the results of the experiments under different scenarios. After enabling MAC-sub layer retransmission all packets are reliably delivered under all models in all scenarios. In other words, the packet loss rate of ATPS under the use of all channel models is decreased to 0%. Hence, Figure 4.14 does not include the results for the packet loss rate. Please note, because of the difference in the packet loss rate of channel models, their number of transmissions, when the MAC sub-layer retransmission

is enabled, is different.

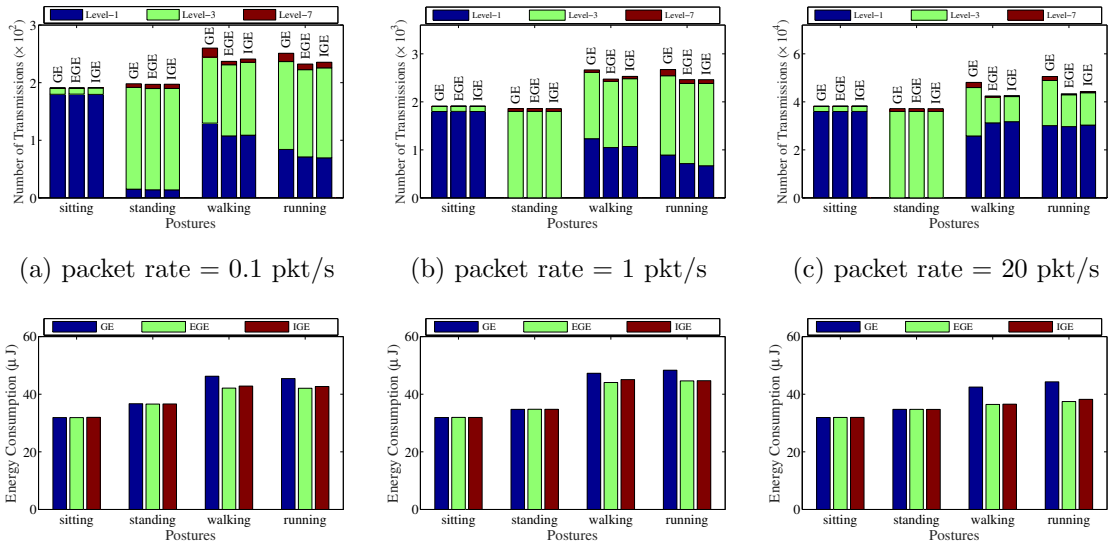

(a) packet rate = 0.1 pkt/s (b) packet rate = 1 pkt/s (c) packet rate = 20 pkt/s

(d) packet rate = 0.1 pkt/s (e) packet rate = 1 pkt/s (f) packet rate = 20 pkt/s

Figure 4.14: Experiments with enabled MAC sub-layer retransmission under different data rates: (a), (b) and (c) show the distribution of power level usage; (d), (e) and (f) show the energy consumption.

In sitting and standing, since GE, EGE, and IGE deliver nearly all packets on their first transmission, enabling retransmission does not affect the performance of the models considerably. Therefore, the number of transmissions and the average per packet energy consumption of ATPS under the use of all channel models remain roughly unchanged. As the packet loss rate of all models in dynamic postures is high, particularly when the packet rate is low (as shown in Figure 4.13), enabling retransmission considerably influences the energy consumption and the number of transmissions of all models. This is more critical in the case of the GE model as is shown in Figure 4.14. For example, when the subject is walking and the packet rate is set to 0.1 pkt/s, enabling retransmission increases the total number of transmissions by 45%, in the GE model, 14% and 12% more than that of EGE and IGE model, respectively. Increasing the packet rate to 20 pkt/s in the same posture reduces the transmission overhead of all channel models but, compared to the same scenario with disabled MAC sub-layer retransmission, the GE model still requires 34% more transmissions which is almost two times more than that of EGE and IGE model. Similarly, in running, the GE model requires many more transmissions compared to the EGE model to deliver all packets while IGE performs almost as well as EGE model. In the case of energy consumption,

the GE model undertakes more energy overhead than the other two models. Compared to EGE and IGE models and regardless of the packet rate, the GE model respectively consumes about 11% and 9% more energy on average to deliver all packets in walking. The results presented in Figures 4.14d, 4.14e, and 4.14f indicate the same trend in the running, where IGE performs almost as well as EGE model but consumes below 91% of the energy used by GE model. The results of the experiments in different scenarios reveal that the proposed IGE model outperforms the GE model and achieves almost the same performance as well as the EGE model but at the cost of lower memory usage.

4.6.3 Comparing Performance of ATPS with the State-of-the-art Protocols

To have a better evaluation of the performance of the proposed IGE model, ATPS protocol which uses the IGE model for channel estimation is compared with the state-of-the-art protocols. In this regard, the previous experiments are repeated, the same experiment setup is used, and the same performance metrics are considered.

Experiments with MAC sub-layer Retransmission Disabled

In this section, it is assumed that the sending node does not retransmit a lost packet so that the experimental results can be compared. Thus, the numbers of transmissions in all scenarios at a given packet rate are the same. The purpose to have this set of experiments is two-fold: (1) it is easy to see the distribution of the power levels used for transmission and the impact of data rate on the performance of different schemes; (2) it will be used as a benchmark to compare and analyse the results for the scenario in which retransmissions are enabled. Figure 4.15 shows the results of the experiments under three different packet rates and four different body postures. For the sake of clarity, the results in *static* and *dynamic* postures are discussed separately.

Static postures: In sitting, the performance of ATPS and DPPI is roughly the same, particularly when the packet rate is high. Both models use power level 1 for more than 94% of transmissions and rarely use power level 7 (below 0.1%). They also consume roughly the same amount of energy and deliver about 94% of the packets. Increasing the packet rate improves the performance of the ATPS because the channel model (i.e., the IGE model) will get more channel feedback (and consequently it will measure more RSSI samples) and thus, it can better understand the channel pattern and the transition probability among different channel states. Similarly, increasing the packet

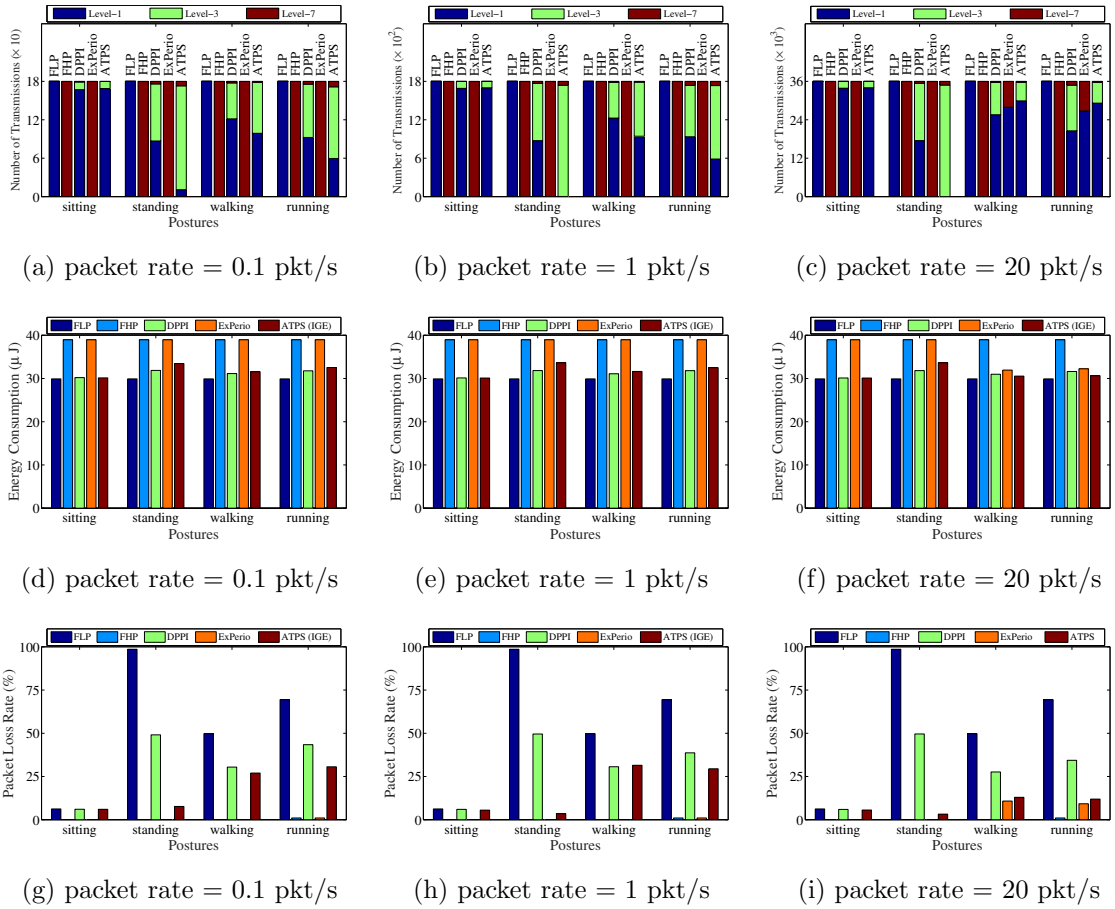

(a) packet rate = 0.1 pkt/s (b) packet rate = 1 pkt/s (c) packet rate = 20 pkt/s

(d) packet rate = 0.1 pkt/s (e) packet rate = 1 pkt/s (f) packet rate = 20 pkt/s

(g) packet rate = 0.1 pkt/s (h) packet rate = 1 pkt/s (i) packet rate = 20 pkt/s

Figure 4.15: Experiments with disabled MAC sub-layer retransmission under different data rates: (a), (b) and (c) show the distribution of power level usage; (d), (e) and (f) show the energy consumption; (g), (h) and (i) show the packet loss rate.

rate improves the performance of DPPI. Since DPPI estimates the channel by averaging the measured RSSI of the last two transmissions, increasing the packet rate reduces the time interval between the transmissions and thus, the averaged RSSI value is a more accurate estimation on the current channel RSSI. In standing, ATPS outperforms DPPI in all packet rates. The DPPI frequently switches between power level 1 and power level 3 due to the adoption of a simple threshold-based method to determine the optimal transmission power level. Hence, it chooses power level 1 for half of its transmissions and uses power level 3 for the other half. Since the channel using low power levels is not very stable, DPPI becomes sensitive to the thresholds, leading to such a ping-pong effect. Moreover, because of the blocked LoS path to the gateway in standing, most of the transmitted packets using power level 1 are dropped. On the other side, ATPS uses

power level 3 for most of its transmissions and delivers more than 96% of the packets at the rate of 20 pkt/s, though, at the cost of a slightly higher energy consumption.

In both sitting and standing, where the channel quality is fixed, ExPerio turns into FHP because there is no periodic motion. Both schemes transmit using the maximum power level and thus produce the maximum potential interference and consume much more energy than that for ATPS. FLP has excellent performance in sitting as the LoS path is available, and low-power communication can deliver the packets. However, it has very poor performance in standing in which almost all packets have been dropped.

Dynamic postures: In both walking and running, since the channel fluctuates between different states, ATPS can learn the channel state transition, estimate the channel fluctuation pattern, buffer the packets when the channel is blocked, and transmit them once the LoS path becomes available. To learn the channel state transition probability, ATPS (i.e., the IGE channel model) needs to measure the channel RSSI upon receiving the channel feedback. When the packet rate is low, learning the channel state transition probability is a slow procedure (as it is a feedback based learning mechanism) and will take a while until ATPS learns the channel pattern. Hence, it cannot accurately schedule the packet transmissions at the beginning and thus, it is possible the sending node transmits the packets using power level 1 when the channel is at the state 3. At the packet rate of 0.1 pkt/s, although ATPS chooses power level 1 for 55% and 33% of its transmission in walking and running, respectively, it drops a large number of packets (about one-third of the packets) due to the inaccurate packet scheduling. With the increase of packet rate, the percentage of transmissions that use power level 1 is increased since the more accurate channel state transition can be quickly obtained with more channel feedback. When the packet rate is 20 pkt/s, ATPS uses power level 1 for more than 80% of transmissions in both walking and running while its packet loss rate is reduced to below 15%. Even though DPPI transmits most packets using power levels 1 and 3, the distribution of power level usage does not change much for different packet rates. Moreover, it drops a large number of packets—more than two and three times higher than that of ATPS in walking and running, respectively. The low performance of DPPI in dynamic postures is not only due to the ping-pong effect but also because the assumption of a linear relationship between power level and channel RSSI does not hold in dynamic postures as discussed in Chapter 2.

In low packet rate scenarios, ExPerio still behaves as FHP as it cannot detect the channel peaks. Therefore, they both potentially produce the maximum interference and consume the maximum amount of energy, though, they deliver almost all packets. When

the packet rate is 20 pkt/s, ExPerio detects the channel peaks and schedules the packets to be opportunistically transmitted at the channel peaks. It opportunistically transmits more than 75% of the packets using level 1 in walking and running however, it still consumes more energy than ATPS and imposes unaffordable computation overhead to the resource-constrained sending node. It is not surprising that both FLP and FHP do not have good performance in dynamic postures due to the frequent change of channel quality.

Experiments with MAC sub-layer Retransmission Enabled

To provide reliable communication, a lost packet is retransmitted. For a more comprehensive comparison among different schemes, the previous experiments are repeated with enabled retransmission at MAC sub-layer. The ways different communication protocols deal with a lost packet are different. FLP and FHP do not make changes on transmission power. ExPerio retransmits each lost packet with the maximum power level. DPPI adjusts its power level to a level between the current level and the maximum level, but ATPS adaptively selects the power level for retransmission based on its new channel estimation. Figure 4.16 shows the results of the experiments under different scenarios. Since retransmission is enabled, the total number of transmissions in different schemes are different due to the difference in packet loss rate. It turns out that the obtained experimental data is highly skewed with many small values and a few large values. To display the small values, the large values are allowed to cut through the plot area and then, they are labelled with the real values.

Static postures: As is expected, enabling retransmission does not considerably increase the energy consumption and the total number of transmissions of ATPS and DPPI in sitting as they deliver almost all packets on their first transmission. In standing, ATPS is the most energy efficient protocol. It consumes only about half of the energy used by DPPI because it quickly detects the channel is stable and thus, it adjusts its transmission power level to level 3 and delivers almost all packets on the first transmission. The reason for the huge energy consumption of DPPI in standing is its high packet loss rate as previously mentioned. Similar to FHP, ExPerio delivers almost all packets and enabling retransmission does not remarkably influence its performance. They both transmit all packets using the maximum power level and compared to ATPS potentially produce more interference. Despite the excellent performance of FLP in sitting, it consumes a huge amount of energy in standing, much more than that of other protocols. Although FLP tries to deliver the lost packets through retransmitting them,

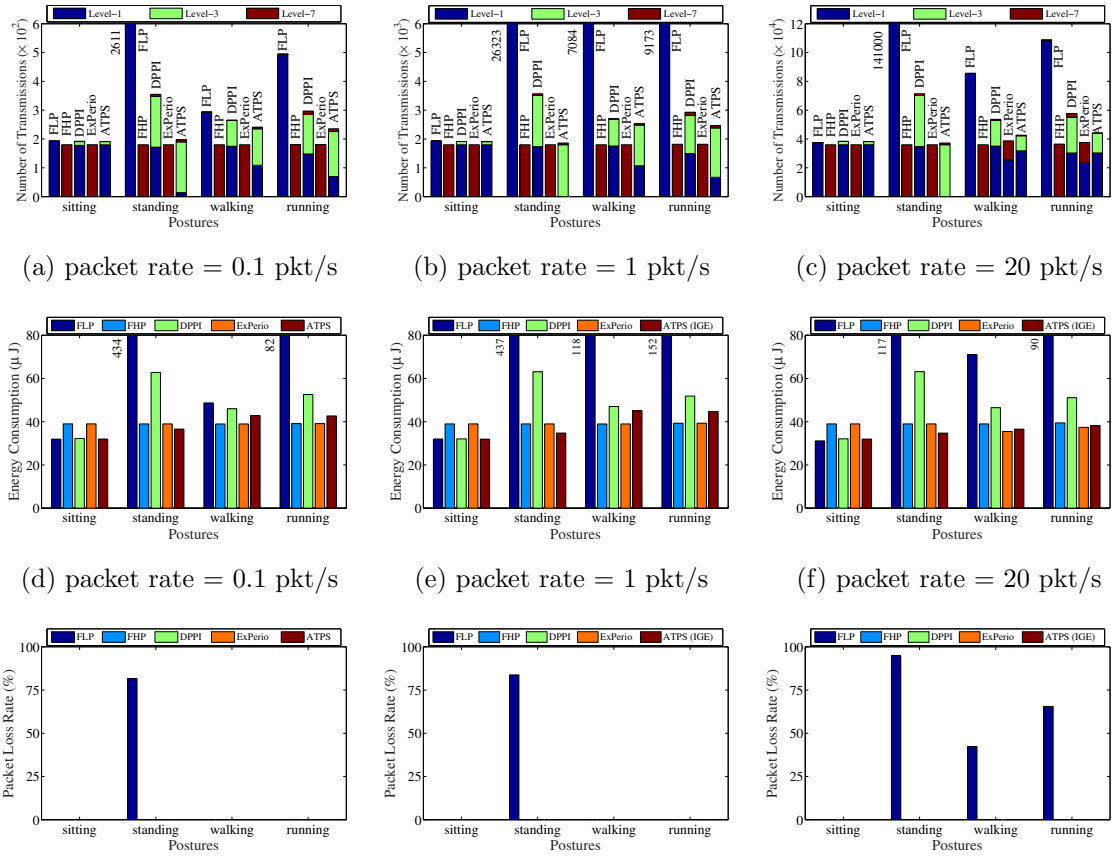

Figure 4.16: Experiments with enabled MAC sub-layer retransmission under different data rates: (a), (b) and (c) show the distribution of power level usage; (d), (e) and (f) show the energy consumption; (g), (h) and (i) show the packet loss rate.

almost all the trials fail because it constantly uses the lowest transmission power level.

Dynamic posture: ATPS has the same trend on power level used in walking and running. As previously shown, when retransmission is disabled, the packet loss rate of ATPS in low packet rate scenarios is high. Hence, enabling packet retransmission increases its number of transmissions and accordingly imposes some energy overhead though, delivers all packets in all scenarios. For example, when the subject is walking and the packet rate is 0.1 pkt/s, ATPS consumes $43\mu J$, about 10% more than that of ExPerio and FHP which use power level 7 for all transmissions. When the packet rate is set to 20 pkt/s, ATPS and ExPerio can efficiently schedule the packets to be transmitted at the channel peaks. Hence, most of the packets are delivered on their first transmission. At this packet rate, the energy consumption of ExPerio and ATPS

in both walking and running are reduced to the same level of the energy usage of FHP and they possibly produce less interference. Packet retransmission enables DPPI to deliver all packets, however, at the expense of a considerable overhead. It transmits about 10% and 20% more than that of ATPS in walking and running, respectively, when the packet rate is low, and about 35% on average when the packet rate is high. It rarely uses the maximum power level and mainly transmits using level 1 and level 3 but still consumes more energy than ATPS. For example, the huge number of transmissions of DPPI at the packet rate of 20 pkt/s increases its energy consumption to up to 33% higher than that of ATPS in the running.

Communication using power level 1 drops all packets when the channel is blocked. Since FLP uses power level 1 even for retransmissions, a lost packet needs to be retransmitted a couple of times until the LoS path becomes available or the number of retransmissions reaches the maximum. Hence, the number of retransmissions in FLP is much more than that of other schemes. For the same reason, it has the maximum energy consumption. In low packet rate scenarios, the time between two adjacent transmissions is larger than the time for a gait cycle. Since the LoS path becomes available in a part of a gait cycle, FLP gets a chance to deliver a lost packet after a couple of retransmissions. Therefore, similar to all other protocols, FLP delivers all packets in walking and running. In high packet rate scenarios, since the time gap between two adjacent transmissions is too short, the channel is constant, and FLP cannot deliver most of the lost packets.

In summary, ATPS is a power-adaptive communication protocol that benefits from the spatio-temporal locality among channel samples. It can learn the channel state transition probability through monitoring the channel RSSI samples. Unlike the ExPerio that is suitable for body postures which present periodic motion patterns (however, at the cost of unaffordable computation overhead), ATPS supports static postures as well. Although its performance in low packet rate scenarios, when the channel state is quickly changing, is slightly low, it still outperforms the state-of-the-art protocols in some of the designed scenarios.

4.7 Discussion

This chapter presents IGE, a new channel model that can accurately predict channel behaviour in WBANs. Experimental evaluation shows that IGE model can accurately predict channel behaviour at high packet rate scenarios. Motivated by the high accuracy of IGE for long-term channel prediction, ATPS, an adaptive transmission power

selection protocol for low-energy and low-interference communication in WBANs is developed. ATPS enables the sending node to benefit from the channel prediction model for scheduling packet transmissions. The experimental results in many scenarios demonstrate that this scheme can self-adapt to channel fluctuation patterns, and choose the most appropriate power level to reduce energy consumption and interference and improve communication reliability. ATPS decreases the usage of high transmission signal power and accordingly reduces energy cost remarkably, without any unacceptable cost at the packet loss rate. Since ATPS learns the channel pattern through monitoring channel samples, it supports only applications with high-rate periodic packet transmission. That is, when the packet rate is low or aperiodic, ATPS cannot capture the channel fluctuation pattern in dynamic postures and thus, it cannot predict the channel. Moreover, since ATPS channel prediction is based on RSSI measurements, a strong external interference may impact its performance. That is, the channel might be overestimated because the interference from an illegitimate transmitter can increase the RSSI value of a receiving packet at the legitimate receiver. However, this problem can be addressed by considering the LQI. In the next chapter, the correlation between body motion pattern and channel pattern is investigated. Then, a new learning scheme is proposed to exploit the channel behaviour based on the locally monitored body motion signal. Since the motion signal is locally monitored, the sending node does not need a high frequency periodic channel sampling. Thus, it is expected that the proposed scheme in the next chapter performs well in low packet rate scenarios.

Chapter 5

Chimp: A Learning-based Power-aware Communication Protocol for Wireless Body Area Networks

5.1 Introduction

The ATPS protocol proposed in the previous chapter benefits from the spatio-temporal locality characteristic of WBANs' channels. ATPS measures channel RSSI and monitors channel fluctuation pattern using a proposed memory efficient Markov chain model to estimate the channel quality and schedule the packet transmission. Although ATPS achieves very good performance in both static and dynamic postures in high packet rate scenarios, it suffers from a few drawbacks: (1) Measured RSSI is highly subject to interference and is influenced by the channel environment (Gharghan, Nordin, and Ismail, 2016). Moreover, the accuracy of measured RSSI by CC2420 deviates ± 6 dBm from the actual RSSI (Texas Instruments, 2007), which is a wide error margin. Such inaccuracy in measured RSSI influences the ATPS performance as it is a threshold based protocol which selects transmission power levels based on the instant measurements of RSSI. (2) ATPS has to exploit the channel fluctuation pattern to estimate the channel quality, therefore, it requires a periodic high-rate channel RSSI sampling. Since ATPS measures channel RSSI samples on receiving the ACK packets, the need for a periodic high-rate channel RSSI sampling requires a periodic high packet rate communication with the gateway. Thus, ATPS can support neither event-driven applications nor

applications with low packet rate.

A desirable solution to overcome the mentioned drawbacks needs to estimate the channel quality locally, without measuring the channel RSSI. The results of the experiments presented in Table 3.1 show the channel quality is highly dependent on the location of the sending node so that when the sending node is in front of the body, the LoS path to the gateway is available and the channel is good, while when the sending node is at the back of the body, the LoS path to the gateway is blocked and the channel is bad. However, localisation methods presented for WBANs are highly inaccurate, energy inefficient, and computationally expensive (Zhu, Zhong, Yu, and Wan, 2013; Hamie, Denis, and Richard, 2012). In the absence of location information, a high-level view on the most of dynamic physical activities (e.g., walking, running, swimming, etc.) reveals that the sending node attached to the wrist is moving between two regions in a way that the LoS communication path is available in one region and blocked in another region. Hence, the sending node should be able to learn this cyclic pattern and select the optimal power level for communication. At the same time, it should be adaptive to learn changed cyclic pattern when user changes his behaviour. To design a communication protocol in which the sending node selects the optimal transmission power level according to its movement pattern, the key challenges below need to be addressed first: (1) how can each sending node locally detect its movement pattern? (2) how can each sending node infer the real-time channel quality from its movement pattern without measuring channel RSSI? (3) how does it select the optimal power level? (4) how does the sending node deal with any changes in the movement/channel pattern due to the changes in the subject's physical activity?

This chapter presents Chimp, a new learning-based power-adaptive communication protocol. In Chimp, each sending node can self-learn the channel status and adaptively choose the best power level for each transmission to reduce energy consumption and interference range while guaranteeing high communication reliability. Chimp is a lightweight communication scheme designed based on learning-automata (Narendra and Thathachar, 2012). Instead of measuring channel RSSI, it uses only the acknowledgment packets from the gateway and the motion data obtained from a local gyroscope sensor to infer the real-time channel quality, without introducing additional communication cost. The key contributions of this chapter are summarised as follows:

- Inspired by the idea of learning automata the power-adaptive communication problem is modelled as a reinforcement learning algorithm. Based on the cost function presented in Section 3.3, a new learning function is designed and its

optimality in choosing the best transmission power level to minimise the cost function is illustrated.

- Experiments are carried out to investigate the relationship between the channel quality and the motion data generated by accelerometer and gyroscope sensors and observed a strong correlation between them during dynamic postures such as walking and running. Based on this observation, the previous learning model is extended by letting each sending node infer the real-time channel quality through the correlation with the motion data. Such an extension avoids frequent channel relearning and makes Chimp capable of quickly finding the best transmission power level in dynamic postures.

- The performance of Chimp is evaluated through many experiments on the TelosB sensor motes under three different data rates in several postures (sitting, standing, walking, and running), and is compared with ATPS and other state-of-the-art protocols as well as the optimal power assignment that is calculated off-line. The experimental results reveal that Chimp outperforms existing state-of-the-art protocols in many postures, achieves almost the same performance as the optimal power assignment when the data rate is relatively high and performs much better than ATPS in low packet rate scenarios.

The rest of this chapter is organised as follows: The learning automata-based modelling which presents the newly designed learning function is given for the power-adaptive communication problem in Section 5.2. Section 5.3 discusses the correlation between channel quality, the location, and the inertial features of the moving sending node, and then the Chimp protocol is presented and analysed. Experimental results for different scenarios are evaluated and discussed in Section 5.4. Section 5.5 concludes this chapter and discusses future work.

5.2 Chimp: Learning-based Power-adaptive Communication

In this section, the power-adaptive communication problem is formulated based on learning automata. Then, a novel reward function is presented that includes the transmission power, interference, and communication reliability. Finally, it is shown

that the designed learning function can find the optimal power level to minimise the transmission cost for static body postures.

5.2.1 Learning-automata Based Power-adaptive Communication

Consider a WBAN composed of one gateway and several sending nodes, in which the sending nodes communicate with the gateway according to the IEEE 802.15.4 beacon-enabled MAC protocol. Each sending node has n transmission power levels (level 1 is the lowest and level n is the highest) and can dynamically adjust its transmission power at a per-transmission level. It is assumed that each packet needs to be sent immediately once generated. The key idea of Chimp is similar to learning automata (Narendra and Thathachar, 2012), which is an adaptive learning method that tries to discover the attributes of the environment through trial and error as illustrated in Figure 5.1a. In Chimp, it is expected that each sending node can adaptively control its transmission power according to the channel quality, i.e., increases the transmission power whenever the channel is bad or decreases it as soon as the channel becomes good. To this end, each sending node needs a continuous interaction with the gateway to estimate the channel quality, and the ACK packet is used for each data transmission to serve for this purpose, as illustrated in Figure 5.1b. At the sending node side, a timer is set up for each packet transmission. If the sending node successfully receives the ACK packet before the timer is expired, the channel is interpreted as good; otherwise, the channel is understood as bad.

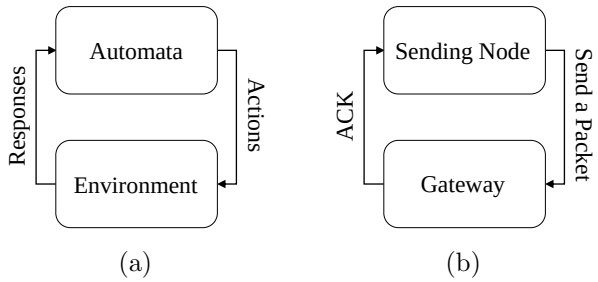

Figure 5.1: Feedback loop between (a) the automata and environment, (b) the sending node and the gateway.

In the following, the adaptive selection of transmission power is modelled as a learning automata that is defined using a quintuple $\{A, B, S, L, G\}$, where:

- $A = \{1, 2, \ldots, n\}$ is a finite set of actions or outputs of the automata, where

$a(t) = i$ represents the selection of power level i for transmission at time t.

- $B = \{0, 1\}$ is the set of responses each of which represents the status of receiving the ACK packet. Let $b(t)$ be the response for the packet sent at time t. $b(t) = 1$ represents the ACK packet is successfully received, and $b(t) = 0$ represents the ACK packet is not received.

- $S = \{s_1, s_2, \ldots, s_m\}$ is a set of internal states, where each state is a vector of selection probabilities that represent the probability of choosing each action. At each time instant t, the automata is in a state $s(t) \in S$, and a transition to another state $s(t+1) \in S$ may occur according to the current state and feedback from the environment. Let $p_i(t)$ denote the probability that the learning automata selects $a(t) = i$ at time t. The state at any time t, denoted by $s(t)$, can be represented as below:

$$s(t) = \{p_1(t), p_2(t), \ldots, p_n(t)\}, \quad \text{where } \sum_{i=1}^{n} p_i(t) = 1. \tag{5.1}$$

- L is a learning function that maps the current state $s(t)$ to a new state $s(t+1)$ based on the response from the environment, that is, $s(t+1) = L(s(t), b(t))$.

- G is a function that determines the next action based on the current state: $a(t+1) = G(s(t))$. The higher the probability of an action in the current state, the larger the probability it will be selected as the next action.

5.2.2 Energy-, Interference-, and Reliability-aware Cost and Reward Function

Since the goal of Chimp is to select the best transmission power to reduce energy consumption and interference, the proposed cost function that was presented in Chapter 3 is used so that each sending node can choose the optimal transmission power to minimise this cost function. In Chimp, the power level used for a packet transmission at time t is determined by randomly selecting a power level i from $A = \{1, 2, 3, \ldots, n\}$ based on its selection probability $p_i(t)$. Therefore, the expected cost for sending a packet can be computed by

$$E[cost] = \sum_{i=1}^{n} p_i(t)\, cost_i. \tag{5.2}$$

The learning function L in a learning automata is a key component that determines the performance regarding both optimality and convergence speed. The Linear Reward Inaction (L_{R-I}) function (Narendra and Thathachar, 2012), as illustrated in Eqns. (5.3) and (5.4), has been widely used.

- If an ACK is received ($b(t) = 1$):

$$\begin{aligned} p_i(t+1) &= p_i(t) + \alpha(1 - p_i(t)), \\ p_j(t+1) &= (1-\alpha)p_j(t), \quad \forall j \in A \text{ and } j \neq i \end{aligned} \tag{5.3}$$

- If an ACK is not received ($b(t) = 0$):

$$\begin{aligned} p_i(t+1) &= p_i(t), \\ p_j(t+1) &= p_j(t), \quad \forall j \in A \text{ and } j \neq i \end{aligned} \tag{5.4}$$

The key idea of the L_{R-I} learning function is: for a power level i that results in a good response, its selection probability $p_i(t)$ is linearly increased by a constant reward factor (α), and the selection probabilities for all the other actions are linearly decreased by the same reward factor. For a power level i that results in a bad response, the selection probabilities are not changed. However, the L_{R-I} learning function does not work for our case, which can be explained as follows: since a higher transmission power will have better channel quality, the probability of receiving the ACK packet using a high transmission power is larger than that for low transmission power levels. Hence, the learning automata will gradually increase the selection probability for the actions with high transmission power and finally select the highest transmission power as the optimal transmission power. It can be seen that the reason why L_{R-I} fails is that all actions in L_{R-I} use the same reward factor (α) which does not reflect the real reward according to the newly designed cost function. Motivated by this, the reward factor is redefined by: (a) letting each action have a separate reward factor to give different rewards to different actions; (b) defining the reward factor of each power level according to its transmission power so that the learning function can give more reward to actions with lower transmission power. The selection probabilities are updated as follows when an ACK is received:

$$\begin{aligned} p_i(t+1) &= p_i(t) + \alpha_i(1 - p_i(t)), \\ p_j(t+1) &= (1-\alpha_i)p_j(t), \quad \forall j \in A \text{ and } j \neq i \end{aligned} \tag{5.5}$$

where $0 < \alpha_i, \alpha_j \ll 1$ and $\frac{\alpha_i}{\alpha_j} = \frac{P_{tx}^j}{P_{tx}^i}$. When the ACK is received, the selection probability of power level i is increased by $\alpha_i\big(1 - p_i(t)\big)$, and the selection probability for any other power level j is decreased by $\alpha_i p_j$. Since $\alpha_i\big(1 - p_i(t)\big) = \alpha_i \sum_{j=1, j\neq i}^{j=n} p_j = \sum_{j=1, j\neq i}^{j=n} \alpha_i p_j$, the sum of all selection probabilities remains equal to 1 after updating the probabilities.

According to the definition of ϵ-optimality for learning automata (Narendra and Thathachar, 2012), a learning function L is ϵ-optimal if the probability of converging to the optimal action is as close to 1 as desired. The following theorem shows that the proposed new learning function is ϵ-optimal in selecting the optimal transmission power level to minimise the cost function.

Theorem 1: For any given channel quality, the proposed learning function is ϵ-optimal in selecting the optimal power level to minimise the cost function if

$$\frac{\alpha_i}{\alpha_j} = \frac{P_{tx}^j}{P_{tx}^i}, \quad and \quad 0 < \alpha_i, \alpha_j \ll 1, \forall i, j \in A. \tag{5.6}$$

From Theorem 1, it is evident that the reward factor for each power level is inversely proportional to the transmission power, which enforces the sending node to choose a low transmission power level if the channel quality is good. By making the reward factor much smaller than 1, it guarantees that the selection probability of the best action will gradually approach to 1. To empirically evaluate the effectiveness of Theorem 1, a set of experiments is carried out for three different postures (1, 3 and 5) given in Figure 3.3. Figure 5.2 shows the experimental results. For each posture, two sub-figures are plotted: the upper one shows the selection probabilities for different power levels over time regarding the number of transmissions, and the lower one shows the cost over the same period. It is clear that the best transmission power level in different postures may not be the same. The best transmission power level for postures 1 and 3 are both power level 3 as they have similar channel quality. The best power level for posture 5 is

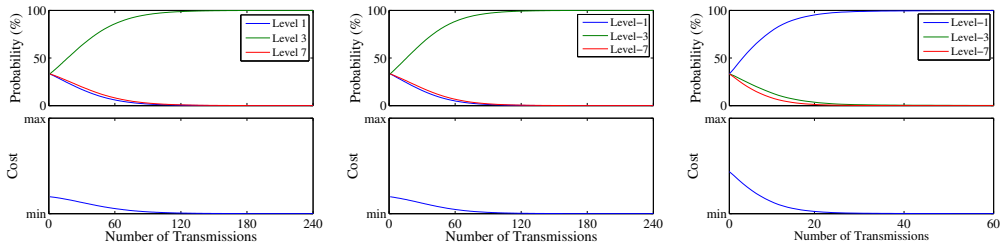

(a) Posture (1) (b) Posture (3) (c) Posture (5)

Figure 5.2: Performance of the designed learning function for different postures.

the lowest power level due to the availability of the LoS path with short transmission distance. The results show it takes about 120 interactions (packet transmissions) in posture 1 and 3 and below 40 transmissions in posture 5 for Chimp to find the best power level. In another point of view, if packet rate is set to 20 pkt/s, Chimp needs only 6 seconds in posture 1 and 3 and below 2 seconds in posture 5 to find the optimal power level. Moreover, the cost is quickly reduced in a few iterations.

5.3 Gyroscope Support for Dynamic Postures

Despite the fact that the previous design can choose the best power level to minimise the cost in static postures, its performance drops in dynamic postures due to the quick changes to the channel quality caused by frequent body movements. To investigate the behaviour of the previously proposed solution in dynamic postures, an experiment is carried out to measure the RSSI for walking and running, where the channel sampling rate is set to 20 samples per second. The upper sub-figures in Figures 5.3a and 5.3b show the measured RSSI of the channel samples within 5 seconds of walking and running, and the lower sub-figures show the expected optimal power levels calculated through an off-line analysis of the relationship between RSSI and the transmission costs of different power levels. From a high-level view, during walking and running (and other similar activities such as swimming), the sending node attached to the wrist is moving between two regions in a way that the LoS communication path is available in one region and blocked in another region. As depicted in the lower sub-figures in Figures 5.3a and 5.3b, an ideal adaptive communication protocol should be able to transmit using a low power

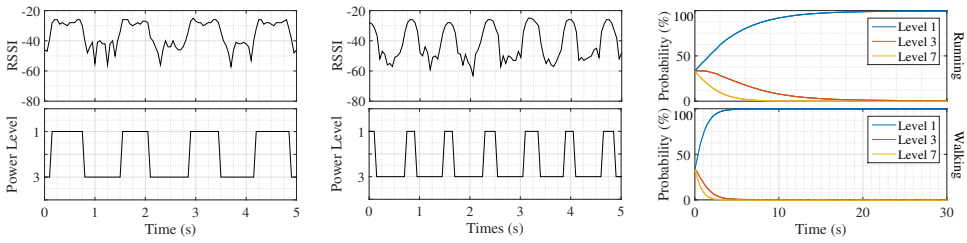

(a) (b) (c)

Figure 5.3: Channel RSSI within 5 seconds of (a) walking and (b) running as well as optimal power levels for communication during the same period and (c) Selection probability trend in Chimp in walking and running.

level when the RSSI is good and switch to a higher power level when it becomes bad. However, as can be seen from Figure 5.3c, which shows the selection probability trend of Chimp in 2 minutes walking and running, Chimp eventually selects a fixed power level instead of cyclically switching between a low power level and a high power level. This is mainly due to the slow convergence speed relative to the channel variation rate. Since Chimp learns based on the feedback, it cannot converge quickly without getting enough feedback.

The above problem can be solved if each sending node knows its real-time location, by which it can remember the communication history at previously observed locations and reduce the overhead caused by relearning the channel quality. However, most localisation methods for WBANs mainly rely on range measurement using RSSI (Zhu *et al.*, 2013) or Time-of-Arrival (ToA) of beacon packets (Hamie *et al.*, 2012), which will not only increase the energy consumption but also produce more overhead and interference. Existing motion tracking schemes (Young, Ling, and Arvind, 2007; Roetenberg, Luinge, and Slycke, 2009; Zhu and Zhou, 2004; Chen, Zhang, Hamel, and Tan, 2014; Kim, Kim, and Jang, 2018) can track the location of body sensors in real time by using inertial measurement sensors such as accelerometer, gyroscope, and magnetometer. However, this tracking is done on a central server instead of at each sending node by letting each sending node frequently send the inertial measurements to the server. As can be seen from Figures 5.3a and 5.3b, the movement of the body parts and the measured RSSI have a strong correlation, and exhibit a cyclic pattern for walking and running. This makes it possible to infer the real-time channel quality through the correlation with the motion data which can be easily obtained locally using an inertial measurement unit without any cost of communication or RSSI measurement. By enabling Chimp to remember the communication history at previously observed motion values, the overhead of channel relearning can be avoided, and each sending node will be able to select the best power level quickly. In the following, Chimp with gyroscope support is presented that exploits this idea.

5.3.1 Correlation Between Channel Quality and Motion Data

Experiments are carried out to investigate the correlation between motion data and RSSI during walking and running using an MPU-9250 sensor board (InvenSense, 2014) that integrates a 3-axis accelerometer, a 3-axis gyroscope, and a 3-axis magnetometer. In our experiments, the full-scale range of the accelerometer and gyroscope readings is adjusted to ± 2 g and ± 250 degrees per second (dps), respectively. Even though the use

of motion sensors can introduce extra energy consumption, the energy consumed for acquiring real-time motion data is negligible in comparison with the energy consumed by wireless communication. For instance, when the sampling rate is 31.25 Hz, the usage of current of MPU-9250 is only $19.8\mu A$ in low power mode. It is further reduced in some modern boards such as the MMA8491Q (Semiconductors, 2007) 3-axis accelerometer for which the usage of current is less than $400nA$ with ultra-fast data output time ($\sim 700\mu s$). During the experiments, the sending node encapsulates the motion data into packets and transmits them to the gateway at the rate of 20 pkt/s. When a packet is received at the gateway, its RSSI is firstly measured, and then the motion data and measured RSSI are recorded for processing.

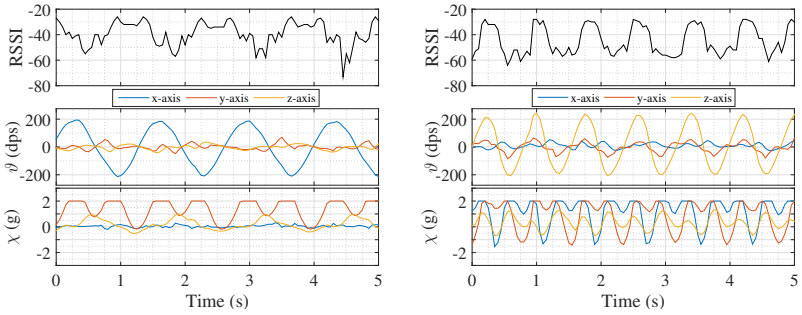

Figure 5.4: RSSI, acceleration and, angular velocity variation during (a) walking (b) running.

Figure 5.4 shows the RSSI, angular velocity (ϑ), and acceleration (χ) of five seconds of walking and running. Since the gateway is attached to the chest, the LoS path between the sending node and the gateway is regularly disconnected, and the RSSI fluctuates with a cyclic pattern that is very similar to a periodic sine wave, which was also reported in (Hauer, 2014a). In the same way, both acceleration and angular velocity exhibit a periodic pattern in most axes except that the changing frequency of acceleration is twice than those for RSSI and angular velocity. Hence, it can be concluded that there is a strong correlation between RSSI and motion data, which enables each sending node to estimate the RSSI (the channel quality) just by measuring the motion data.

Considering the channel samples and motion data as discrete time-series data, the correlation between RSSI and angular velocity or RSSI and acceleration can be discussed more precisely by calculating the Pearson's correlation coefficient (Sharma, 2005). Table 5.1 shows the correlation coefficients between RSSI and acceleration as

Table 5.1: Correlation Coefficients Between RSSI and Motion Data

Posture	$corr(RSSI, \vartheta)$			$corr(RSSI, \chi)$		
	x	**y**	**z**	**x**	**y**	**z**
Walking	0.91	0.71	-0.80	0.52	0.43	0.79
Running	-0.49	-0.80	-0.84	-0.74	-0.80	-0.50

well as the correlation between RSSI and angular velocity. The coefficients in the table are high enough to justify the correlation between RSSI and motion data in the test WBAN, which indicates that channel quality fluctuation in the current configuration (and possibly in many different configurations) can be predicted by monitoring the motion data. Since the motion data measured by accelerometer and gyroscope are from the same source (body movement), acceleration and angular velocity are correlated as well. However, unlike acceleration from the accelerometer, angular velocity from the gyroscope is less noisy and is unrelated to the strength of the outer forces. For example, when the subject is in an elevator or driving, the accelerometer may show some acceleration variation while the location of the sending node relative to the gateway has not been changed. Due to the reasons above, gyroscope data is chosen to be used for estimating channel quality.

From both Figure 5.4 and Table 5.1 and analysing different RSSI and motion data of different users, it can be observed that RSSI and angular velocity exhibit much stronger correlation on the axis with the highest peak-to-peak amplitude of inertial data. For example, the most robust correlation occurs on the x-axis for walking, but on z-axis for running. Since the measured gyroscope data from all three axes are from the same source, they are correlated and thus, it is better to select the axis with the highest peak-to-peak amplitude, however, multivariate correlation techniques can be applied. A simple axis detection module (Yang, He, and Yu, 2009) is used to detect the axis with the highest peak-to-peak amplitude in real time by monitoring the angular velocity on all axes. The axis detection algorithm works in the following three steps: it smooths the noisy signal, corrects the baseline, and detects the signal peaks. Since the gyroscope data is very smooth and not subject to drift, the axis detection algorithm can find the signal peaks with very low delay. The algorithm monitors the measured gyroscope samples on each axis and looks for the local extremums. To this end, it uses two variables to keep the latest observed local maximum and local minimum. Once the local extremums are not changed for a few samples, the peak-to-peak amplitude of the gyroscope signal on each axis is calculated by subtraction of the local extremums.

Finally, the axis with the maximum peak-to-peak amplitude is selected. Since the peak detection monitors only a small window of gyroscope samples within the short distance of a peak candidate, it does not impose a considerable computation overhead.

5.3.2 Chimp with Gyroscope Support

Motivated by the correlation between channel quality and angular velocity, the gyroscope support is integrated into Chimp so that it would be able to learn this correlation and estimate the channel quality through just locally measured angular velocity. However, despite the existence of such a correlation, there is no one-to-one mapping between their values. In fact, there are situations with equal angular velocities but different RSSIs. Figure 5.5 shows the RSSI measurement and its corresponding angular velocity (ϑ) and angular acceleration (Δ) for 3 seconds of walking and running. The angular acceleration is computed based on the measured angular velocity data. The small red asterisks in the angular velocity diagrams represent the time instances with almost equal angular velocities but different RSSIs. As can be seen from the angular acceleration diagrams, the sign (i.e., the direction) of the angular accelerations ($\delta \in \{+, -\}$) for such time instances are different. Hence, each pair of ϑ and δ can be mapped to a unique limited RSSI range. On the other hand, as shown in Figure 5.5, the channel quality is not fluctuating remarkably with a small variation of the angular velocity. Therefore, the angular velocity range $[-\Theta, +\Theta]$ is partitioned into k exclusive sub-ranges θ_1 to θ_k where $\bigcup_{m=1}^{k} \theta_m = [-\Theta, +\Theta]$ and $\theta_i \cap \theta_j = \emptyset \ \forall i, j \in \{1, 2, \ldots, m\}$. For the sake of

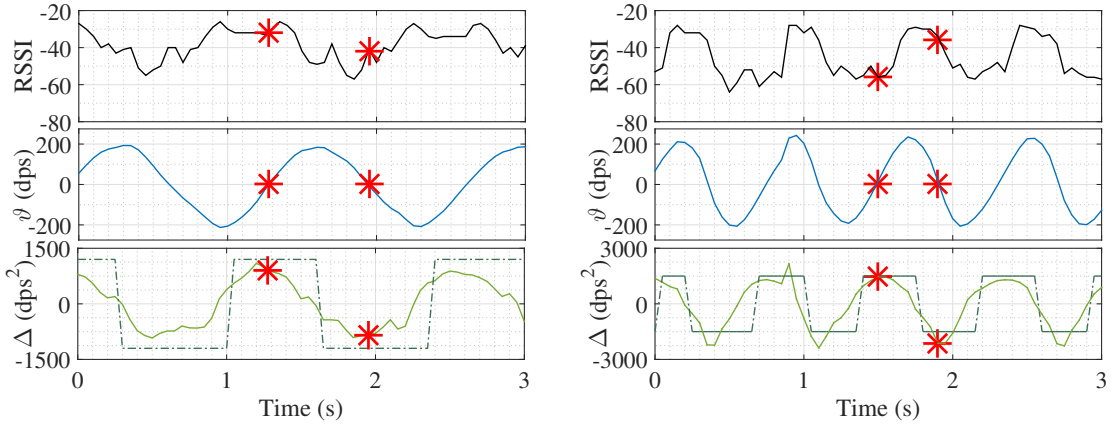

Figure 5.5: RSSI, angular velocity, and angular acceleration during (a) walking, (b) running.

simplicity of the explanation, all velocity sub-ranges are assumed to have equal length of $\frac{2\Theta}{k}$. Thus, each θ_m is defined as:

$$\theta_m = [(-\Theta + (m-1) \times \frac{2\Theta}{k}), (-\Theta + m \times \frac{2\Theta}{k})], \text{ where } m \in \{1, \ldots, k\}. \tag{5.7}$$

A separate internal state $s_{\{\theta_m,\delta\}}(t)$ is defined for each pair of θ_m and δ. Hence, the internal state of the learning automata at time t becomes

$$s(t) = \{s_{\{\theta_1,+\}}(t), \ldots, s_{\{\theta_k,+\}}(t), s_{\{\theta_1,-\}}(t), \ldots, s_{\{\theta_k,-\}}(t)\}.$$

Each internal state $s_{\{\theta_m,\delta\}}(t)$ is a set of probability $P_{\{i,\theta_m,\delta\}}(t)$ that represents the selection probability of a power level i under angular velocity range θ_m and angular acceleration sign δ, i.e., $s_{\{\theta_m,\delta\}}(t) = \{P_{\{1,\theta_m,\delta\}}(t), P_{\{2,\theta_m,\delta\}}(t), \ldots, P_{\{n,\theta_m,\delta\}}(t)\})$, where n is the number of power levels. Once a packet is generated at time t, Chimp measures the current angular velocity (ϑ) from the selected axis, maps it to the corresponding sub-range ($\left\lceil \frac{\Theta+\vartheta}{l} \right\rceil$), and calculates the average angular acceleration. Based on the calculated (θ_m, δ), it retrieves the corresponding internal state $s_{\{\theta_m,\delta\}}(t)$ and randomly selects a power level i based on the probabilities determined by $s_{\{\theta_m,\delta\}}(t)$ to transmit the packet. Depending on the feedback, Chimp updates $s_{\{\theta_m,\delta\}}(t)$ according to Eqn. (5.5). Note that the Chimp just updates $s_{\{\theta_m,\delta\}}(t)$, and the other internal states remain unchanged.

Algorithm 4 gives the pseudocode of Chimp. Roulette wheel selection (Back, 1996) is used to select the transmission power level based on the probabilities given in $s_{\{\theta_m,\delta\}}(t)$ (line 3-8). For small velocity sub-ranges, the channel quality is fixed in each sub-range and Chimp can minimise the expected transmission cost. By minimising the expected transmission cost in all sub-ranges, Chimp minimises the expected transmission cost in a dynamic posture like walking.

Complexity Analysis: The Chimp algorithm has two key modules: (1) the use of roulette wheel selection for power level selection (line 3-8), and (2) the update of the selection probabilities after the ACK packet is received (line 10-17). Since both modules have the complexity of $O(n)$ where n is the number of power levels, the time complexity of Chimp is $O(n)$. In our implementation Chimp requires roughly $10n + 17$ single arithmetic operations plus another 5 operations on average for the axis detection module. Since Chimp only uses power level 1, 3, and 7, it uses only about 52 single arithmetic operations per transmission. Such a low-complexity algorithm imposes very little energy overhead. Based on the TelosB platform, the energy consumed by computations in

Algorithm 4: Chimp pseudocode including roulette wheel for random power selection and learning module

Input : ϑ, δ

$m \leftarrow \lceil \frac{\Theta+\vartheta}{l} \rceil$; /* find the current angular velocity sub-range θ_m */

$fetch\big(s_{\{\theta_m,\delta\}}(t)\big)$; /* fetch corresponding internal state for the given θ_m and δ */

$P \leftarrow 0$; $i \leftarrow 0$;

$rnd \leftarrow rand()$; /* generate a random number in [0,1] */

do

  $i = i + 1$;

  $P = P + p_{\{i,\theta_m,\delta\}}(t)$;

while $rnd > P$;

$send(i)$; /* send packet with power level i */

if *ACK is received* **then**

  $p_{\{i,\theta_m,\delta\}} = p_{\{i,\theta_m,\delta\}} + \alpha_i \times (1 - p_{\{i,\theta_m,\delta\}})$;

  for $j = 1, \ldots, n$ **do**

    if $j \neq i$ **then**

      $p_{\{j,\theta_m,\delta\}} = (1 - \alpha_i) \times p_{\{j,\theta_m,\delta\}}$;

    end

  end

end

Chimp is around $56.4nA$ per each transmission. However, the energy consumed by the radio to send a 41-byte data packet using power level 7 is $9.9\mu A$, which is about 175 times more than the energy consumption on computation.

In Chimp the angular velocity range is partitioned into k sub-ranges with each sub-range having two classes. The state for each class is represented by the selection probabilities for n power levels. Therefore, the memory space complexity of Chimp is $O(nk)$. Please note that since n and k are usually small numbers (in our setup, n is 3, and k is 10), the memory complexity of Chimp is not high. Moreover, Chimp can be programmed to benefit from dynamic memory allocation. Therefore, it can adaptively add new classes when the fluctuation range of the angular velocity is increased (e.g., in dynamic postures) or remove the useless classes and free the allocated memory when the fluctuation range of angular velocity is decreased (e.g., in static postures).

5.4 Experimental Evaluation

In this section, the performance of Chimp is evaluated through many experiments based on the following three metrics as explained in Section 4.6: power level usage, energy consumption, and packet loss rate.

Parameter	Value	Parameter	Value
Power levels	$\{1, 3, 7\}$	Packet rate	0.1, 1, 20 pkt/s
Data packet length	41 Bytes	ACK packet length	13 Bytes
k	10	Number of participants	3
The length of each scenario	30 minutes	$\{\alpha_1, \alpha_3, \alpha_7\}$	{0.316, 0.0494, 0.005}

Table 5.2: Experiment parameters

5.4.1 Experiment Setup

The same setup as presented in Section 3.1 is adapted with the sending node attached to the wrist and the gateway mounted on the chest. The experiment parameters are summarised in Table 6.1. Power levels 1, 3, and 7 are chosen for transmitting 41-byte data packets. Similar to the experiments in the previous chapter, this setup assumes the packets are generated at a constant rate of 0.1 pkt/s, 1 pkt/s, and 20 pkt/s and are transmitted to the gateway according to IEEE 802.15.4 beacon-enabled MAC protocol. The experiments are performed on three participants. In each experiment, the participants were asked to stay in the following four representative postures in human's daily activities in the same indoor environment, with each posture lasting for 30 minutes: sitting with folded hand, standing upright, walking, and running. To fairly analyse the performance of Chimp, it is necessary to compare it with other well-known protocols (including ExPerio, DPPI, FLP, and FHP) under the same conditions. Hence, the same simulation setup with the same RSSI traces as presented in Section 4.6 is used. Moreover, Chimp is compared with the following two schemes:

(1) ATPS (Chapter 4): It monitors channel RSSI samples to exploit the spatio-temporal dependency between them through which, it can estimate the channel fluctuation pattern and schedule its transmissions.

(2) optimal scheme: The RSSI samples are collected for each experiment, based on what the best power level for each packet transmission is computed in an off-line

manner. That is, for each transmission, the optimal scheme knows the channel RSSI and accordingly selects the transmission power for communication with the lowest transmission cost.

5.4.2 Experiments with MAC Sub-layer Retransmission Disabled

For all experiments in this section, retransmission at the MAC sub-layer is disabled. Hence, for a given packet rate, the numbers of transmissions in all implemented schemes are the same. Once a new packet is generated the backoff period is randomly set between 0 to $2^{BE} - 1 \times t_{b_{off}}$ where $t_{b_{off}}$ is $320\mu s$ and BE (binary exponent) is initially set to macMinBE which is 3. Once the backoff is expired, the sending node performs clear channel assessment (cca) and sends the packet if the channel is free. Otherwise, the sending node increases the BE (considering that it should not be more than macMaxBE which is 5) and runs backoff period again. As previously mentioned, this set of experiments helps to analyse the impact of packet rate on the distribution of the power levels used for transmission in different protocols. Moreover, it provides a benchmark to compare and analyse the results for the scenario in which retransmission is enabled. Figure 5.6 shows the experimental results under three packet rates in terms of power-level usage, energy consumption, and packet loss rate. For the sake of clarity, the experimental results are discussed under the headings of *static* and *dynamic* postures, separately.

Static postures: In sitting, the performance of Chimp, ATPS, and DPPI is very close to that of the optimal scheme, especially in high packet rate cases. They transmit almost all packets using power level 1, consume roughly the same amount of energy, and deliver more than 94% of the packets. With the increase of packet rate, the performance of Chimp, ATPS, and DPPI is also improved. This is because: (a) Chimp needs to learn the channel quality at the beginning. In high packet rate scenarios, the learning automata can quickly converge to the optimal power level as it receives more channel feedback in very short time; (b) IGE model using by ATPS gets more channel feedback and thus, can exploit the channel burstiness and can estimate the channel state transition probability more accurately; (c) DPPI adjusts the transmission power based on the RSSI measurements of the past two packet transmissions. In high packet rate scenarios, the interval between two adjacent packet transmissions becomes small, which makes the channel estimation more accurate.

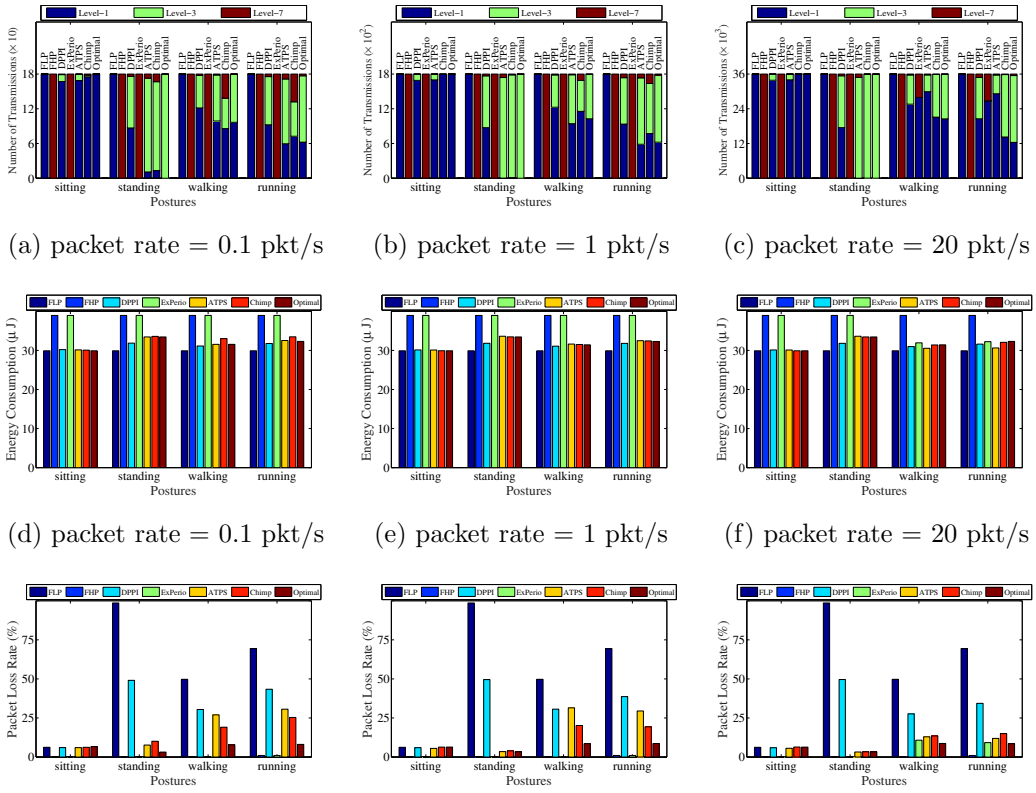

(a) packet rate = 0.1 pkt/s (b) packet rate = 1 pkt/s (c) packet rate = 20 pkt/s

(d) packet rate = 0.1 pkt/s (e) packet rate = 1 pkt/s (f) packet rate = 20 pkt/s

(g) packet rate = 0.1 pkt/s (h) packet rate = 1 pkt/s (i) packet rate = 20 pkt/s

Figure 5.6: Experiments with disabled MAC sub-layer retransmission under different data rates: (a), (b) and (c) show the distribution of power level usage; (d), (e) and (f) show the energy consumption; (g), (h) and (i) show the packet loss rate.

In standing, Chimp and ATPS perform as well as the optimal scheme and much better than DPPI. Despite the packet rate, DPPI always transmits half of the packets using power level 1 and another half using power level 3. However, it drops almost 50% of the packets. It is observed that the low performance of DPPI in standing is mainly because of the ping-pong effect as described in Section 2.3 and 4.6.3. ATPS has the same trend on power level used in different packet rates and always transmits below 4% of the packets using power level 7. But, increasing the packet rate to 20 pkt/s improves the performance of Chimp. It reduces the selection probability of power level 7 to about 0 and achieves a low packet loss rate of 3.4%, almost as well as the optimal scheme.

In different static postures, ExPerio and FHP transmit using power level 7, produce the maximum potential interference, and consume much more energy than that for Chimp. Conversely, FLP always transmits using the minimum power level. It consumes the minimum amount of energy and potentially produces the minimum interference but

delivers a few percent of the packets in standing.

Dynamic postures: For both walking and running, the distribution of power levels used in Chimp approaches that of the optimal scheme with the increase of packet rate. When the packet rate is 0.1 pkt/s, Chimp uses more power level 7 due to the impact of channel learning. Increasing the packet rate to 1 pkt/s reduces the usage of power level 7 to one-third of that at 0.1 pkt/s. In the same scenario, Chimp delivers 10% more packets than that of ATPS in both walking and running, while the two protocols consume almost the same amount of energy. With the increase of packet rate, the percentage of transmissions that use power level 7 is reduced since the best transmission power level can be quickly obtained with more channel feedback. When the packet rate is 20 pkt/s, the distribution of power levels used in Chimp perfectly matches that in the optimal scheme. Even though ATPS transmits more packets using power level 1, it cannot achieve a lower packet loss rate and energy consumption. Moreover, the packets must undertake some transmission delay. Similarly, DPPI transmits most of packets using power levels 1 and 3 but, the distribution of power level usage does not change much for different data rates. Moreover, it drops many packets—at a rate up to two times higher than that of Chimp. It is worth considering that, when the data rate is set to 0.1 pkt/s and 1 pkt/s, ExPerio still behaves as FHP because it cannot get enough channel feedback to detect the channel peak. Therefore, it potentially produces the maximum interference and consumes the maximum energy.

When the data rate is 20 pkt/s, ExPerio can detect the channel peaks and schedule the packets to be opportunistically transmitted at the channel peaks. Using opportunistic transmission, ExPerio transmits more than 75% of the packets using power level 1 but adjusts the maximum power level of the rest of transmissions. In walking and running, ExPerio has a smaller packet loss rate than Chimp while they almost consume the same amount of energy. The analysis of real measurements reveals that the transmission delay imposed by ExPerio and ATPS is about 10.4 and 5.6 slots on average in walking and running, respectively. This makes ExPerio and ATPS not suitable for applications with stringent delay requirements such as motion tracking and gaming. Moreover, ExPerio does not benefit from the use of power level 3 and is sensitive to any change in motion patterns. Once three consecutive packets transmitted with power level 1 are lost, ExPerio assumes the channel pattern has been changed and starts the detection and learning phase again, which consumes more energy. Above all, ExPerio is computationally very expensive as discussed before, which negatively affects its usability in low-power resource-constrained body sensors. It is not surprising that both FLP and

FHP do not have good performance in dynamic postures due to the frequent change of channel quality.

5.4.3 Experiment with MAC Sub-layer Retransmission Enabled

Due to the critical nature of the patient's vital signals, health-related applications of WBANs require ultra reliable packet transmission with above 99% delivery rate (Henna and Sarwar, 2018). Thus, this section repeats the previous experiments with enabled retransmission at MAC sub-layer. That is, the communication protocols can retransmit a lost packet to provide more reliable communication. To do so, the IEEE 802.15.4 beacon-enabled MAC protocol illustrated in Figure 4.11b is used. Accordingly, the newly generated packet is transmitted during CFP. If the transmitted packet is lost, the sending node schedules the packet to be transmitted in CAP. The maximum number of retransmissions is set to 3, 15, and 15 for the packet rate of 20 pkt/s, 1 pkt/s, and 0.1 pkt/s, respectively. Once a packet is dropped, FLP and FHP do not make changes on their transmission power. ExPerio retransmits each lost packet with the maximum power level and DPPI adjusts its power level to a level between the current level and the maximum level. ATPS makes a new channel estimation and accordingly selects the appropriate power level and Chimp adaptively selects the power level for retransmission based on the selection probabilities of different power levels. Figure 5.7 shows the results of the experiments under different scenarios. Since retransmission is enabled, the packet loss rate of most of the schemes is almost reached to zero whereas their total number of transmissions and accordingly their average energy consumption is increased. Moreover, the total number of transmissions in different schemes are different due to the difference in packet loss rate. It turns out that the obtained experimental data is highly skewed with many small values and a few large values. To display the small values, the large values can cut through the plot area and are labelled with the real values.

Static postures: In sitting, Chimp, ATPS, and DPPI perform as well as the optimal scheme. Since they deliver almost all packets on their first transmission, enabling retransmission does not influence their performance remarkably. In standing, DPPI requires many packet retransmissions since it has very high packet loss rate as shown in subfigures (d), (e), and (f) of Figure 5.6, thereby consuming much more energy. Both Chimp and ATPS are the most energy efficient protocols in this posture as

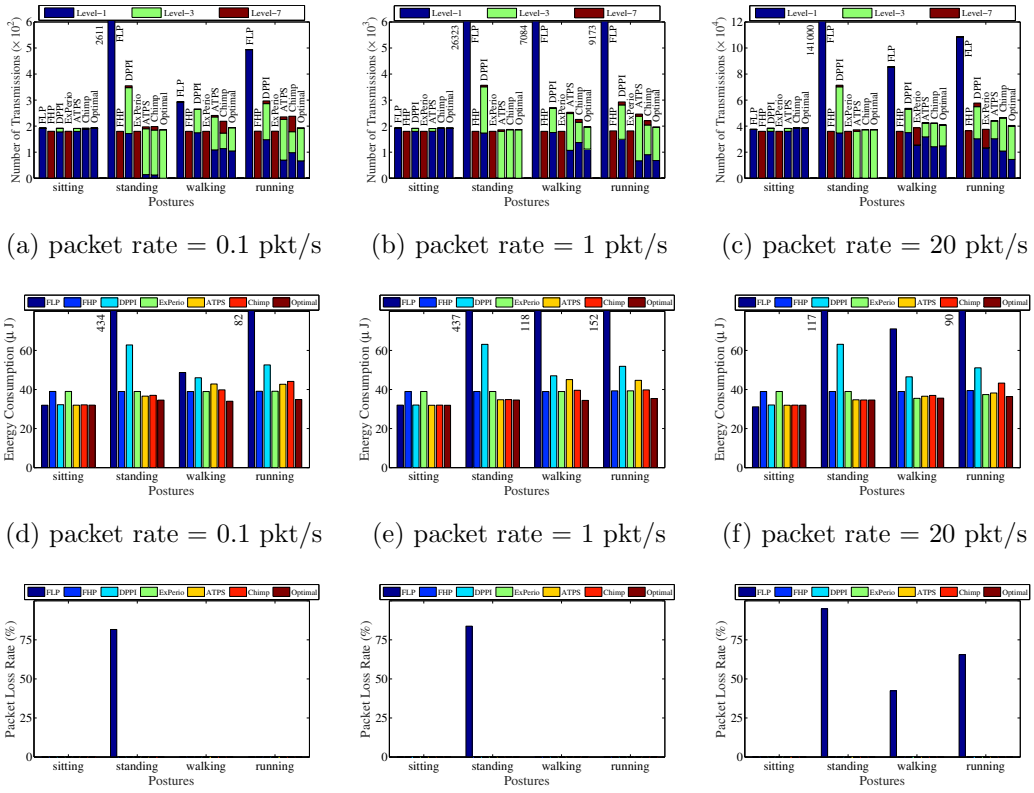

(a) packet rate = 0.1 pkt/s (b) packet rate = 1 pkt/s (c) packet rate = 20 pkt/s

(d) packet rate = 0.1 pkt/s (e) packet rate = 1 pkt/s (f) packet rate = 20 pkt/s

(g) packet rate = 0.1 pkt/s (h) packet rate = 1 pkt/s (i) packet rate = 20 pkt/s

Figure 5.7: Experiments with enabled MAC sub-layer retransmission under different data rates: (a), (b) and (c) show the distribution of power level usage; (d), (e) and (f) show the energy consumption; (g), (h) and (i) show the packet loss rate.

they are imposed by only a few percent of packet retransmission overhead, and their performance is very close to that of the optimal scheme regarding all the three evaluation metrics. Since both ExPerio and FHP use the maximum power level, they deliver nearly all of the packets on the first transmission. Therefore, the overhead of enabling retransmission on the performance of ExPerio and FHP is negligible. However, they consume more energy and possibly produce much more interference in comparison with Chimp and ATPS. As shown in Figure 5.7, all schemes except FLP achieve nearly 100% on packet delivery reliability. Since FLP uses a fixed low transmission power, the channel quality is very bad in standing, and almost all transmissions failed. Hence, enabling retransmissions significantly increase the energy consumption without much improvement in communication reliability.

Dynamic postures: Chimp has the same trend on power level used in walking and running. With the increase in data rate, the distribution of power level used in Chimp is

very close to that of the optimal scheme. As can be seen, at the packet rate of 1 pkt/s, Chimp is the most energy efficient protocol. It consumes below 90% of the energy used by ATPS. As previously shown, when retransmission is disabled, the packet loss rate of Chimp at low packet rate scenarios is slightly high, though it is usually lower than that of ATPS. Hence, enabling packet retransmission increases the number of transmissions and accordingly imposes some energy overhead in these scenarios. However, the impact of retransmission overhead can be ignored if the posture lasts longer. Except in the running at 20 pkt/s, where ATPS predicts the channel peaks very well, the total number of transmissions of Chimp is lower than that of ATPS.

Enabling retransmission imposes a considerable overhead to DPPI. On average, it transmits 25% more than that of Chimp in both walking and running which also increases its energy consumption to up to 35% higher than that of Chimp. The performance of ExPerio in low packet rate scenarios is the same as the performance of FHP. They both use the maximum power level and deliver almost all packets on the first transmission. Therefore, the retransmission overhead is negligible but at the cost of possibly producing much more interference. At the packet rate of 20 pkt/s, ExPerio reduces its energy consumption by opportunistically transmitting many packets using power level 1. Since it delivers about 90% of the packets on the first transmission, enabling retransmission does not impose a remarkable overhead. In walking, the number of transmissions in ExPerio is comparable to that of Chimp. However, it potentially produces much more interference. As previously explained, FLP has the maximum energy consumption and its number of retransmissions is much more than that of other schemes because a lost packet is retransmitted until the LoS path becomes available or the number of retransmissions reaches the maximum.

In summary, Chimp is a reinforcement learning-based communication protocol that can work efficiently in both static and dynamic postures. ATPS does not work well for dynamic postures when the packet rate is low. In other words, when the packet rate is low, the IGE channel model used by ATPS does not get enough feedback to exploit the channel state transition probability and predict the channel peaks. This is the same for ExPerio. Although the performance of Chimp is highly dependent on the packet rate as well, its performance is quickly improved even in low packet rate scenarios as the posture lasts longer because, instead of measuring channel RSSI, it monitors the locally measured gyroscope samples which are correlated with channel RSSI fluctuations.

5.4.4 Impact of k on the Performance of Chimp

Chimp benefits from the correlation between channel quality and gyroscope data so that it can estimate the channel quality just based on the locally measured angular velocity. The velocity range is partitioned into k sub-ranges, and Chimp learns the average channel quality in each sub-range. A set of experiments was conducted to evaluate the impact of k on the performance of Chimp. A participant was asked to walk for 30 minutes and the packet rate was set to 20 pkt/s. The experiment is repeated for different values of k from 2 to 34 with an equal gap of 4. As can be seen from Figure 5.8, different settings on k do not have a big impact on the distribution of power level selection and energy consumption but do make big differences on the packet loss rate. By increasing k from 2, the packet loss rate first decreases and reaches to the minimum when $k = 10$, and then increases and becomes relatively stable when $k > 20$. This can be explained as follows: for small values of k, each sub-range observes a broad range of RSSI samples with a large variance, and thus cannot reflect the instantaneous channel quality. On the other hand, when k is too large, Chimp will not be able to receive enough feedback to learn the channel accurately in each velocity sub-range.

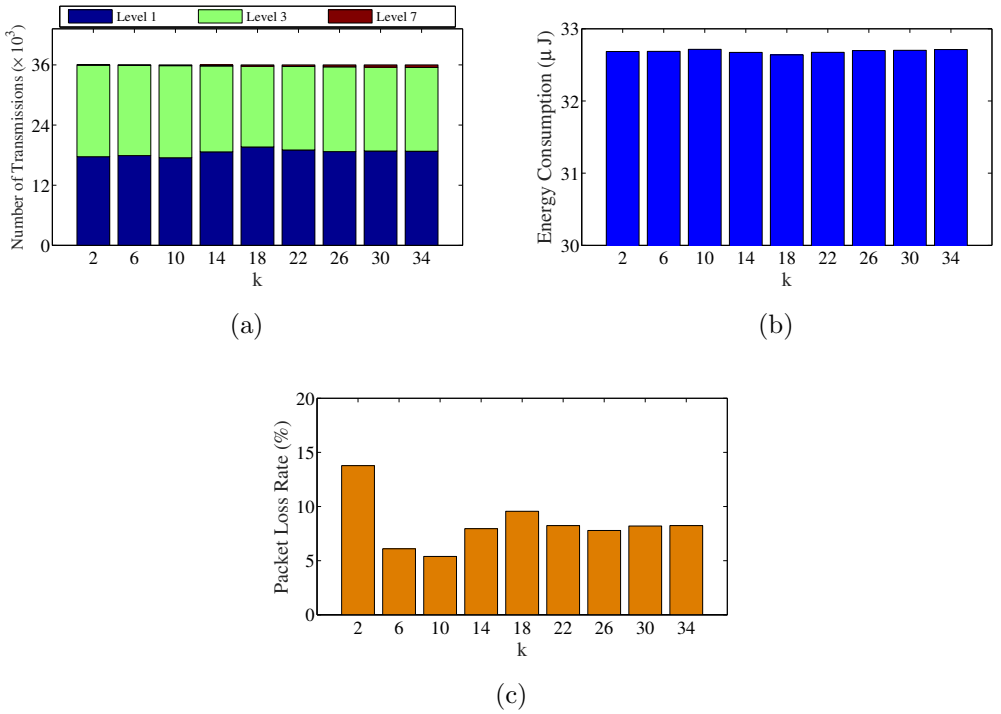

Figure 5.8: (a) distribution of usage of power levels, (b) energy consumption, (c) packet-loss rate

5.5 Discussion

Motivated by the idea of learning automata, this chapter introduced Chimp, a learning-based power-aware communication protocol for WBANs. Chimp is a lightweight communication protocol which adaptively adjusts the transmission power level of the sending node. It can self-learn the channel quality and can find the optimal power level to minimise the transmission cost. By conducting several experiments, it shown Chimp outperforms the state-of-the-art protocols in some of the designed scenarios, however, it still suffers from poor performance in extremely low packet rate scenarios. Because of its learning-based nature, it does not need any prior information about the network topology, body posture, or even the location of the sending node on the body. It exploits the correlation between body motion patterns and channel quality fluctuation, through which, it can locally estimate the channel without measuring the channel RSSI. Unlike ATPS that might be affected by noise from illegitimate transmitters, Chimp gradually increases the selection probability of higher power levels to overcome the noise. Chimp supports dynamic postures even in low packet rate scenarios. However, because of the trial and error nature of Chimp, its learning speed is relatively low and its performance in scenarios with extremely low transmission rate or in scenarios which does not last long is significantly degraded. Moreover, since it exploits the correlation between body motion patterns and channel fluctuation pattern, it only supports those physical activities that show a periodic motion pattern (e.g., walking and running) or static motion pattern (e.g., sitting). Hence, if the user moves his body parts randomly, Chimp cannot find the optimal power. The next chapter investigates the impact of combining the learning ability of Chimp with information about the real-time location of the sending node. It is expected that by knowing the real-time location, the sending node can quickly find the optimal communication power level, through which it can perform well in scenarios with extremely low packet rates.

Chapter 6

Tuatara: Learning, and Location-based Power-adaptive Communication Protocol

6.1 Introduction

The Chimp protocol presented in the previous chapter uses learning-automata and exploits the correlation between channel quality and motion data provided by a local gyroscope to enable the sending node to self-learn the channel quality. Although Chimp achieves high performance in both static and dynamic postures even when the packet rate is relatively low, it has a few **drawbacks** as below: (1) Since Chimp has no prior knowledge about the channel quality and since it learns the optimal power level through trial and error, its learning time directly depends on its number of trials (i.e., transmissions). Hence, its performance is considerably decreased in applications with extremely low packet rate, especially when the subject's activity is frequently changed. (2) Since Chimp benefits from the correlation between the channel quality and the periodic motion patterns of the sending node, it has to relearn the correlation whenever the motion patterns are changed (for example when the subject changes his walking speed). Relearning the channel quality imposes a considerable overhead to the sending node. (3) When the motion patterns are aperiodic or when the subject moves his body parts randomly or casually, for example, when the subject pulls out his hand from his pocket to grab a cup, Chimp cannot find the optimal power level quickly because its learning speed is too low to learn the channel in a small fraction of time.

The experimental results presented in Table 3.1 (Chapter 3) revealed the correlation

between the location of the sending node and the channel quality. Hence, a desirable solution to overcome the mentioned problems in Chimp is to simply enable the sending node to know its location relative to the gateway before transmission so it can estimate the channel quality and adaptively adjust its transmission power level to the optimal level. Although this solution looks very straightforward, three **key challenges** need be addressed first: (1) how can each sending node locally know its location before transmission with insignificant communication overhead? (2) how can each sending node choose the optimal transmission power level at each location? (3) how to deal with short term and long term channel fluctuation due to frequent blockage by body parts, while the location of the sending node is fixed? For example, when part of the user's clothes accidentally blocks the LoS communication path.

In this chapter, Tuatara, a novel power-adaptive communication protocol, is presented to enable each sending node to quickly find the optimal transmission power level in all postures. It supports a wide range of applications in WBANs from applications with extremely low packet rate scenarios to applications with periodic high packet rate, whether the body part movement is a random movement, or it has a periodic pattern. Tuatara is a location-aware communication protocol which adjusts the transmission power level according to the location of the sending node. To estimate the location of the sending node, it utilises the forward kinematic model of body movement and combines the anatomical constraints on movements of body parts with the locally measured orientation of the sending node captured by inertial sensors. Assuming a prior knowledge of the average channel quality in different locations is provided, Tuatara predicts the channel once the location of the sending node is estimated with a reasonable communication and processing overhead. The key contributions of this chapter are as follows:

- A set of systematic experiments using the TelosB platform is conducted to accurately measure the channel RSSI in different locations around the human body. Experimental result confirms the correlation between the location of the sending node and the channel quality. Moreover, it reveals that small changes in the location of the sending node do not considerably affect the channel quality. Accordingly, a rough estimation on the location of the sending node is enough to select the optimal transmission power level.

- A localisation algorithm is proposed to enable the sending node to locally estimate its location relative to the gateway. This algorithm combines anatomical

limitations of human body movements with the orientation information of the sending node captured by motion sensors.

- Tuatara, a location-based communication protocol is proposed that can adjust its transmission power level based on the real-time location information provided by the location estimation algorithm and prior knowledge about the channel quality in each location. Since the channel quality between the sending node and the gateway is not constant, even when the location of the sending node is fixed (as it might be unexpectedly blocked by clothes or other objects), Tuatara is extended to benefit from the learning ability of Chimp. So, it can monitor the history of communications in every single location and can learn the channel and adjust the transmission power level to the new optimal level whenever the channel is changed.

- The performance of Tuatara is evaluated through many experiments on the TelosB sensor motes under different packet rates and physical activities. Then, the results are compared with Chimp and ATPS as well as optimal power assignment that is calculated off-line. The experimental results show Tuatara outperforms Chimp in almost all scenarios, especially when the packet rate is low. Compared to ATPS, Tuatara reduces the potential interference in low packet rate scenarios and saves more energy. Although in high packet rate scenarios ATPS may perform slightly better, it is at the cost of imposing some transmission delay to the sending node.

The rest of this chapter is organised as follows: Section 6.2 discusses the correlation between the channel quality and the location of the sending node and presents the motivations. Section 6.3 gives a short overview of Tuatara. In Section 6.4 the idea of orientation estimation using inertial data and anatomical limitations of human body movements is discussed. Power level selection scheme is presented in Section 6.5. The learning algorithm and the computation overhead of Tuatara is discussed in Section 6.6. Section 6.7 presents the experimental results and Section 6.8 concludes this chapter and discusses the future work.

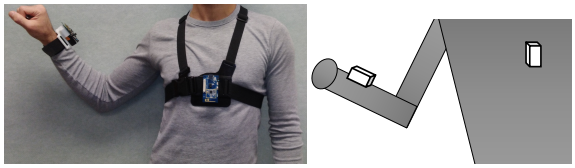

(a) (b)

Figure 6.1: Setup of the experiment.

6.2 Experimental Characterisation of Channel Behaviour

To systematically investigate the channel behaviour and its relationship with the location of the sending node, a series of experiments are carried out using the TelosB sensor motes. Similar to the previous experiments, the setup in the experiments in this chapter includes a wrist mounted sending node communicating with a gateway attached to the chest as shown in Figure 6.1. However, our proposed scheme is not limited to this setup, and can support different setups regardless of the location of the sending nodes.

Since the movement of the shoulder joint is a spherical rotation (Cheng, 2000), a spherical coordinate system centred at the shoulder as shown in Figure 6.2a is used to uniquely define the location of the wrist relative to the shoulder. In this coordinate system, the z-axis is parallel to the body trunk with $+z$-axis pointing upward from the leg to the head, x-axis is parallel to the shoulder line with $+x$-axis pointing out from the right shoulder, and the y-axis is perpendicular to the xz plane with $+y$-axis in front of the trunk. As illustrated in Figure 6.2b, every single relative location of the wrist can be defined using spherical coordinates (d, α, β) where

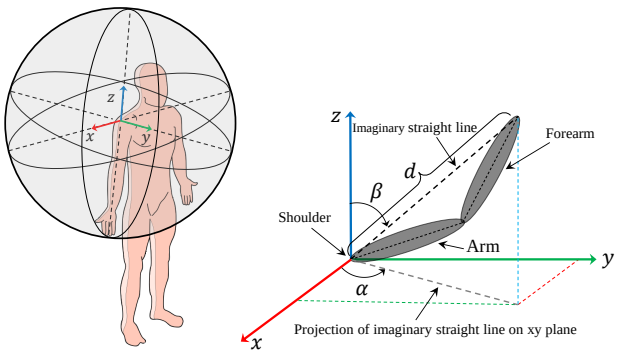

(a) (b)

Figure 6.2: (a) Shoulder centred coordinate system, (b) Location of the wrist is identified by a triple of (d, α, β).

d: length of the imaginary straight line that connects the wrist to the shoulder.

α: angle between $+x$ axis and the projection of the imaginary straight line onto the xy plane in anticlockwise direction.

β: angle between imaginary straight line and $+z$ axis.

Since the location of the shoulder relative to the gateway is almost constant, the location of the wrist relative to the gateway can be easily calculated by adding the coordinates of the shoulder relative to the gateway. The area around the shoulder is

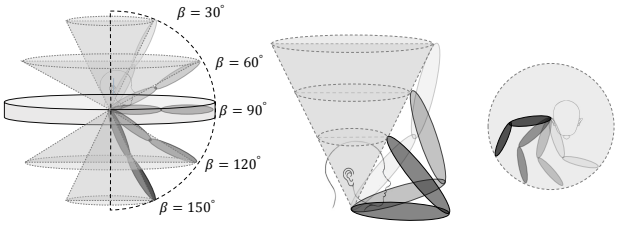

(a) (b)

Figure 6.3: (a) Partitioning the area around shoulder into cones. (b) bending elbow and moving arm and forearm horizontally to sweep all locations on the surface of a cone.

partitioned into a couple of cones as shown in Figure 6.3a. The spherical coordinates of all locations on the surface of the same cone have the same β. To sweep all locations on the surface of a single cone, the other two parameters d and α are changed accordingly. Assuming L is the length of arm plus forearm, d is set to take values from $\{L, \frac{3}{4}L, \frac{1}{2}L, \frac{1}{4}L\}$ by bending the elbow as illustrated in Figure 6.3b. For each value of $\{\beta, d\}$, the subject moves his arm and forearm horizontally to increase α step by step from its minimum to its maximum accessible value with a step size of 20°. Figure 6.4 shows the top view of the movements for different settings of α and d, when $\beta = 90^o$.

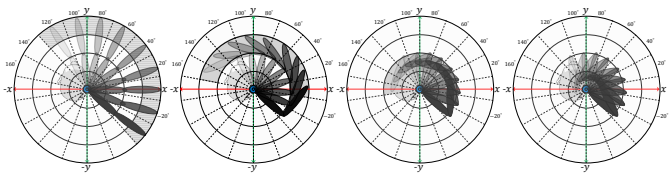

(a) $d = L$ (b) $d = \frac{3}{4}L$ (c) $d = \frac{1}{2}L$ (d) $d = \frac{1}{4}L$

Figure 6.4: Top view of a single cone and sweeping the accessible locations by changing α.

(a) (b)

Figure 6.5: A physiotherapist assists the subject to keep his wrist in the right location.

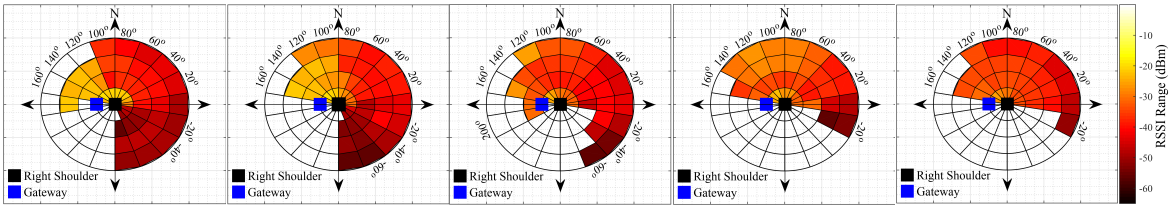

(a) $\beta = 30°$ (b) $\beta = 60°$ (c) $\beta = 90°$ (d) $\beta = 120°$ (e) $\beta = 150°$

Figure 6.6: RSSI heat map in different locations around the gateway.

During the process of collecting RSSI samples, a physiotherapist assisted the subject and set his wrist in the predetermined locations by measuring the angle and the distance using a goniometer and a metre, as illustrated in Figure 6.5. At each accessible location, the sending node transmits 1000 packets to the gateway with power level 32, and the gateway measures the RSSI of each received packet. Assuming the subject is facing north, Figure 6.6 shows the summarised top-view RSSI heat map of communication with power level 32 in all accessible locations. As is expected, the experiment results confirm the relationship between the relative location of the sending node and the channel quality.

To further analyse the results, the optimal transmission power level at each location is calculated based on a four steps method presented in Chapter 5 that is: (1) A transmission power level set of three power levels {1, 3, 7} are used for communication as is already justified in Chapter 3. (2) As previously presented the transmission cost of a power level i is defined proportional to its signal power over its communication reliability. (3) Through RSSI mapping method, the communication reliability of power levels (Level 1, 3, and 7) is obtained and since the transmission signal power of all power levels are known, the transmission cost of all power levels at each channel quality (represented by channel RSSI of power level 32) can be calculated. (4) Then, for each location with an available average RSSI, the power level with the minimum transmission cost is selected as the optimal power level. Figure 6.7 shows the optimal transmission

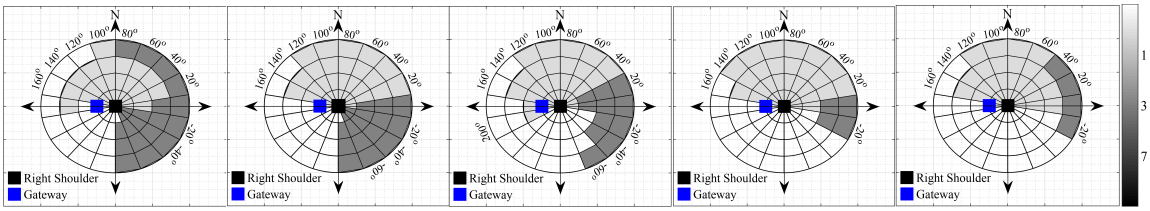

(a) $\beta = 30^\circ$ (b) $\beta = 60^\circ$ (c) $\beta = 90^\circ$ (d) $\beta = 120^\circ$ (e) $\beta = 150^\circ$

Figure 6.7: Optimal power level in different locations around the gateway.

power level at each location.

According to the results, the **key observations** are: (1) Although the results confirm the relationship between the channel quality and the relative location of the sending node, it also shows the channel quality (and consequently the optimal transmission power level) is not sensitive to the small changes of the location of the sending node. More precisely, the channel quality of the locations (i.e., the sub-zones) in the same neighbourhood is almost similar. These observations also implicitly reveal that the channel quality more depends on horizontal movements (changing α) than vertical movements (changing β). (2) Power level 1 is the optimal power level in most of the locations close to the gateway with available LoS path to the gateway and power level 3 is the optimal power level in locations with a long distance or with blocked LoS path to the gateway. Hence, power level 7 is not necessary except in those situations the channel is suffering from a long-term deep fading. For example, when the subject is sleeping with his wrist beneath his body.

The **key conclusion** based on the above observations is that energy efficient and low-interference reliable power adaptive communication is possible if the sending node can locally estimate its relative location. In other words, since the optimal power level in a wide range of locations is almost constant, a rough estimation of the location of the sending node can provide acceptable performance.

6.3 Overview of Tuatara

The key idea of Tuatara is to explore the correlation between the channel quality and the position of the sending node relative to the gateway to dynamically adjust the transmission power, aiming to save energy, reduce interference, and improve communication reliability. There are two challenges in implementing such an idea in WBANs:

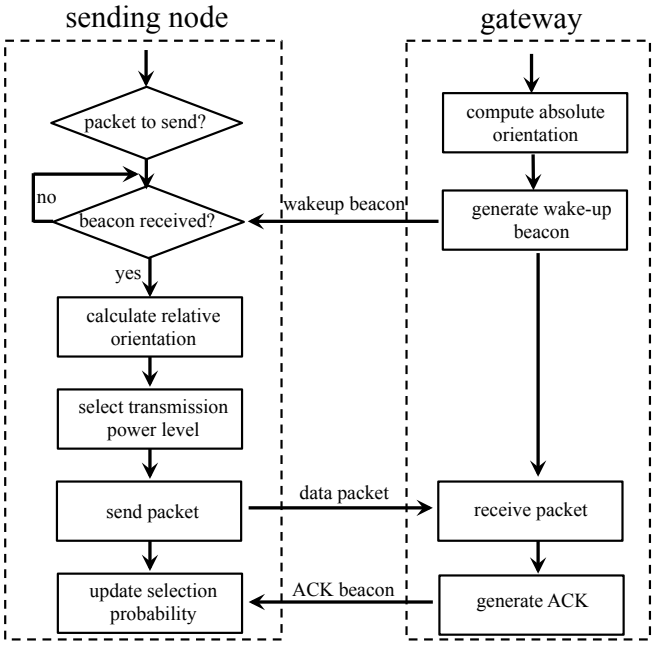

Figure 6.8: Flowchart of Tuatara

(1) each sensor node should have a priori knowledge on the relationship between channel quality and relative position for all accessible locations, i.e., the best power level for each accessible location; (2) each sending node can obtain its location relative to the gateway instantaneously. The first challenge can be addressed through a measurement campaign as depicted in Section 6.2. Since the human body ratios for different people are more or less the same, such knowledge can be pre-coded in the sensor nodes and further refined through reinforcement learning based on the communication between the sensor node and the gateway to characterise the minor difference among users. The focus of the rest of this chapter is on addressing the second challenge.

Tuatara uses a modified version of RI-MAC (Sun, Gurewitz, and Johnson, 2008), a receiver-initiated medium access control protocol in which a sensor node can transmit packets only after it receives a wakeup beacon from the gateway. The flowchart of Tuatara is shown in Figure 6.8. It has the following three key modules:

- **Localisation module**: following the forward kinematic model, this module estimates the instantaneous relative location of the sending node at a coarse-grain level by combining the orientation captured by an IMU with the anatomical constraints in body movements. The accessible area around the human body is partitioned into several blocks based on parameters α, β and d in the classical spherical coordinate system. This module outputs the block(s) in which the

sending node might be located.

- **Power level selection module**: the localisation module can output multiple blocks due to the infeasibility in obtaining accurate location estimation using a single IMU, especially if the sensor node is attached to the body part such as the wrist that connects to the body trunk through the elbow joint. Moreover, a single block can contain multiple sub-zones with different optimal power levels, depending on the granularity of block partition. Hence, a probabilistic power selection method is used in Tuatara. A vector of power selection probabilities $\{p_1, p_2, \cdots, p_n\}$ is defined so that p_i is the probability of selecting power level i as the transmission power level and n is the number of power levels. This module will compute the optimal vector of power selection probabilities based on the output of the localisation module and the correlation between channel quality and relative position, aiming to minimise the transmission cost metric given in Section 6.2. The actual power level used for packet transmission is selected according to the probabilities given in the optimal power level selection vector.

- **Learning module**: due to the slight difference in body ratios for different users, the optimal power level selection vector corresponding to each block needs to be refined. Moreover, it can change over time due to the changes of the propagation environment, e.g., changing clothes and rooms, interference from other un-coordinated WBANs, etc. This module refines the selection probability vector for each block based on the ACK beacon in RI-MAC using a trial and error learning mechanism.

The cost metric given in Chapter 3 does consider the impact of interference. Based on this metric, Tuatara will choose a low transmission power level if it can achieve good communication reliability. In the presence of interference from other co-existing networks, the learning model will adjust the power level probabilities to maintain good communication reliability. It can be further combined with other strategies such as channel switching to mitigate interference, however, such a combination is out of the scope of this thesis.

6.4 IMU-based Location Estimation

In order to determine the location of the wrist relative to the chest (i.e., the sending node relative to the gateway) a basic skeletal model (a tree of joints) with two joints

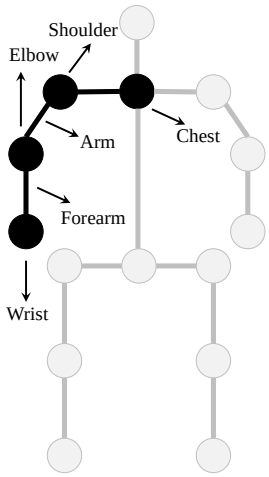

Figure 6.9: Basic skeletal body model

(shoulder and elbow) and three links (chest, arm, and forearm) is used as is shown in Figure 6.9. There are two kinematic models to describe the movement of such an articulated body model:

- **Inverse kinematics:** It aims to find the body posture and set the joint angles assuming the location of the leaf nodes in the tree model (i.e., the wrist in this case) is known (Young, 2010; Aristidou and Lasenby, 2009). In other words, inverse kinematics models the possible angles of joints through which the known location of the leaf nodes can be met. To do so, inverse kinematics applies complex body motion models and movement constraints to the joint angles and uses computationally expensive heuristic algorithms to find the most possible body postures. Inverse kinematics has many applications in different areas of computer science. In robotics, inverse kinematics is used to determine and control the possible orientation of a chain of arms so that the end-effector can reach to a desirable location (Murray, 2017; Glower, Agasti, Bakke, Johnson, and Ratan, 2018). It is also used in computer graphic and video games (Aristidou, Lasenby, Chrysanthou, and Shamir, 2018) to animate and control virtual objects and creatures. Inverse kinematics is very popular in the field of biomechanical modelling (Trinler and Baker, 2018), computer-aided ergonomics (Miehling, Schuhhardt, Paulus-Rohmer, and Wartzack, 2015), and rehabilitation medicine (Murphy, Rammer, Vinehout, Caballero, Cornwell, Fritz, and Harris, 2018) where the human models are developed for simulation and prediction purposes.

- **Forward kinematic:** It aims to find the relative location of the leaf nodes only

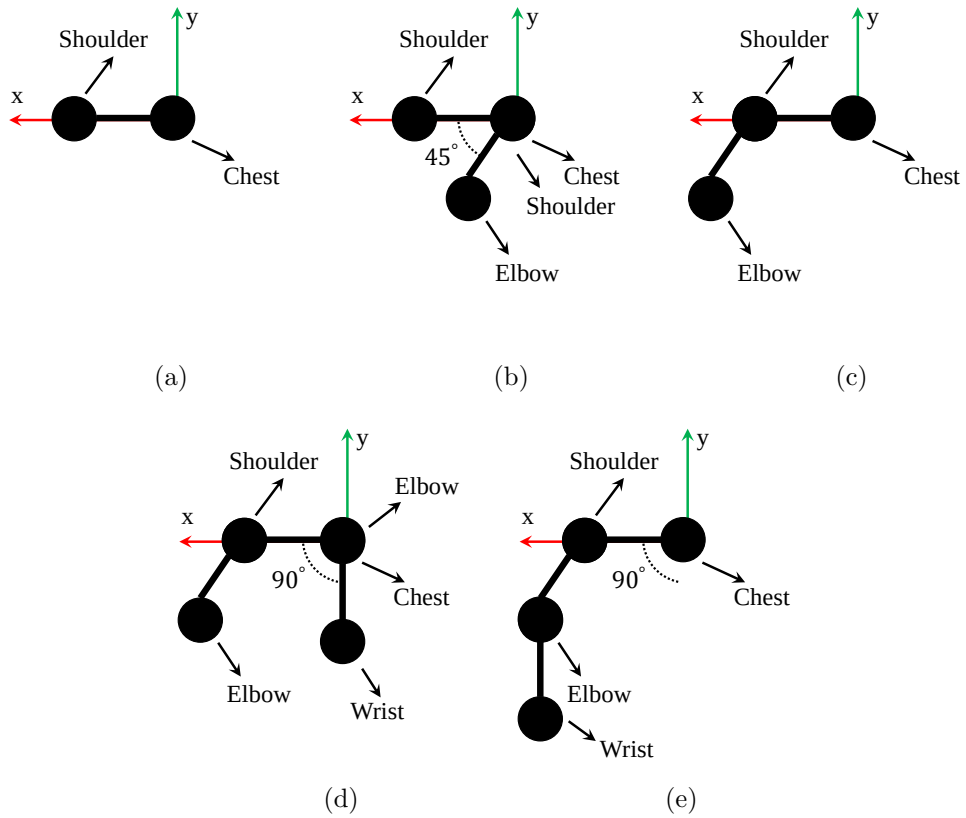

Figure 6.10: The process of applying forward kinematics in a simple 2-dimensional example of localisation of the wrist

by knowing the length and the relative orientation of the links (arm and forearm in this case). Consider the chest as the root of the tree, the location of the wrist can be found by traversing the tree starting from the chest and applying the orientation and accumulating the position as each joint is traversed. Figure 6.10 shows the process of applying forward kinematics model in a simple 2-dimensional example to find the location of the wrist relative to the chest. Assume the subject's arm and forearm have a 45° and 90° rotation, respectively, in counterclockwise direction. At the first step of applying forward kinematics, the unrotated vector $\vec{s}$ from chest to the shoulder is placed at the origin of the coordinate system (Figure 6.10a). Similarly, in the second step, the unrotated vector $\vec{a}$ (representing the subject's arm) is placed at the origin of the coordinator system. Then, it is rotated 45° (Figure 6.10b) and added to $\vec{s}$ (Figure 6.10c) to yield the final location of the elbow, relative to the chest. At the third step, the same process is applied to the vector $\vec{f}$ (representing the subject's forearm). That is, the unrotated $\vec{f}$ is placed at the origin of the coordinate system. Then, it is rotated 90° (Figure 6.10d)

and added to the $\vec{a}$ (Figure 6.10e) to give the location of the wrist relative to the chest.

Many IMU-based motion tracking solutions have been developed that utilise forward kinematics and can achieve even centimetre-level localisation accuracy (Young *et al.*, 2007; Roetenberg *et al.*, 2009; Salehi, Bleser, Schmitz, and Stricker, 2013; Tjhai and O'Keefe, 2019). However, these schemes are not suitable for the design here due to the following two reasons: (1) multiple IMU sensing devices are needed to track flexible body segments such as arm and leg, which not only increases the system cost and complexity but also reduces the system practicability; (2) each IMU sensing device needs to frequently send its measurements to a central device (e.g., a PC) where locations of the sensing devices are calculated. To facilitate location-based power level selection, the calculated location must be sent back to each sensor node timely before each transmission, which is not only infeasible due to quick changes on postures but also does not worth it due to the large energy overhead caused by the two-way communication.

Since highly accurate location estimation is not necessary for power level selection, a novel IMU-based location estimation algorithm is designed that allows each sensor node to *locally* estimate its rough location in real time without the need of any extra IMU sensing device. The **key idea** of the algorithm is to combine the biomechanical constraints of body movements with the measured orientation of the sending node relative to the gateway. Since the absolute orientation of the gateway is carried in every beacon message for either wakeup or acknowledgment, each sending node can instantaneously calculate its orientation relative to the gateway based on its local IMU measurements and the received gateway orientation. As illustrated in

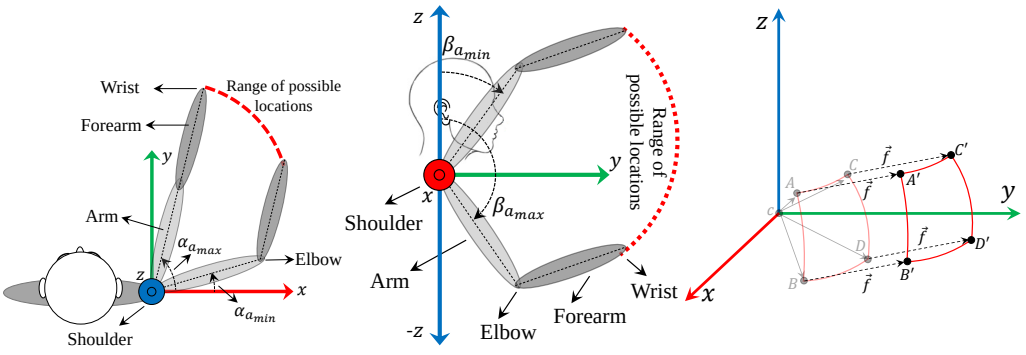

Figure 6.11: *RoPL* of the wrist relative to the shoulder in different views (a) top view, (b) side view, (c) front view.

Figure 6.11a and 6.11b, for any given orientation of the forearm, the orientation of the arm, represented by (α_a, β_a), is constrained by the biomechanical constraints of arm movements, that is,

$$\alpha_{a_{min}} \leq \alpha_a \leq \alpha_{a_{max}}, \quad \beta_{a_{min}} \leq \beta_a \leq \beta_{a_{max}}.$$

Here, the imaginary line in Figure 6.2b coincides with the straight dotted line in the arm. Assuming the lengths of arm and forearm are known a priori, the Range of Possible Locations (*RoPL*) of arm can be estimated based on $[\alpha_{a_{min}}, \alpha_{a_{max}}]$ and $[\beta_{a_{min}}, \beta_{a_{max}}]$, and then the *RoPL* of the wrist (i.e., sending node) can be calculated by further taking into account the length of the forearm and its relative orientation, as illustrated in Figure 6.11c. In what follows, the details on calculating the relative orientation of forearm, quantifying the anatomical constraints of arm, and calculating the *RoPL* of the wrist is presented.

6.4.1 Calculation of Relative Orientation for Forearm

$\{\alpha_f, \beta_f\}$ is used to represent the orientation of the forearm relative to the human body trunk. Figure 6.12 illustrates the three-step routine used to calculate $\{\alpha_f, \beta_f\}$.

The *first step* is to generate the absolute orientation of the forearm relative to the earth based on the IMU measurements. Madgwick filter (Madgwick, 2010), a lightweight fusion algorithm, is used at the sending node to locally combine all inertial motion data measured by MPU-9250 into a single quadruple quaternion ($q = [q_o, q_x, q_y, q_z]$) to represent the absolute orientation of forearm in 3D space. Quaternion-based representation is used since it is safe from gimbal lock problem (Kane, Likins, and Levinson, 1983; Mitchell and Rogers, 1965; Spring, 1986) and has less complexity than other methods such as Euler angles (Favre, Jolles, Siegrist, and Aminian, 2006). Throughout this section, the quaternion notation system presented in (Craig, 2005) is used, in which ${}^b_a q$ represents the orientation of segment (or frame) a relative to segment b. Accord-

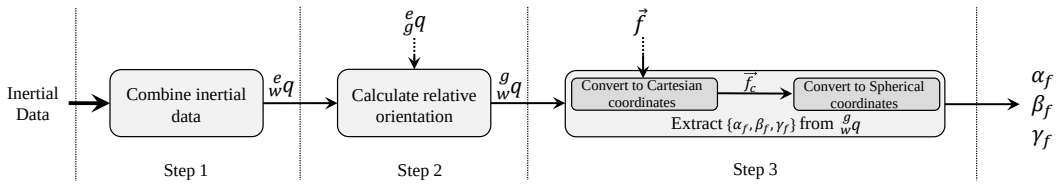

Figure 6.12: State diagram of extracting the relative orientation of the sending node at wrist from inertial data

ingly, ${}^{e}_{w}q = \{{}^{e}_{w}q_o, {}^{e}_{w}q_x, {}^{e}_{w}q_y, {}^{e}_{w}q_z\}$ is the quaternion-based representation of the absolute orientation of the wrist (w) relative to the earth (e).

The *second step* is to calculate the orientation of the forearm relative to the gateway attached to the body trunk, i.e., ${}^{g}_{w}q$. To this end, the gateway embeds its quaternion-based representation of its absolute orientation (i.e., ${}^{e}_{g}q$) into the wake up beacon packet. Then, the gateway periodically wakes up, following the RI-MAC protocol, and broadcasts a wakeup beacon including its absolute orientation $\left({}^{e}_{g}q\right)$ to inform sending node for communication. If the sending node has a data packet to send, it first extracts ${}^{e}_{g}q$ from the beacon packet and then calculates its relative orientation as below:

$$ {}^{g}_{w}q = {}^{e}_{w}q \otimes {}^{e}_{g}q^* \tag{6.1} $$

where $\otimes$ is quaternion product and ${}^{e}_{g}q^* = \{{}^{e}_{g}q_o, -{}^{e}_{g}q_x, -{}^{e}_{g}q_y, -{}^{e}_{g}q_z\}$ is the conjugate of ${}^{e}_{g}q$.

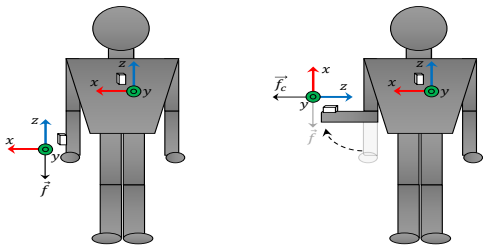

(a) (b)

Figure 6.13: Orientation of the wrist relative to the chest (a) anatomy position, (b) any other position.

The *third step* is to extract α_f and β_f from ${}^{g}_{w}q$. Figure 6.13a shows the anatomical posture where the sending node and the gateway have the same orientation. Take anatomical posture as a reference and assume $\vec{f} = \{f_x, f_y, f_z\}$ is a 3D vector representing forearm in the Cartesian coordinate system in this posture. Therefore, any orientation of forearm relative to the gateway (Figure 6.13b) is shown by $\vec{f_c}$ and is calculated as follows (Kuipers *et al.*, 1999):

$$ \vec{f_c} = {}^{g}_{w}q \otimes \vec{f} \otimes {}^{g}_{w}q^* \tag{6.2} $$

Please note that since $\vec{f}$ is a 3D vector, a 0 is inserted at the first element to provide a four elements vector for quaternion product ($\vec{f} = \{0, f_x, f_y, f_z\}$). In the same way, $\vec{f_c}$ is a four-element vector so, its first element needs to be removed. Considering $|\vec{f_c}|$ as the length of $\vec{f_c}$, the second sub-step calculates α_f and β_f, as below :

$$\alpha_f = \arctan\left(\frac{f_{c_y}}{f_{c_x}}\right), \quad \beta_f = \arccos\left(\frac{f_{c_z}}{|\vec{f}_c|}\right). \tag{6.3}$$

6.4.2 Estimation of the Orientation of Arm

Without attaching an IMU on the arm, it is impossible to measure its orientation $\{\alpha_a, \beta_a\}$. Instead, its orientation is estimated by considering the anatomical limitations on the movement of arm and forearm. The major movements of the arm can be summarised as follows:

- **Horizontal flexion/extension** is the horizontal movement of arm away from or toward the trunk in the xy plane, as illustrated in Figure 6.14a. This type of movement can be represented by α_a. According to (American College of Sports Medicine, 2013; Norkin and White, 2016), $-45^\circ \leq \alpha_a \leq 130^\circ$, as depicted in Figure 6.14b.

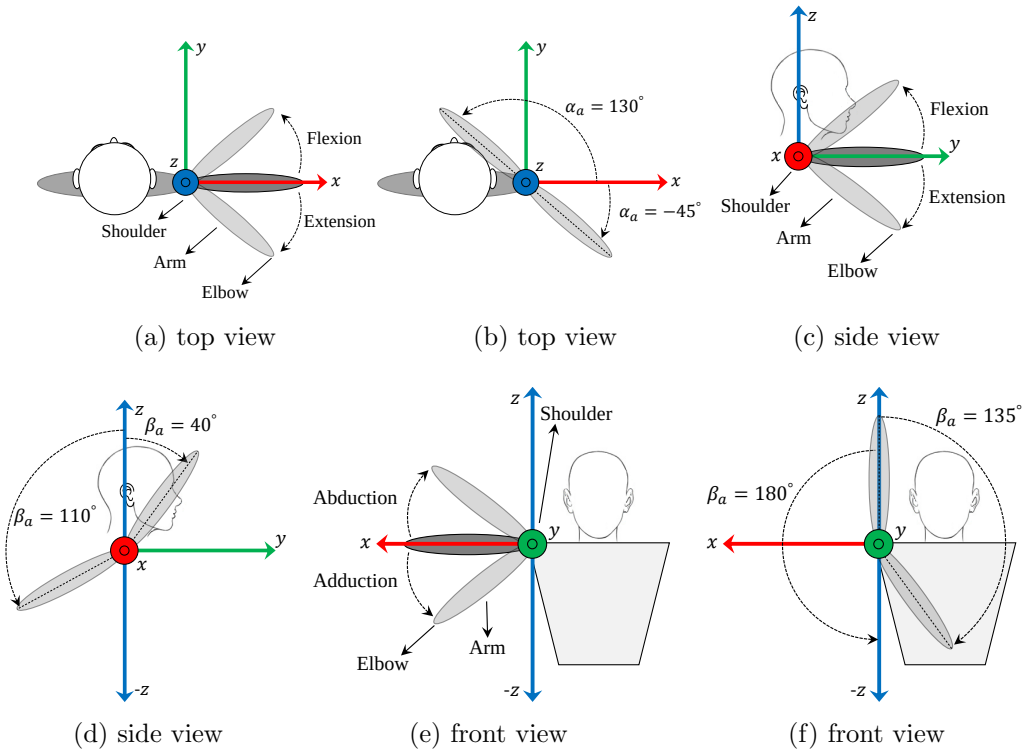

(a) top view (b) top view (c) side view

(d) side view (e) front view (f) front view

Figure 6.14: (a) horizontal flexion/extension; (b) RoM of horizontal flexion/extension; (c) vertical flexion/extension; (d) RoM of vertical flexion/extension; (e) vertical abduction/adduction; (f) RoM of vertical abduction/adduction.

- **Vertical flexion/extension** is the vertical movement of arm away from or toward the trunk in yz plane and is represented by β_a (Figure 6.14c). According to (American College of Sports Medicine, 2013; Norkin and White, 2016), $0^\circ \leq \beta_a \leq 180^\circ$, as depicted in Figure 6.14d.

- **Vertical abduction/adduction** is the vertical movement of arm away from or toward the trunk in the xz plane and can be represented by β_a (Figure 6.14e). As shown in Figure 6.14f, the range of vertical abduction/adduction of arm is between 0° and 180° according to (American College of Sports Medicine, 2013; Norkin and White, 2016).

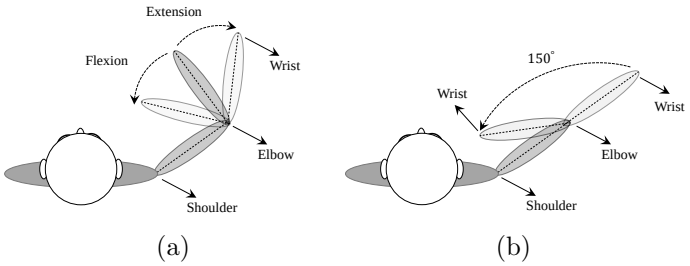

Figure 6.15: Movement of elbow joint (a) horizontal flexion/extension (b) range of horizontal flexion/extension.

To more accurately estimate the real-time orientation of arm, the dependencies between the orientation of arm and forearm is also considered. Since the arm and forearm is connected via the elbow, there is a relationship between their orientations. In horizontal flexion/extension shown in Figure 6.15, the elbow is opened in one direction (extension) until it meets a stop where arm and forearm are in the same direction and the elbow angle (the angle from forearm to arm in anticlockwise direction) is about 180° (American College of Sports Medicine, 2013; Norkin and White, 2016). In another direction, the elbow joint is closed (flexion) until the anterior surface of the forearm meets the biceps, where the elbow angle is around 30° (American College of Sports Medicine, 2013; Norkin and White, 2016). Based on these limitations, α_a can be further restricted by α_f as follows:

(1) $\alpha_a \leq \alpha_f$: α_a cannot exceed α_f, otherwise the elbow angle can be larger than 180° which is impossible.

(2) $\alpha_f - \alpha_a \leq 150^\circ$: this is because the elbow angle cannot be smaller than 30° as illustrated in Figure 6.15b.

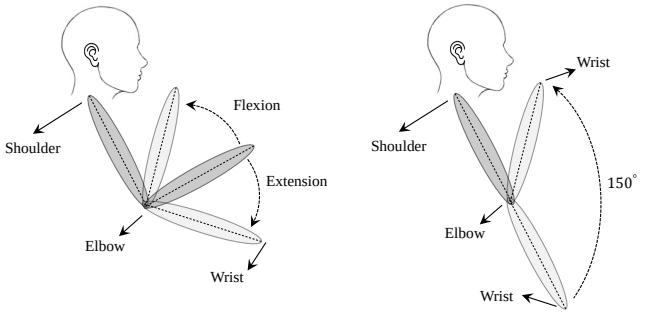

(a) (b)

Figure 6.16: Movement of elbow joint (a) vertical flexion/extension (b) range of vertical flexion/extension.

For a given α_f captured by the sending node at the wrist, α_a can be estimated based on the above two constraints and the limitation on horizontal flexion/extension as below:

$$\max\big(-45°, (\alpha_f - 150°)\big) \leq \alpha_a \leq \min\big(\alpha_f, 130°\big). \tag{6.4}$$

Similar limitations can be applied to restrict the range of β_a. As shown in Figure 6.16, the limitations on vertical flexion/extension of the elbow joint does not allow β_a to be bigger than β_f in most of daily activities, that is,

$$0° \leq \beta_f \leq \beta_a \leq 180°. \tag{6.5}$$

Even though more anatomical limitations on the movement of arm and forearm can be considered to enhance the localisation accuracy, it will increase the complexity of the localisation procedure as well. Since this scheme does not require highly accurate location of the sending node, it is found that estimating location of the sending node based on the above-mentioned limitations can achieve a good trade-off between complexity and performance. Next section explains how to estimate the *RoPL* of the sending node relative to the gateway based on (α_f, β_f) and (α_a, β_a).

6.4.3 Estimation of *RoPL*

As illustrated in Figure 6.17, three coordinate systems C_g, C_s, and C_e are defined with the origin at the gateway, shoulder and elbow, respectively. The axes in C_s and C_e are in the same direction as those in C_g. $\vec{f}$ and $\vec{a}$ are used to represent the 3D vector of forearm and arm in C_e, and C_s respectively, and $\vec{s}$ denotes the vector of the shoulder in C_g. Since the axes in C_e are in the same direction as those in C_g, the forearm has the

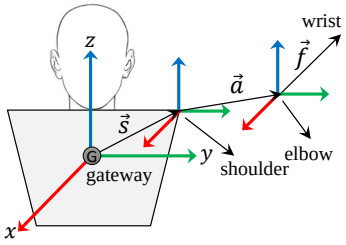

Figure 6.17:

same a_f and β_f in both C_g and C_e. Let (f_x, f_y, f_x) be the coordinate of the wrist in C_e. It is calculated as below:

$$f_x = |\vec{f}| \sin(\beta_f) \cos(\alpha_f), \quad f_y = |\vec{f}| \sin(\beta_f) \sin(\alpha_f), \quad f_z = |\vec{f}| \cos(\beta_f). \tag{6.6}$$

In the same way, the coordinate of the elbow in C_s, denoted by (a_x, a_y, a_z), is calculated using (α_a, β_a) and $\vec{a}$. Since the positions of the shoulder relative to the gateway is almost fixed, the coordinate of the shoulder in C_g, which is denoted by (s_x, s_y, s_z) is constant over time. Hence the coordinate of the wrist in C_g, denoted by (x, y, z), can be computed as follows:

$$x = s_x + a_x + f_x, \quad y = s_y + a_y + f_y, \quad z = s_z + a_z + f_z. \tag{6.7}$$

As discussed in Section 6.4.2, for each measured pair of (α_f, β_f), the orientation of arm is estimated as a range of angles. Since the movement of the elbow is a spherical rotation around the shoulder joint, the *RoPL* for the elbow is a convex surface on a sphere centred at the shoulder with a radius of $|\vec{a}|$ and bounded by four points A, B, C, and D, where the four points correspond to $\{\alpha_{a_{\min}}, \beta_{a_{\min}}\}$, $\{\alpha_{a_{\min}}, \beta_{a_{\max}}\}$, $\{\alpha_{a_{\max}}, \beta_{a_{\min}}\}$ and $\{\alpha_{a_{\max}}, \beta_{a_{\max}}\}$, respectively. Figure 6.18a and Figure 6.18b show the possible orientations of arm caused by changing β_a and α_a, respectively, and Figure 6.18c shows the *RoPL* for the elbow. Once the *RoPL* for the elbow is obtained, the *RoPL* for the wrist, bounded by four points A′, B′, C′, and D′ as illustrated in Figure 6.18c, can be calculated based on Equation (6.7).

Since $\vec{s}$, $|\vec{f}|$, and $|\vec{a}|$ are constant, the *RoPL* of the wrist is a function of α_f and β_f. According to the mutual relationship between the *RoPL* of the wrist and the corresponding (α_f, β_f), there is no need to calculate the *RoPL* of the wrist. Instead, it is identified by the corresponding (α_f, β_f) and is represented by $RoPL(\alpha_f, \beta_f)$ in the following sections.

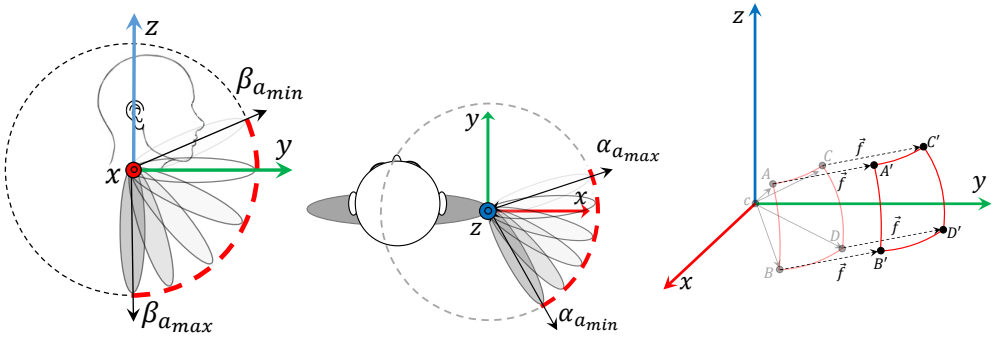

(a) (b) (c)

Figure 6.18: *RoPL* of the elbow relative to the shoulder (a) side view; (b) top view; (c) front view;

6.5 Power Level Selection Module

The power level selection module has two following phases: (1) The **setup phase** which aims to provide the sending node with a priori knowledge about the optimal power level in different $RoPL(\alpha_f, \beta_f)$; (2) The **communication phase** which transmits the packet with the power level selected based on the knowledge about the optimal power level in the current $RoPL(\alpha_f, \beta_f)$. In what follows, these phases are discussed.

6.5.1 Setup Phase

A $RoPL(\alpha_f, \beta_f)$ may include several sub-zones with different optimal power levels. Thus, a probability set $p_{\{\alpha_f,\beta_f\}} = \{p_1, p_2, \ldots, p_n\}$ is defined for each $RoPL(\alpha_f, \beta_f)$ where n is the number of power levels and p_i is the probability that power level i is the optimal power level in $RoPL(\alpha_f, \beta_f)$. Let L_i be the number of locations in the given $RoPL(\alpha_f, \beta_f)$ with power level i as the optimal power level and L_T be the total number of locations in $RoPL(\alpha_f, \beta_f)$, the selection probability of power level i in $RoPL(\alpha_f, \beta_f)$ is:

$$p_i = \frac{L_i}{L_T}$$

Since α_f ($\alpha_f \in [-180^o, 180^o]$) and β_f ($\beta_f \in [0^o, 180^o]$) belong to a wide range of angles, using a separate set of selection probabilities for each $RoPL(\alpha_f, \beta_f)$ extremely increases the memory usage. To compensate the memory overhead, several $RoPL(\alpha_f, \beta_f)$ in the same neighbourhood are grouped to create a Class of Locations ($CoL_{k,j}$) with a single selection probability set. To do so, the range of α_f and β_f are partitioned into

N_{α_f} and N_{β_f} sub-ranges with the length of $\frac{360}{N_{\alpha_f}}$ and $\frac{180}{N_{\beta_f}}$, respectively. Hence, there will be $N_{\alpha_f} \times N_{\beta_f}$ exclusive pairs of $\big([\alpha_{f_{min}}, \alpha_{f_{max}}], [\beta_{f_{min}}, \beta_{f_{max}}]\big)$ each of which identifies a separate $CoL_{k,j}$ as below:

$$CoL_{k,j} = [(k-1) \times \frac{360}{N_{\alpha_f}} - 180 \leq \alpha_f \leq k \times \frac{360}{N_{\alpha_f}} - 180\,, \\ (j-1) \times \frac{180}{N_{\beta_f}} \leq \beta_f \leq j \times \frac{180}{N_{\beta_f}}], 1 \leq k \leq N_{\alpha_f},\ 1 \leq j \leq N_{\beta_f} \quad (6.8)$$

Algorithm 5 is the pseudocode of the setup phase. It receives the length of forearm and $\vec{s}$ as the input. Although the length of arm and forearm in people with different heights is not the same but, the ratio of the length of the arm relative to the length of the forearm $\left(\frac{|\vec{a}|}{|\vec{f}|}\right)$ is about 1.2 on average (Hale and Richer, 1986; Hogarth, 2003; Goldfinger, 1991). Accordingly, line 1 calculates the length of arm. Using nested for loops (line 2-3), all *CoLs* from $CoL_{1,1}$ to $CoL_{N_{\alpha_f}, N_{\beta_f}}$ are explored. Considering k and j, line 4 defines the $CoL_{k,j}$ (i.e., defines α_f and β_f sub-ranges). Line 5 initialises the array L with n elements (where n is the number of power levels) to zero. Each element $L[i]$ will be used to show the frequency of observation of power level i as the optimal power level in the current *CoL*. Line 6-24 explores all *RoPLs* belonging to a $CoL_{k,j}$ using nested loops. In each iteration of the outer loop, all values of α_f in the current $CoL_{k,j}$ are explored (line 6). For each value of α_f, the inner loop scans all values of β_f (line 7). Line 8 calculates the location of the wrist relative to the elbow using Eqn. (6.6). For each pair of (α_f, β_f), all locations in the corresponding $RoPL(\alpha_f, \beta_f)$ is explored. To this end, the range of α_a and β_a is estimated based on the Eqns. (6.4) and (6.5) (line 9-12). Each $RoPL(\alpha_f, \beta_f)$ includes several locations that is explored using the third nested loops (line 13-22). In each iteration of the for loops, a single pair of α_a and β_a is considered through which one of the possible locations of the elbow relative to the shoulder is calculated (line 15). Having location of the wrist relative to the elbow, location of the elbow relative to the shoulder, and location of the shoulder relative to the chest, line 16 calculates the location of the wrist relative to the chest using Eqn. (6.7). Then, the calculated location is fed into the *loc_to_pow* function. *loc_to_pow* is a function that takes a location (x, y, z) in the $RoPL(\alpha_f, \beta_f)$ and returns the corresponding optimal power level for communication at that location through mapping the given location to the sub-zones depicted in Figure 6.7 (line 17). If the location is not accessible by the wrist, the function returns 0. If the returned value is not 0, the corresponding element in L is increased by one. Therefore, the value of

Algorithm 5: Setup phase

Input : $|\vec{f}|$, $\vec{s}$

$|\vec{a}| = 1.2 \times |\vec{f}|$
for $k = 1, \ldots, N_{\alpha_f}$ **do**
  for $j = 1, \ldots, N_{\beta_f}$ **do**
    define the $CoL_{k,j}$
    $L[1, .., n] \leftarrow 0$ `/* set the array to 0 */`
    for $\alpha_f = \alpha_{f_{min}}, \ldots, \alpha_{f_{max}}$ **do**
      for $\beta_f = \beta_{f_{min}}, \ldots, \beta_{f_{max}}$ **do**
        calculate f_x, f_y, f_z
        `/* determine the` $RoPL_{\{\alpha_f, \beta_f\}}$ `*/`
        $\alpha_{a_{min}} = max\big(-45, (\alpha_f, -150)\big)$
        $\alpha_{a_{max}} = min\big(\alpha_f, 130\big)$
        $\beta_{a_{min}} = \beta_f$
        $\beta_{a_{max}} = 180$
        for $\alpha_a = \alpha_{a_{min}}, \ldots, \alpha_{a_{max}}$ **do**
          for $\beta_a = \beta_{a_{min}}, \ldots, \beta_{a_{max}}$ **do**
            calculate a_x, a_y, a_z
            calculate x, y, z
            $pwr = loc\_to\_pow\big(x, y, z\big)$
            if $pwr \neq 0$ **then**
              $++L[pwr]$
            end
          end
        end
      end
    end
    $L_T = L[1] + L[2] + \cdots + L[n]$
    for $i = 1 \ldots n$ **do**
      $p_{\{i, CoL_{k,j}\}} = \frac{L[i]}{L_T}$
    end
  end
end

an element $L[i]$ represents the number of locations in the current $CoL_{k,j}$ with power level i as the optimal power level. Once all locations in a $CoL_{k,j}$ are explored, the total number of accessible locations is calculated (line 25) and the selection probability of each power level i (i.e., $p_{\{i,CoL_{k,j}\}}$) is calculated by dividing $L[i]$ by the L_T (line 26-28).

Let's consider an example to see how much memory can be saved by grouping a couple of *RoPL* into a single *CoL*. Assume a separate *RoPL* is defined for each integer value of α_f and β_f. That is, there will be about 360×180 ranges of possible locations because $-180^o \leq \alpha_f \leq 180^o$ and $0^o \leq \beta_f \leq 180^o$. Assuming a 4 byte variable is required to keep the selection probability of each power level i in each *RoPL*, more than $250 \times n$ kB memory is required to store the selection probabilities of n power levels in all *RoPLs*, which is unaffordable for tiny sending nodes. Partitioning the whole area around the shoulder into $N_{\alpha_f} \times N_{\beta_f}$ classes reduce the memory usage of the algorithm to $\frac{250 \times n}{N_{\alpha_f} \times N_{\beta_f}}$ kB. However, there is a tradeoff between the memory usage of the algorithm and the accuracy of the selection probabilities. That is, compared to a *RoPL*, for a *CoL* the selection probabilities are averaged over a wider range of locations and thus, the randomly selected power level has less chance to be the optimal transmission power level at a specific location.

6.5.2 Communication Phase

Unlike the setup phase which is run once, the communication phase is run every time a packet is generated. That is, once a packet is generated, the sending node measures the real-time α_f and β_f based on which the current *CoL* is determined. Then, the corresponding selection probability set initialised in the setup phase is considered. Finally, based on the roulette wheel selection scheme (Back, 1996) a transmission power level is randomly selected and the packet is sent. Algorithm 6 shows the pseudo code of the communication phase. As can be seen, the communication phase gets α_f and β_f as the input. Line 1-2 determines the current $CoL_{k,j}$. Line 4 generates a uniformly distributed random number and then, the while loop (line 5-8) selects power level i accordingly. Finally, the packet is transmitted using power level i (line 9).

6.6 Learning Module

As explained before, the randomly selected power level is not necessarily the optimal power level because: (1) the selection probability set is averaged over a wide range of locations possibly from different sub-zones; (2) the probabilities (which are pre-coded to

Algorithm 6: Communication phase

Input : α_f, β_f

/* Localisation module: determines $CoL_{k,j}$ */

$k = \lfloor \frac{180+\alpha_f}{N_{\alpha_f}} \rfloor$

$j = \lfloor \frac{\beta_f}{N_{\beta_f}} \rfloor$

/* Power selection module */

$P \leftarrow 0$; $i \leftarrow 0$;

$rnd \leftarrow rand()$; /* generate a random number in [0,1] */

do

  $++i$;

  $P = P + p_{\{i,CoL_{k,j}\}}$;

while $rnd > P$;

$send(i)$; /* send packet with power level i */

the sending node) are generally exploited from collected data of different users and thus, it does not perfectly match for every user. Hence, Learning Automata (LA) (Narendra and Thathachar, 2012), a feedback-based reinforcement learning scheme is used to refine the selection probability sets. In combination with *CoLs*, LA enables the sending node to remember the history of communications at each *CoL* and learn from it, based on which, the sending node can gradually update the selection probabilities at each *CoL*. For each $CoL_{k,j}$ a separate selection probability set $s_{k,j}$ is defined. Hence, the internal state of the LA at time t is:

$$s(t) = \{s_{1,1}(t), s_{1,2}(t), \ldots, s_{N_{\alpha_f}, N_{\beta_f}}(t)\}$$

$s_{k,j}(t)$ is a set of probabilities $p_{\{i,CoL_{k,j}\}}(t)$ that represents the selection probability of a power level i in class $CoL_{k,j}$. In other words:

$$s_{k,j}(t) = \{p_{\{1,CoL_{k,j}\}}(t), p_{\{2,CoL_{k,j}\}}(t), \ldots, p_{\{n,CoL_{k,j}\}}(t)\}$$

where n is the number of power levels. After sending a packet using a randomly selected power level i, the selection probability set corresponding to the current $CoL_{k,j}$ is updated upon receiving the ACK packet. That is, according to the learning function below, $p_{\{i,CoL_{k,j}\}}(t)$ is increased and the selection probability of other power levels is decreased:

$$p_{\{i,CoL_{k,j}\}}(t+1) = p_{\{i,CoL_{k,j}\}}(t) + \alpha_i(1 - p_{\{i,CoL_{k,j}\}}(t)),$$
$$p_{\{ii,CoL_{k,j}\}}(t+1) = (1-\alpha_i)p_{\{ii,CoL_{k,j}\}}(t),\ \forall ii \neq i \tag{6.9}$$

where $0 < \alpha_i \ll 1$ is the reward factor corresponding to power level i. It is shown that by setting $\frac{\alpha_i}{\alpha_{ii}} = \frac{P_{tx}^{ii}}{P_{tx}^{i}}$, the learning function finds the optimal power level in each $CoL_{k,j}$.

Algorithm 7: Tuatara

Input : α_f, β_f

`/* Localisation module: determines` $CoL_{k,j}$ `*/`

1 $k = \lfloor \frac{180+\alpha_f}{m_{\alpha_f}} \rfloor$

2 $j = \lfloor \frac{\beta_f}{m_{\beta_f}} \rfloor$

`/* Power selection module */`

3 $P \leftarrow 0$; $i \leftarrow 0$;

4 $rnd \leftarrow rand()$; `/* generate a random number in [0,1] */`

5 **do**

6 $\quad ++i$;

7 $\quad P = P + p_{\{i,CoL_{k,j}\}}$;

8 **while** $rnd > P$;

9 $send(i)$; `/* send packet with power level` i `*/`

`/* Learning module */`

10 **if** *ACK is received* **then**

11 $\quad p_{\{i,CoL_{k,j}\}} = p_{\{i,CoL_{k,j}\}} + \alpha_i \times (1 - p_{\{i,CoL_{k,j}\}})$;

12 $\quad$ **for** $ii = 1, \ldots, n$ **do**

13 $\quad\quad$ **if** $ii \neq i$ **then**

14 $\quad\quad\quad p_{\{ii,CoL_{k,j}\}} = (1-\alpha_i) \times p_{\{ii,CoL_{k,j}\}}$;

15 $\quad\quad$ **end**

16 $\quad$ **end**

17 **end**

Algorithm 7 gives the pseudocode of Tuatara, including the power selection module and the learning module. Similar to Algorithm 5 Tuatara gets the real-time orientation of the forearm (α_f and β_f) as input from the localisation algorithm, through which it can find the current class of locations by calculating the indexes of the class (line 1-2). Then, the packet is transmitted using a randomly selected power level (line 3-9). Once

the ACK packet is received, the selection probability of the used power level is increased depending on its reward factor and thus, the selection probability of other power levels are decreased. As demonstrated in Chapter 5, LA finds the optimal transmission power level after a couple of transmissions. Different from Chimp, Tuatara remembers the selection probabilities in previously observed locations, making its behaviour stable when the motion patterns of the user are changed during a physical activity. Moreover, it is expected that Tuatara supports a wider range of physical activities including activities with aperiodic motion patterns, even in extremely low packet rate scenarios.

6.6.1 Complexity Analysis

The first phase of Tuatara that calculates the selection probabilities of different power levels in the different classes of location is run once and imposes a fixed limited computation overhead to the sending node thus, its overhead is ignorable. The second phase of Tuatara has three key modules: (1) finding the indexes of the current class of locations, (2) using Roulette wheel selection for selecting the transmission power level, and (3) updating the selection probabilities after receiving the ACK packet. The first module requires a constant number of operations. The time complexity of the other two modules is $O(n)$ where n is the number of power levels. Therefore, the time complexity of Tuatara is $O(n)$. In the implementation, the second phase of Tuatara requires $10n$+20 single arithmetic operations for each transmission. However, the transmission power level set is limited to three power levels (i.e., $n = 3$) and thus, Tuatara uses around 50 single arithmetic operations. Accordingly, the energy overhead of Tuatara is limited to below $54.5nA$ per transmission based on the TelosB platform, that is almost at the level of energy usage of Chimp but about 180 times lower than the energy consumed by the radio to send a 41-byte data packet using power level 7. In Tuatara, the accessible locations by the wrist around the shoulder are partitioned into $N_{\alpha_f} \times N_{\beta_f}$ classes. For each class of locations, a separate internal state represented by the selection probabilities for n power levels are defined. Hence, the memory complexity of Tuatara is $O(n \times N_{\alpha_f} \times N_{\beta_f})$.

6.7 Experimental Evaluation

This section includes performing several experiments to evaluate the performance of Tuatara regarding its energy consumption, distribution of usage of power levels, and the packet loss rate. To provide a comprehensive view on the performance of Tuatara,

Table 6.1: Experiment parameters

Parameter	value
Power levels	$\{1, 3, 7\}$
data rate	0.1, 1, 20 pkt/s
Data packet length	41 Bytes
ACK packet length	13 Bytes
m_{α_f}	12
m_{β_f}	6
Number of participants	3
The length of each scenario	30 minutes
$\{\alpha_1, \alpha_3, \alpha_7\}$	{0.316, 0.0494, 0.005}

it is compared with the optimal scheme and the previously proposed communication protocols (ATPS and Chimp) using the same channel RSSI traces and under the same experiment setup.

Table 6.1 summarises the experiment parameters. A small set of power levels including level 1, 3, and 7 are used for reliable and energy efficient packet transmission, however, a wider range of power levels can be used. The data packet size and ACK packet size is set to 41 and 13 Bytes, respectively. The experiments are performed under three different packet rates (0.1 pkt/s, 1 pkt/s, and 20 pkt/s) and two different MAC sub-layer retransmission modes: disabled retransmission and enabled retransmission. Besides the previously considered postures (sitting, standing, walking, and running), the performance of the schemes in a scenario with a mixed posture is considered. In this scenario, the subject repeatedly stays in the four mentioned postures in a row and in the following order: sitting, walking, standing, and running, with each posture lasting for 30 seconds and the whole scenario lasting for 30 minutes. Instead of staying in a completely static or dynamic posture, the mixed posture helps to evaluate the performance limits of the schemes when schemes must quickly find the optimal power.

6.7.1 Experimental Result with Disabled MAC Sub-layer Retransmission

For all experiments in this section, retransmission at MAC Sub-layer is disabled. That is, every single packet is transmitted only once whether it is received at the gateway or not. Hence, the total number of transmissions in all schemes are the same and thus, it is possible to analyse the behaviour of a communication protocol in a single scenario in which retransmission is enabled. Figure 6.19 shows the results of the experiments. For the sake of clarity, the experimental results in *static* and *dynamic* postures are discussed separately.

Static postures: In sitting, all protocols achieve roughly the same performance, very close to the optimal scheme. They choose power level 1 for almost all transmissions, especially when the packet rate is high, though ATPS transmits a few percent of the packets using level 3. The energy consumption and the packet loss rate of all protocols in this posture is very similar to that of the optimal scheme. In standing, all protocols consume almost the same amount of energy. In this posture, Tuatara, like the optimal scheme, selects power level 3 for more than 99% of transmissions. Unlike Tuatara that has the same trend on power level used in different packet rates, ATPS and Chimp use other power levels causing a higher packet loss rate. Tuatara achieves the lowest packet loss rate, almost as low as the packet loss rate of the optimal scheme. For example, at the packet rate of 0.1 pkt/s, the packet loss rates of Chimp and ATPS is respectively about three and two times more than that of Tuatara. However, increasing the packet rate reduces the packet loss rate of ATPS and especially Chimp. The reason for such a good performance of Tuatara is its prior knowledge about the channel quality in different locations. For example in standing, the class of locations estimated by the localisation algorithm mostly includes sub-zones with power level 3 as the optimal power level. That is, the selection probability of power level 3 in this posture is initially very close to 1. This is the same for sitting because Tuatara finds the current class of locations includes sub-zones with power level 1 as the optimal power level.

Dynamic postures: In dynamic postures, where the packet loss rate of all protocols is raised, Tuatara is the most reliable communication protocol. Its loss rate at the packet rate of 0.1 pkt/s and 1 pkt/s is below 70% of that of Chimp in the both walking and running. Although increasing the packet rate decreases the packet loss rate of all protocols, especially for ATPS and Chimp (as is shown in Figure 6.19), Tuatara is still more reliable. The usage of different power levels in Tuatara is very similar to that of

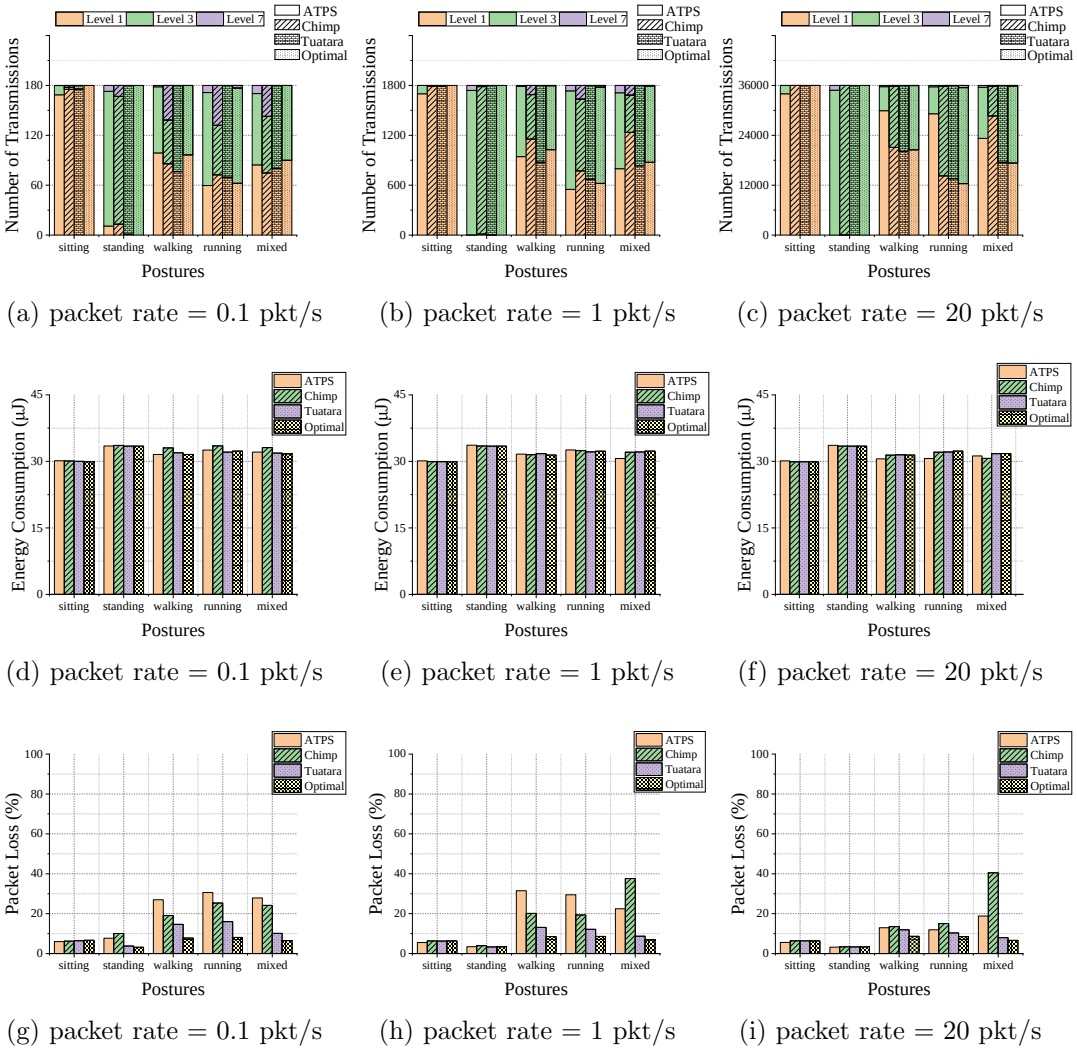

(a) packet rate = 0.1 pkt/s (b) packet rate = 1 pkt/s (c) packet rate = 20 pkt/s

(d) packet rate = 0.1 pkt/s (e) packet rate = 1 pkt/s (f) packet rate = 20 pkt/s

(g) packet rate = 0.1 pkt/s (h) packet rate = 1 pkt/s (i) packet rate = 20 pkt/s

Figure 6.19: Experiments with disabled MAC sub-layer retransmission under different data rates: (a), (b) and (c) show the distribution of power level usage; (d), (e) and (f) show the energy consumption; (g), (h) and (i) show the packet loss rate.

the optimal scheme. Through estimating the location of the sending node, Tuatara appropriately selects power level 1 when it expects the sending node is in front of the body trunk and switches to level 3 when it predicts the sending node is at the back of the body trunk. Compared to Chimp which uses power level 3 for 33% of transmissions and power level 7 for 26% of transmissions in the running at the packet rate of 0.1 pkt/s, Tuatara potentially produces less interference by nearly ignoring power level 7 and adjusting power level 3 for about 62% of transmissions. However, increasing packet rate to 20 pkt/s enables Chimp to quickly converge the usage of different power levels

close to that of Tuatara and the optimal scheme. Please note the usage of power level 1 in walking in all protocols is higher than that in the running because the LoS path in walking lasts longer. It is worth considering that in high packet rate scenarios, ATPS transmits most of the packets using power level 1. Hence, it potentially produces less interference and consumes less energy compared to the other protocols, however, at the cost of imposing some transmission delay and slightly higher packet loss rate.

Mixed postures: As is expected, the performance of Tuatara is nearly similar to its average performance in all other postures and very close to that of the Optimal scheme. The performance of ATPS and particularly Chimp is significantly reduced in mixed posture. The limits of Chimp appears when the data rate is reached to 20 pkt/s. As the results show, Chimp uses power level 1 for many of its transmissions at the packet rate of 20 pkt/s (more than 80%) that compared to Tuatara results in slightly lower energy usage, however, at the cost of almost 40% packet loss rate, 5 times more than that of Tuatara. Similarly, ATPS drops a lot of packets (up to 30%) though, the distribution of usage of power levels in ATPS is somewhat similar to that of Tuatara and Optimal scheme. Chimp tries to learn the correlation between the channel pattern and the angular velocity pattern of the sending node. In static postures like sitting and standing, regardless of the real location of the sending node, the measured angular velocity is almost zero as there is no considerable motion. In the designed mixed posture, the subject starts by sitting for 30 seconds. During this period, Chimp receives about 600 feedback (at the data rate of 20 pkt/s) which is enough to converge the selection probability of power level 1 to almost 1 (as the LoS is available). In other words, Chimp learns that the optimal power at zero velocity is power level 1. After 30 seconds of walking, the subject stands for 30 seconds. In this posture, the velocity is again zero, thus, Chimp selects level 1 with the probability of almost 1, as it was learned before. Communication with power level 1 in standing drops almost all packets as the LoS path is blocked, however, Chimp does not reduce the selection probability of power level 1 because of the lack of a penalising mechanism. In other words, there is no mechanism in Chimp that allows the sending node to reduce the selection probability of a power level which is no longer optimal. However, assuming Chimp has a penalising mechanism, it still suffers from a very slow convergence rate which makes the process of resetting the selection probabilities very inefficient. For the same reason, the optimal power levels that are learned in the walking at different velocities are not useful in the running, result in increasing packet loss rate, wasting energy, and a higher number of transmissions. Please note, a similar problem happens if the mixed posture starts with

another posture. For example, if the subject starts by standing, Chimp learns power level 3 is the optimal power level at zero velocity and thus, it selects power level 3 in sitting and increases potential interference. Compared to the Chimp, ATPS is more efficient regarding almost all performance metrics. It properly adapts the transmission power levels while the posture is changing and thus, it delivers almost all packets.

6.7.2 Experimental Result with Enabled MAC Sub-layer Retransmission

This section repeats the previous experiments with enabled MAC sub-layer retransmission. That is, a lost packet is retransmitted up to 15 times when the packet rate is low and up to 3 times when the packet rate is high. Once a packet is dropped, Tuatara, similar to Chimp, randomly selects a transmission power level based on the roulette wheel section scheme and retransmits the packet. Similarly, ATPS makes a new channel prediction and selects a transmission power level and accordingly retransmits the packet. Figure 6.20 presents the results of the experiments. Since enabling retransmission helps the protocols to deliver almost all packets in low data rate scenarios, Figure 6.20 does not present the results for the packet loss rate at the packet rate of 0.1 pkt/s and 1 pkt/s. For the sake of clarity, the results of the experiments are discussed under the headings of *static*, *dynamic*, and mixed posture, separately.

Static postures: In sitting, since all protocols deliver almost all packets on the first transmission, they perform as well as the optimal scheme. They use power level 1 for almost all transmissions and reduce the energy consumption and the potential interference of the sending node to almost its lowest level. However, ATPS selects power level 3 for a few percent of transmissions, but it does not significantly influence the energy consumed and the potential interference produced by ATPS. In standing, Tuatara, similar to the optimal scheme, uses power level 3 for almost all transmissions and delivers most of the packets on the first transmission, even at low packet rate scenarios. Despite the packet rate, the performance of Tuatara in standing is very close to that of the optimal scheme. Unlike Tuatara that has prior knowledge about the optimal power level in each position, Chimp and ATPS require some feedback to learn the optimal power level. For example, Chimp drops some of the packets at the beginning of the communication for which, enabling retransmission increases its total number of transmissions and imposes some negligible energy overhead. This is more remarkable at the packet rate of 0.1 pkt/s where Chimp transmits 6% more than that

of Tuatara. However, increasing the packet rate reduces the learning overhead of Chimp and ATPS and improves their performance to the level of Tuatara and the optimal scheme.

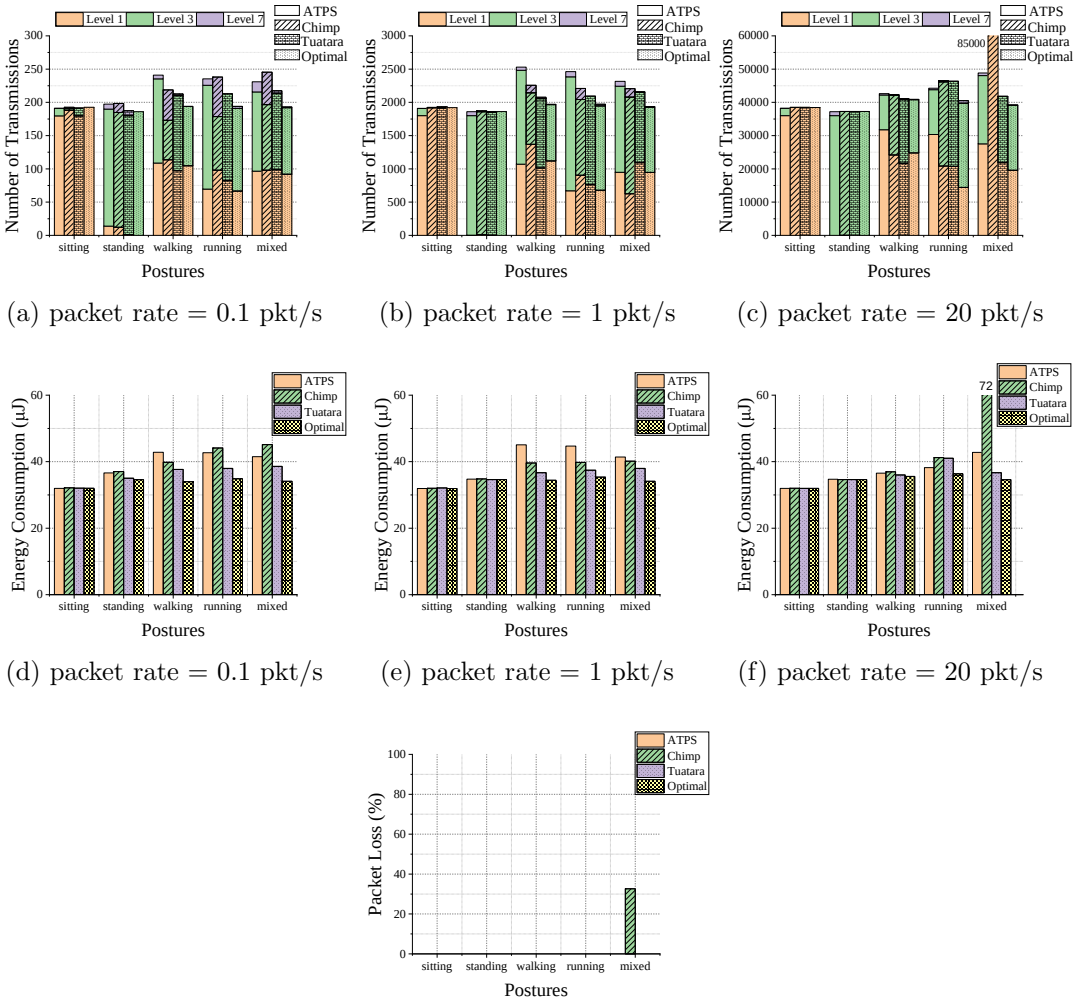

(a) packet rate = 0.1 pkt/s (b) packet rate = 1 pkt/s (c) packet rate = 20 pkt/s

(d) packet rate = 0.1 pkt/s (e) packet rate = 1 pkt/s (f) packet rate = 20 pkt/s

(g) packet rate = 20 pkt/s

Figure 6.20: Experiments with enabled MAC sub-layer retransmission under different data rates: (a), (b) and (c) show the distribution of power level usage; (d), (e) and (f) show the energy consumption and (g) show the packet loss rate.

Dynamic postures: In dynamic postures, Tuatara is the most energy efficient protocol in most of the scenarios. For example, Tuatara saves 5.6% and 13.6% of the energy used by Chimp and ATPS in walking, when the packet rate is 0.1 pkt/s. The reason for such a low energy usage of Tuatara is two-fold: (1) it delivers most of the packets on the first transmission and thus, enabling retransmission does not impose a significant

retransmission overhead. For example, in the running, and at the packet rate of 0.1 pkt/s Tuatara transmits 11% fewer packets than that of Chimp and ATPS; (2) Unlike Chimp and ATPS that try to learn the channel pattern based on trial and error, Tuatara has prior knowledge about the channel quality in different locations and can select the appropriate power level for each transmission. As is shown in Figure 6.20, Chimp uses power level 7 for 21% of transmissions in the running at 0.1 pkt/s which is a waste of energy as the results of the optimal scheme shows power level 3 is high enough for reliable communication in this posture.

With the increase in the packet rate, the energy consumption and the distribution of power level used in Chimp is very close to that of Tuatara. They both have a very similar usage of power levels and consume almost the same amount of energy in walking and running at 20 pkt/s. Please note, although ATPS outperforms Chimp and Tuatara in running at 20 pkt/s in terms of used energy and produced potential interference, the packets undertake some transmission delay which is not acceptable for many applications.

Mixed postures: Unlike ATPS that achieves better results in high data rate scenarios, Chimp has its worst performance at the packet rate of 20 pkt/s. Even at the presence of enabled MAC layer retransmission, Chimp drops more than 30% of the packets as it uses power level 1 for most of its transmissions. Such a high number of packet transmission increases the energy usage of Chimp to more than twice of that of Tuatara. The average performance of ATPS is much better than Chimp. It delivers all packets and consumes much less energy than Chimp. However, compared to Tuatara, it transmits more packets and thus, consumes more energy and produces a higher potential interference as it is based on the idea of trial and error.

6.7.3 Impact of m_{α_f} and m_{β_f} on the performance of Tuatara

As discussed before, Tuatara benefits from the correlation between the channel quality and the location of the sending node. Under the absence of the accurate location of the sending node, α_f and β_f are partitioned into m_{α_f} and m_{β_f} sub-ranges, to provide *CoLs*. Using a higher number of *CoLs* saves memory, however, at the cost of lower accuracy of the estimated location. This section considers the impact of m_{α_f} and m_{β_f} on the performance of Tuatara. To do so, a subject was asked to walk for 30 minutes and the RSSI samples were collected at the rate of 20 pkt/s. Then, the experiments were repeated with different cluster numbers from $m_{\alpha_f} = 2$ and $m_{\beta_f} = 2$ to $m_{\alpha_f} = 20$ and $m_{\beta_f} = 12$ with a gap of 2.

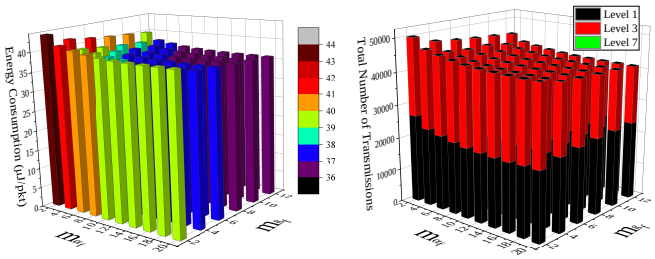

(a) Energy consumption (b) Distribution of power levels

Figure 6.21: Performance of Tuatara under different m_{α_f} and m_{β_f}.

Figure 6.21 shows the results of the experiments. As is expected, increasing the number of clusters has positive effects on reducing energy consumption and particularly the total number of transmissions. The improvement is more significant when the number of total clusters are increased from 4 ($m_{\alpha_f} = 2$ and $m_{\beta_f} = 2$) to 72 ($m_{\alpha_f} = 12$ and $m_{\beta_f} = 6$). This can be explained as follows: when there are a few clusters, each cluster represents a broad range of locations with a wide variety of channel qualities. Thus, once a packet is generated, there is a low chance for the selected power level to be the optimal one. Increasing the number of clusters narrows the range of possible locations (and consequently decreases the variety of channel qualities) represented by each cluster. Hence, the selected transmission power has a higher chance to be the optimal level. On the other hand, increasing the number of clusters from 72 does not have a big impact on the performance of Tuatara which is discussed as follows: when the clusters are narrow enough to represent a limited range of locations and channel qualities, splitting a cluster into two clusters is not only a waste of memory, but also Tuatara will receive fewer channel feedbacks per each cluster, results in slower channel learning.

6.8 Discussion

Tuatara is a novel protocol for power adaptive communication in WBANs. Considering the real-time orientation of the sending node relative to the gateway and applying anatomical constraints, Tuatara gives a rough estimation of the real-time location of the sending node. Then, in combination with a priori knowledge about the channel quality in different locations around the body, Tuatara predicts the channel quality. Finally, it selects the appropriate transmission power level based on the predicted channel quality. Because of the initial knowledge about the channel quality in different

locations, Tuatara performs very well even in extremely low packet rate scenarios. The experiments conducted on the real-world channel RSSI samples show Tuatara performs better than the state-of-the-art protocols in many scenarios and its performance is very close to that of the optimal scheme in a wide range of postures. Tuatara is a lightweight protocol and does not impose a considerable computation overhead to the sending node. Tuatara is adaptive to quick channel fluctuations and can revise its prior knowledge about the channel quality when it becomes invalid.

Chapter 7

Conclusions and Future Work

This thesis focuses on the design of power-adaptive communication protocols for resource-constrained WBANs. The main idea is to estimate the highly unstable channels in WBANs and adaptively adjust the transmission power level of the sending node to a low power level when the LoS path to the gateway is available and switch to a high power level when the LoS path is blocked. With the aim of jointly reducing energy consumption, the usage of high power levels, and the packet loss rate, a transmission cost function has been presented to combine all performance parameters into a single metric. Then, three topology independent communication protocols named ATPS, Chimp, and Tuatara have been proposed aiming at reducing transmission cost in different applications of WBANs. ATPS exploits channel burstiness using a Markov chain model and schedules the packets to be transmitted in a bursty fashion when the channel is expected to be good. However, it only supports applications with periodic packet transmission. Sustaining the advantages of ATPS it has been suggested that Chimps supports a wider range of applications. Chimp benefits from the idea of learning automata to exploit the correlation between channel quality fluctuations and motion patterns, through which it can predict the channel quality by locally monitoring the motion signal. Chimp works based on trial and error and thus, it does not achieve a good performance in extremely low packet rate scenarios. Hence, Tuatara is proposed to achieve better performance results in all applications under different packet rate scenarios. By combining the locally measured orientation of the sending node with the anatomical constraints on body movements, Tuatara gives a rough estimation of the location of the sending node. Then, using the prior knowledge of the optimal power level in each location, the sending node can quickly adjust its transmission power level. The rest of this chapter summarises the contributions and presents potential future

research directions.

7.1 Conclusions

This section summarises all chapters and discusses the advantages and disadvantages of the proposed communication protocols.

Chapter 1 introduced WBAN and its applications. This chapter presented the characteristics of WBANs and discussed the most important challenges in designing a communication protocol for resource-constrained body sensors. Three major performance metrics including energy consumption, communication reliability, and interference were described and the reason why a fixed-power communication protocol cannot achieve high performance in WBANs was explained.

Chapter 2 gave the important background knowledge on the IEEE standards, frequency bands, and channel characteristics of WBANs. This chapter presented a comprehensive literature review of communication protocols in WBANs. Moreover, the disadvantages of multi-hop communication protocols and the necessity of designing a one-hop communication protocol for WBANs were discussed.

Chapter 3 described the properties of the TelosB mote and the CC2420 radio chip as the hardware platform for the test WBAN based on the results of comprehensive experiments and measurements. A WBAN testbed with a sending node attached to the wrist and a gateway mounted on the chest was designed. Then, a unified cost function that reflects all performance metrics were presented and justified in this chapter.

Chapter 4 analysed the characteristics of channels of WBANs and presented a new channel model called **IGE**. Motivated by the accuracy of IGE model in predicting the channel behaviour at high packet rate scenarios, **ATPS** was designed. ATPS enables the sending node to estimate the channel quality and buffer the packets when the LoS path is blocked and transmit them in a bursty fashion when the LoS path is available. The experimental results show ATPS can self-learn the channel fluctuation pattern and adaptively adjust the transmission power level to save energy while achieving high communication reliability. Since ATPS learns the channel pattern through monitoring channel samples, it supports only applications with a constant high packet rate. When the motion patterns are aperiodic or when the subject moves his body parts randomly or casually, for example, when the subject pulls out his hand from his pocket to grab a cup, ATPS cannot learn the channel pattern. However, when the posture is static (e.g., in sitting and standing), ATPS has a good performance even in low packet rate

scenarios.

Chapter 5 introduced **Chimp** to solve the mentioned problems in ATPS. This chapter described the idea of learning automata and showed how the problem of finding the optimal power level can be mapped to the learning automata. Then, a new learning function was developed to help the sending node to find the optimal transmission power level. Instead of expensive channel measurements, Chimp tries to learn the correlation between body motion patterns and channel pattern. Since the motion patterns are measured locally, Chimp can estimate the channel without measuring the channel RSSI. Hence, unlike ATPS, it supports event-driven applications as well as the applications with periodic packet transmission. Chimp achieves excellent performance in both static and dynamic postures when the packet rate is high. However, since it is a trial and error based learning algorithm, its learning overhead in low packet scenarios is high and thus, its performance is low. Since channel estimation in Chimp is based on monitoring of the correlation between the motion patterns of the sending node and the channel quality, with any change in the user's physical activity (even as simple as changing his walking speed) Chimp has to relearn the correlation between the motion data and the channel quality.

Chapter 6 proposed **Tuatara**. Tuatara is a location- and learning-based communication protocol for WBANs which was presented to solve the problem of Chimp in low packet rate scenarios. This chapter carried out a set of experiments to show the channel quality between the sending node and the gateway is highly dependent on the location of the sending node. Motivated by this, a lightweight localisation algorithm was developed that can estimate the location of the sending node using the locally measured orientation information in combination with anatomical constraints on body movements. With prior knowledge about the optimal power level in different accessible locations of the sending node around the body, once a new packet is generated, Tuatara estimates the location of the sending node and transmits the packet using the appropriate power level. Since the channel quality even in a fixed location of the sending node is not necessarily constant, Tuatara benefits from the idea of learning automata so that it can keep updating the selection probability of transmission power levels in every given location. Since the location information is provided locally, Tuatara can support both event-driven applications and applications with periodic packet transmission. Moreover, since it has prior knowledge about the optimal power level in different locations, the learning automata do not impose a considerable learning overhead and thus, it achieves very good performance, close to that of the optimal scheme. For the same reason, as

Tuatara is location-based, changing the walking speed or moving body parts randomly does not affect its performance.

7.2 Future Work

The focus of this thesis is on designing power-adaptive communication protocols for WBANs. However, there are still several aspects to be investigated as follows:

(1) As explained, the trial and error nature of learning automata imposes a considerable overhead to Chimp, especially when the packet rate is low. This problem can be solved if the learning speed of Chimp is increased. To do so, one solution is to revise the learning function to increase the convergence rate. Alternatively, the reward function of the current learning function can be redefined so that it is a function of not only the transmission signal power but also a function of transmission cost at the current channel quality. Hence, separate RSSI thresholds for different power levels should be defined. Once an ACK packet is received, its RSSI is measured. Since the channel is symmetric, the measured RSSI shows the channel quality from the sending node side to the gateway as well. If the measured RSSI falls into the threshold of the selected transmission power level i, then the reward function can select a higher reward to increase the selection probability of power level i. The third solution suggests the sending node benefits from the information about the channel fluctuation pattern provided by the user's physical activity. The use of WBANs in healthcare applications has brought the wearable physical activity detection systems into focus. These systems commonly use motion sensors and pattern matching algorithms to detect the user's physical activity (Wang, Gu, Chen, Tao, and Lu, 2010; Wang, Gu, Tao, and Lu, 2012). Since the channel fluctuation pattern is highly dependent on the user's physical activity (as shown in Chapter 4), a novel communication protocol can be developed in which, the sending node uses the physical activity information to quickly estimate the channel fluctuation pattern.

(2) During the whole thesis, it is assumed the WBAN test-bed includes sending nodes and a gateway where the sending nodes have to directly communicate with the gateway in a one-hop star topology. Since IEEE standards for WBANs support both one-hop and two-hop star topologies, motivated by the proposed communication protocols, new protocols can be developed to support two-hop communications as well. For example, Chimp can simultaneously consider the link to the gateway as well as the links to all one-hop neighbours and ask neighbours to relay its packet to the gateway,

when the LoS path is blocked for a while.

Bibliography

Abidi, B., Jilbab, A., and Mohamed, E. H. (2018). An energy efficiency routing protocol for wireless body area networks. *Journal of medical engineering & technology*, *42*(4), 290–297.

Alpcan, T., Başar, T., Srikant, R., and Altman, E. (2002). CDMA uplink power control as a noncooperative game. *Wireless Networks*, *8*(6), 659–670.

American College of Sports Medicine (2013). *ACSM's guidelines for exercise testing and prescription*. Lippincott Williams & Wilkins.

Anwar, M., Abdullah, A., Altameem, A., Qureshi, K., Masud, F., Faheem, M., Cao, Y., and Kharel, R. (2018). Green Communication for Wireless Body Area Networks: Energy Aware Link Efficient Routing Approach. *Sensors*, *18*(10), 3237.

Aristidou, A. and Lasenby, J. (2009). *Inverse kinematics: a review of existing techniques and introduction of a new fast iterative solver*. University of Cambridge, Department of Engineering.

Aristidou, A., Lasenby, J., Chrysanthou, Y., and Shamir, A. (2018). Inverse kinematics techniques in computer graphics: A survey. In *Computer Graphics Forum*, Volume 37, 35–58. Wiley Online Library.

Arriola, A., Sancho, J., Brebels, S., Gonzalez, M., and De Raedt, W. (2011). Stretchable dipole antenna for body area networks at 2.45 GHz. *IET Microwaves, Antennas & Propagation*, *5*(7), 852–859.

Bachlin, M., Forster, K., and Troster, G. (2009). SwimMaster: a wearable assistant for swimmer. In *Proceedings of the 11th International Conference on Ubiquitous Computing*, 215–224. ACM.

Back, T. (1996). *Evolutionary algorithms in theory and practice: evolution strategies, evolutionary programming, genetic algorithms*. Oxford university press.

Baek, W.-S., Kim, D.-M., Bashir, F., and Pyun, J.-Y. (2013). Real life applicable fall detection system based on wireless body area network. In *IEEE Consumer Communications and Networking Conference (CCNC)*, 62–67.

Barroca, N., Saraiva, H. M., Gouveia, P. T., Tavares, J., Borges, L. M., Velez, F. J., Loss, C., Salvado, R., Pinho, P., Goncalves, R., *et al.* (2013). Antennas and circuits for ambient RF energy harvesting in wireless body area networks. In *IEEE 24th International Symposium on Personal Indoor and Mobile Radio Communications (PIMRC)*, 532–537. IEEE.

Blessey, R. L., Hislop, H. J., Waters, R. L., and Antonelli, D. (1976). Metabolic energy cost of unrestrained walking. *Physical Therapy*, *56*(9), 1019–1024.

Braem, B., Latre, B., Moerman, I., Blondia, C., and Demeester, P. (2006). The wireless autonomous spanning tree protocol for multihop wireless body area networks. In *3rd Annual International Conference on Mobile and Ubiquitous Systems*, 1–8. IEEE.

Casselman, J., Onopa, N., and Khansa, L. (2017). Wearable healthcare: Lessons from the past and a peek into the future. *Telematics and Informatics*, *34*(7), 1011–1023.

Chaganti, V., Hanlen, L., and Smith, D. (2014). Are narrowband wireless on-body networks wide-sense stationary? *IEEE Transactions on Wireless Communications*, *13*(5), 2432–2442.

Chan, J. C., Leung, H., Tang, J. K., and Komura, T. (2011). A virtual reality dance training system using motion capture technology. *IEEE Transactions on Learning Technologies*, *4*(2), 187–195.

Chávez-Santiago, R., Nolan, K. E., Holland, O., De Nardis, L., Ferro, J. M., Barroca, N., Borges, L. M., Velez, F. J., Goncalves, V., and Balasingham, I. (2012). Cognitive radio for medical body area networks using ultra wideband. *IEEE Wireless Communications*, *19*(4).

Chen, X., Zhang, J., Hamel, W. R., and Tan, J. (2014). An inertial-based human motion tracking system with twists and exponential maps. In *IEEE International Conference on Robotics and Automation (ICRA)*, 5665–5670. IEEE.

Chen, Y., Yu, G., Zhang, Z., Chen, H.-h., and Qiu, P. (2008). On cognitive radio networks with opportunistic power control strategies in fading channels. *IEEE Transactions on Wireless Communications*, *7*(7).

Cheng, P. L. (2000). A spherical rotation coordinate system for the description of three-dimensional joint rotations. *Annals of Biomedical Engineering*, *28*(11), 1381–1392.

Chi, Y. M. and Cauwenberghs, G. (2010). Wireless non-contact EEG/ECG electrodes for body sensor networks. In *International Conference on Body Sensor Networks*, 297–301. IEEE.

Chiang, M., Hande, P., Lan, T., Tan, C. W., *et al.* (2008). Power control in wireless cellular networks. *Foundations and Trends® in Networking*, *2*(4), 381–533.

Ciemins, E., Coon, P., Peck, R., Holloway, B., and Min, S.-J. (2011). Using telehealth to provide diabetes care to patients in rural Montana: findings from the promoting realistic individual self-management program. *Telemedicine and e-Health*, *17*(8), 596–602.

Clawson, J., Patel, N., and Starner, T. (2010). Dancing in the Streets: The design and evaluation of a wearable health game. In *International Symposium on Wearable Computers (ISWC)*, 1–4. IEEE.

Cotton, S. L., Conway, G. A., and Scanlon, W. G. (2009). A time-domain approach to the analysis and modeling of on-body propagation characteristics using synchronized measurements at 2.45 GHz. *IEEE Transactions on Antennas and Propagation*, *57*(4), 943–955.

Craig, J. J. (2005). *Introduction to robotics: mechanics and control*, Volume 3. Pearson/Prentice Hall Upper Saddle River, NJ, USA:.

Dodson, C. C. and Cordasco, F. A. (2008). Anterior glenohumeral joint dislocations. *Orthopedic Clinics*, *39*(4), 507–518.

Ehyaie, A., Hashemi, M., and Khadivi, P. (2009). Using relay network to increase life time in wireless body area sensor networks. In *IEEE International Symposium on a World of Wireless, Mobile and Multimedia Networks & Workshops (WoWMoM)*, 1–6. IEEE.

Elias, J. (2014). Optimal design of energy-efficient and cost-effective wireless body area networks. *Ad Hoc Networks*, *13*, 560–574.

Elias, J. and Mehaoua, A. (2012). Energy-aware topology design for wireless body area networks. In *IEEE International Conference on Communications (ICC)*, 3409–3410.

Elliott, E. O. (1963). Estimates of Error Rates for Codes on Burst-Noise Channels. *Bell System Technical Journal*, *42*(5), 1977–1997.

Fang, G., Dutkiewicz, E., Yu, K., Vesilo, R., and Yu, Y. (2010). Distributed inter-network interference coordination for wireless body area networks. In *Global Telecommunications Conference (GLOBECOM)*, 1–5. IEEE.

Favre, J., Jolles, B., Siegrist, O., and Aminian, K. (2006). Quaternion-based fusion of gyroscopes and accelerometers to improve 3D angle measurement. *Electronics Letters*, *42*(11), 612–614.

Foschini, G. J. and Miljanic, Z. (1993). A simple distributed autonomous power control algorithm and its convergence. *IEEE Transactions on Vehicular Technology*, *42*(4), 641–646.

Gaetano, D., Sipal, V., McEvoy, P., Ammann, M., Brannigan, C., Keating, L., and Horgan, F. (2013). Footwear-centric body area network with directional UWB antenna. *Electronics Letters*, *49*(14), 860–861.

Ghamari, M., Janko, B., Sherratt, R. S., Harwin, W., Piechockic, R., and Soltanpur, C. (2016). A survey on wireless body area networks for ehealthcare systems in residential environments. *Sensors*, *16*(6), 831.

Gharghan, S. K., Nordin, R., and Ismail, M. (2016). Energy efficiency of ultra-low-power bicycle wireless sensor networks based on a combination of power reduction techniques. *Journal of Sensors*, *2016*.

Gilbert, E. N. (1960). Capacity of a Burst-Noise Channel. *Bell System Technical Journal*, *39*(5), 1253–1265.

Glower, J., Agasti, A., Bakke, J., Johnson, K., and Ratan, A. (2018). Inverse Kinematics for a Barn-Door Equatorial Platform. In *IEEE International Conference on Electro/Information Technology (EIT)*, 0118–0122.

Goldfinger, E. (1991). *Human anatomy for artists: The elements of form*. New York: Oxford University Press.

Grimm, G., Guilmin, G., Poppen, F., Vlaming, M. S., and Hohmann, V. (2009). The personal hearing system–A software hearing aid for a personal communication system. *EURASIP Journal on Advances in Signal Processing*, *2009*(1), 1–9.

Hale, R. B. and Richer, P. (1986). *Artistic Anatomy*. Watson-Guptill PublicationsPitman Publishing.

Hall, P., Ricci, M., and Hee, T. (2002). Measurements of on-body propagation characteristics. In *Antennas and Propagation Society International Symposium*, Volume 2, 310–313. IEEE.

Hamie, J., Denis, B., and Richard, C. (2012). Constrained decentralized algorithm for the relative localization of wearable wireless sensor nodes. In *IEEE Sensors*, 1–4.

Hanlen, L., Chaganti, V., Gilbert, B., Rodda, D., Lamahewa, T., and Smith, D. (2010). Open-source testbed for body area networks: 200 sample/sec, 12 hrs continuous measurement. In *IEEE 21st International Symposium on Personal, Indoor and Mobile Radio Communications Workshops (PIMRC)*, 66–71. IEEE.

Hauer, J.-H. (2014a). Leveraging human mobility for communication in body area networks. *ACM Transactions on Sensor Networks (TOSN)*, *10*(3), 1–39.

Hauer, J.-H. (2014b). Towards reliable communication in low-power wireless body area networks.

Heinzelman, W. R., Chandrakasan, A., and Balakrishnan, H. (2000). Energy-efficient communication protocol for wireless microsensor networks. In *Proceedings of the 33rd annual Hawaii international conference on System Sciences*, 10–pp. IEEE.

Henna, S. and Sarwar, M. A. (2018). An Adaptive Backoff Mechanism for IEEE 802.15. 4 Beacon-Enabled Wireless Body Area Networks. *Wireless Communications and Mobile Computing*, *2018*.

Hogarth, B. (2003). *Dynamic anatomy*. Watson-Guptill Publications.

Horton, J., Cameron, A., Devaraj, D., Hanson, R., and Hajkowicz, S. (2018). Workplace Safety Futures: The impact of emerging technologies and platforms on work health and safety and workers compensation over the next 20 years.

Huyghe, B., Rogier, H., Vanfleteren, J., and Axisa, F. (2008). Design and manufacturing of stretchable high-frequency interconnects. *IEEE Transactions on Advanced Packaging*, *31*(4), 802–808.

IEEE LAN/MAN Standards Committee (2011). 802.15.4 - IEEE Standard for Local and Metropolitan Area Networks–Part 15.4: Low-Rate Wireless Personal Area Networks (LR-WPANs). *IEEE std*, 314.

IEEE LAN/MAN Standards Committee (2012). 802.15.6 - IEEE Standard for Local and Metropolitan Area Networks - Part 15.6: Wireless Body Area Networks (WBAN). *IEEE std*, 271.

InvenSense (2014). MPU-9250 datasheet. *https://www.invensense.com/wp-content/uploads/2015/02/PS-MPU-9250A-01-v1.1.pdf*.

Kane, T. R., Likins, P. W., and Levinson, D. A. (1983). Spacecraft dynamics. *New York, McGraw-Hill Book Co, 1983, 445 p.*.

Kazemi, R., Vesilo, R., and Dutkiewicz, E. (2011). A novel genetic-fuzzy power controller with feedback for interference mitigation in wireless body area networks. In *73rd Vehicular Technology Conference (VTC)*, 1–5. IEEE.

Kim, E. C., Park, S., Cha, J. S., and Kim, J. Y. (2010). Improved performance of UWB system for wireless body area networks. *IEEE Transactions on Consumer Electronics*, *56*(3).

Kim, S., Kim, S., and Eom, D.-S. (2013). RSSI/LQI-based transmission power control for body area networks in healthcare environment. *IEEE Journal of Biomedical and Health Informatics*, *17*(3), 561–571.

Kim, Y.-J., Kim, J.-I., and Jang, W. (2018). Quaternion Joint: Dexterous 3-DOF Joint representing quaternion motion for high-speed safe interaction. In *IEEE/RSJ International Conference on Intelligent Robots and Systems (IROS)*, 935–942. IEEE.

Kindt, P., Jing, H., Peters, N., and Chakraborty, S. (2015). ExPerio-Exploiting periodicity for opportunistic energy-efficient data transmission. In *IEEE Conference on Computer Communications (INFOCOM)*, 82–90.

Klann, M. (2008). Tactical navigation support for firefighters: The LifeNet ad-hoc sensor-network and wearable system. In *International Workshop on Mobile Information Technology for Emergency Response*, 41–56. Springer.

Kosma, M., Cardinal, B. J., and Rintala, P. (2002). Motivating individuals with disabilities to be physically active. *Quest*, *54*(2), 116–132.

Kuipers, J. B. *et al.* (1999). *Quaternions and rotation sequences*. Princeton University Press, Princeton.

Lee, W., Lee, B.-D., and Kim, N. (2014). Hybrid transmission power control for wireless body sensor systems. *International Journal of Distributed Sensor Networks*, *10*(10), 259181.

Leonov, V. (2013). Thermoelectric energy harvesting of human body heat for wearable sensors. *IEEE Sensors Journal*, *13*(6), 1–8.

Li, G., Lee, B.-L., and Chung, W.-Y. (2015). Smartwatch-based wearable EEG system for driver drowsiness detection. *IEEE Sensors Journal*, *15*(12), 7169–7180.

Liao, L.-D., Chen, C.-Y., Wang, I.-J., Chen, S.-F., Li, S.-Y., Chen, B.-W., Chang, J.-Y., and Lin, C.-T. (2012). Gaming control using a wearable and wireless EEG-based brain-computer interface device with novel dry foam-based sensors. *Journal of NeuroEngineering and Rehabilitation*, *9*(1), 5.

Lin, J.-C. (2008). Least-squares channel estimation for mobile OFDM communication on time-varying frequency-selective fading channels. *IEEE Transactions on Vehicular Technology*, *57*(6), 3538–3550.

Lin, S., Zhang, J., Zhou, G., Gu, L., Stankovic, J. A., and He, T. (2006). ATPC: adaptive transmission power control for wireless sensor networks. In *ACM Conference on Embedded Networked Sensor Systems*, 223–236.

Liu, B., Yan, Z., and Chen, C. W. (2017). Medium access control for wireless body area networks with QoS provisioning and energy efficient design. *IEEE Transactions on Mobile Computing*, *16*(2), 422–434.

Lu, Y., Wang, W., Chen, L., Zhang, Z., and Huang, A. (2014). Opportunistic forwarding in energy harvesting mobile delay tolerant networks. In *IEEE International Conference on Communications (ICC)*, 526–531. IEEE.

Luo, J., Rosenberg, C., and Girard, A. (2010). Engineering wireless mesh networks: joint scheduling, routing, power control, and rate adaptation. *IEEE/ACM Transactions on Networking (TON)*, *18*(5), 1387–1400.

Luo, N., Dai, W., Li, C., Zhou, Z., Lu, L., Poon, C. C., Chen, S.-C., Zhang, Y., and Zhao, N. (2016). Flexible piezoresistive sensor patch enabling ultralow power cuffless blood pressure measurement. *Advanced Functional Materials*, *26*(8), 1178–1187.

Madgwick, S. (2010). An efficient orientation filter for inertial and inertial/magnetic sensor arrays. *Report x-io and University of Bristol (UK)*, *25*.

Mahapatro, J., Misra, S., Manjunatha, M., and Islam, N. (2012). Interference-aware channel switching for use in WBAN with human-sensor interface. In *4th International Conference on Intelligent Human Computer Interaction (IHCI)*, 1–5. IEEE.

Mahmood, A. S., Jafer, E., Hussain, S., and Fernando, X. (2017). Wireless body area network development for remote patient health observing. In *IEEE Humanitarian Technology Conference (IHTC)*, 26–31.

Maitra, T. and Roy, S. (2019). PBDT: an Energy-Efficient Posture based Data Transmission for Repeated Activities in BAN. *Mobile Networks and Applications*, 1–13.

McWhinney, E. (1971). *The international law of communications*. BRILL.

Miehling, J., Schuhhardt, J., Paulus-Rohmer, F., and Wartzack, S. (2015). Computer aided ergonomics through parametric biomechanical simulation. In *ASME 2015 International Design Engineering Technical Conferences and Computers and Information in Engineering Conference*, V01BT02A016–V01BT02A016. American Society of Mechanical Engineers.

Milenkovic, A., Otto, C., and Jovanov, E. (2006). Wireless sensor networks for personal health monitoring: Issues and an implementation. *Computer Communications*, *29*(13-14), 2521–2533.

Miniutti, D., Hanlen, L., Smith, D., Zhang, A., Lewis, D., Rodda, D., and Gilbert, B. (2008). Narrowband channel characterization for body area networks. *IEEE P802*, 15–08.

Mitchell, E. and Rogers, A. (1965). Quaternion parameters in the simulation of a spinning rigid body. *Transactions of the Society for Computer Simulation*, *4*(6), 390–396.

Movassaghi, S., Abolhasan, M., Lipman, J., Smith, D., and Jamalipour, A. (2014). Wireless Body Area Networks: A survey. *IEEE Communications Surveys & Tutorials*, *16*(3), 1658–1686.

Movassaghi, S., Abolhasan, M., and Smith, D. (2014). Cooperative scheduling with graph coloring for interference mitigation in wireless body area networks. In *Wireless Communications and Networking Conference (WCNC)*, 1691–1696. IEEE.

Murphy, M. P., Rammer, J. R., Vinehout, K. L., Caballero, M. R., Cornwell, C. M., Fritz, J. M., and Harris, G. F. (2018). Inverse Kinematic Assessment of Rehabilitative Therapy in Children Using Orthotics. In *2018 40th Annual International Conference of the IEEE Engineering in Medicine and Biology Society (EMBC)*, 2813–2816. IEEE.

Murray, R. M. (2017). *A mathematical introduction to robotic manipulation*. CRC press.

Narayanaswamy, S., Kawadia, V., Sreenivas, R. S., and Kumar, P. (2002). Power control in ad-hoc networks: Theory, architecture, algorithm and implementation of the COMPOW protocol. In *European Wireless Conference*, Volume 2002, 156162. Florence, Italy.

Narendra, K. S. and Thathachar, M. A. (2012). *Learning automata: an introduction*. Courier Corporation.

Nelson, C. L., Sloan, M. K., Jin, R. Y., Jiang, F., Chen, J.-C., Anderson III, A. E., and Liamos, C. T. (2017). Glucose measuring device for use in personal area network. US Patent 9,730,584.

Norkin, C. C. and White, D. J. (2016). *Measurement of joint motion: a guide to goniometry*. FA Davis.

Novatchkov, H. and Baca, A. (2012). Machine learning methods for the automatic evaluation of exercises on sensor-equipped weight training machines. *Procedia Engineering*, *34*, 562–567.

Pantazis, N. A. and Vergados, D. D. (2007). A survey on power control issues in wireless sensor networks. *IEEE Communications Surveys & Tutorials*, *9*(4), 86–107.

Prabh, S., Royo, F., Tennina, S., and Olivares, T. (2012). BANMAC: an opportunistic MAC protocol for reliable communications in body area networks. In *IEEE International Conference on Distributed Computing in Sensor Systems (DCOSS)*, 166–175.

Preuschl, E., Baca, A., Novatchkov, H., Kornfeind, P., Bichler, S., and Boecskoer, M. (2010). Mobile Motion Advisor–a feedback system for physical exercise in schools. *Procedia Engineering*, *2*(2), 2741–2747.

Qiao, D., Choi, S., Jain, A., and Shin, K. G. (2003). Adaptive transmit power control in IEEE 802.11 a wireless LANs. In *The 57th IEEE Semiannual Vehicular Technology Conference (VTC)*, Volume 1, 433–437. IEEE.

Quwaider, M. and Biswas, S. (2009a). On-body packet routing algorithms for body sensor networks. In *IEEE Conference on Networks and Communications (NETCOM'09)*, 171–177. IEEE.

Quwaider, M. and Biswas, S. (2009b). Probabilistic routing in on-body sensor networks with postural disconnections. In *ACM International Symposium on Mobility Management and Wireless Access*, 149–158.

Quwaider, M. and Biswas, S. (2010). DTN routing in body sensor networks with dynamic postural partitioning. *Ad Hoc Networks*, *8*(8), 824–841.

Quwaider, M., Rao, J., and Biswas, S. (2010). Transmission power assignment with postural position inference for on-body wireless communication links. *ACM Transactions on Embedded Computing Systems (TECS)*, *10*(14), 27.

Rafiq, Y. (2015). *Online Markov Chain Learning for Quality of Service Engineering in Adaptive Computer Systems*. Ph. D. thesis, University of York.

Rappaport, T. S. *et al.* (1996). *Wireless communications: principles and practice*, Volume 2. prentice hall PTR New Jersey.

Reusens, E., Joseph, W., Latré, B., Braem, B., Vermeeren, G., Tanghe, E., Martens, L., Moerman, I., and Blondia, C. (2009). Characterization of on-body communication channel and energy efficient topology design for wireless body area networks. *IEEE Transactions on Information Technology in Biomedicine*, *13*(6), 933–945.

Roetenberg, D., Luinge, H., and Slycke, P. (2009). Xsens MVN: full 6DOF human motion tracking using miniature inertial sensors. *Xsens Motion Technologies BV, Tech. Rep*, *1*.

Rozanov, A. (1967). *Stationary random processes*. Holden-Day.

Saleem, S., Ullah, S., and Yoo, H. S. (2009). On the security issues in wireless body area networks. *JDCTA*, *3*(3), 178–184.

Salehi, S., Bleser, G., Schmitz, N., and Stricker, D. (2013). A low-cost and lightweight motion tracking suit. In *IEEE 10th International Conference on Ubiquitous*

Intelligence and Computing and 10th International Conference on Autonomic and Trusted Computing (UIC/ATC), 474–479. IEEE.

Sanneck, H. A. and Carle, G. (1999). Framework model for packet loss metrics based on loss runlengths. In *Electronic Imaging*, 177–187. International Society for Optics and Photonics.

Semiconductors, N. (2007). MMA8491Q datasheet. *www.nxp.com/docs/en/data-sheet/MMA8491Q.pdf*.

Seo, D., Neely, R. M., Shen, K., Singhal, U., Alon, E., Rabaey, J. M., Carmena, J. M., and Maharbiz, M. M. (2016). Wireless recording in the peripheral nervous system with ultrasonic neural dust. *Neuron*, *91*(3), 529–539.

Sharma, A. K. (2005). *Text book of correlations and regression*. Discovery Publishing House.

Shen, Q., Liu, J., Yu, H., Ma, Z., Li, M., Shen, Z., and Chen, C. (2013). Adaptive cognitive enhanced platform for WBAN. In *IEEE/CIC International Conference on Communications in China (ICCC)*, 739–744. IEEE.

Sipal, V., Gaetano, D., McEvoy, P., and Ammann, M. (2014). Bandwidth scaling of fading properties of on-body wireless channel in body area networks. In *10th International Conference on Communications (COMM)*, 1–4. IEEE.

Sipal, V., Gaetano, D., McEvoy, P., and Ammann, M. J. (2015). Impact of hub location on the performance of wireless body area networks for fitness applications. *IEEE Antennas and Wireless Propagation Letters*, *14*, 1522–1525.

Smith, D., Zhang, J., Hanlen, L., Miniutti, D., Rodda, D., and Gilbert, B. (2009). Temporal correlation of dynamic on-body area radio channel. *Electronics Letters*, *45*(24), 1212–1213.

Smith, D. B., Lamahewa, T., Hanlen, L. W., and Miniutti, D. (2011). Simple prediction-based power control for the on-body area communications channel. In *IEEE International Conference on Communications (ICC)*, 1–5. IEEE.

Snyders, H. W. (2010). Wearable golf swing training aid and method of using the same. US Patent 7,686,699.

Song, S., Lim, J.-S., Baek, S. J., and Sung, K.-M. (2002). Variable forgetting factor linear least squares algorithm for frequency selective fading channel estimation. *IEEE Transactions on Vehicular Technology*, *51*(3), 613–616.

Spring, K. W. (1986). Euler parameters and the use of quaternion algebra in the manipulation of finite rotations: a review. *Mechanism and Machine Theory*, *21*(5), 365–373.

Stutzman, W. L. and Thiele, G. A. (2012). *Antenna theory and design*. John Wiley & Sons.

Sun, G., Wang, K., Yu, H., Du, X., and Guizani, M. (2019). Priority-based medium access control for wireless body area networks with high-performance design. *IEEE Internet of Things Journal*.

Sun, Y., Gurewitz, O., and Johnson, D. B. (2008). RI-MAC: a receiver-initiated asynchronous duty cycle MAC protocol for dynamic traffic loads in wireless sensor networks. In *Proceedings of the 6th ACM Conference on Embedded Network Sensor Systems*, 1–14. ACM.

Syed, A. R. and Yau, K.-L. A. (2013). On cognitive radio-based wireless body area networks for medical applications. In *IEEE Symposium on Computational Intelligence in Healthcare and e-health (CICARE)*, 51–57. IEEE.

Takiff, L. and Aiken, G. (2010). A real-time, wearable elemental carbon monitor for use in underground mines. In *13th North American Mine Ventilation Symposium*.

Texas Instrument (2006). MSP430F1611 datasheet. *https://www.ti.com/lit/ds/symlink/msp430f1611.pdf*.

Texas Instruments (2007). CC2420 datasheet. *http://www.ti.com/lit/ds/symlink/cc2420.pdf*.

Tjhai, C. and O'Keefe, K. (2019). Using step size and lower limb segment orientation from multiple low-cost wearable inertial/magnetic sensors for pedestrian navigation. *Sensors*, *19*(14), 3140.

Tong, L. and Zhao, Q. (1999). Joint order detection and blind channel estimation by least squares smoothing. *IEEE Transactions on Signal Processing*, *47*(9), 2345–2355.

Trinler, U. and Baker, R. (2018). Estimated landmark calibration of biomechanical models for inverse kinematics. *Medical engineering & physics*, *51*, 79–83.

Tselishchev, Y., Boulis, A., and Libman, L. (2012). Variable scheduling to mitigate channel losses in energy-efficient body area networks. *Sensors*, *12*(11), 14692–14710.

Tselishchev, Y., Libman, L., and Boulis, A. (2011). Reducing transmission losses in body area networks using variable TDMA scheduling. In *International Symposium on a World of Wireless, Mobile and Multimedia Networks (WoWMoM)*, 1–10. IEEE.

Tudor-Locke, C. (2002). Taking steps toward increased physical activity: Using pedometers to measure and motivate. *President's Council on Physical Fitness and Sports Research Digest*.

UC Berkeley (2004). TelosB datasheet. *http://www.eecs.harvard.edu/ konrad/projects/shimmer/referen sky-datasheet.pdf*.

Vallejo, M., Recas, J., Garca del Valle, P., and Ayala, J. (2013). Accurate Human Tissue Characterization for Energy-Efficient Wireless On-Body Communications. *Sensors*, *13*(6), 7546–7569.

Vaz, A., Ubarretxena, A., Zalbide, I., Pardo, D., Solar, H., Garcia-Alonso, A., and Berenguer, R. (2010). Full passive UHF tag with a temperature sensor suitable for human body temperature monitoring. *IEEE Transactions on Circuits and Systems II: Express Briefs*, *57*(2), 95–99.

Wang, L., Gu, T., Chen, H., Tao, X., and Lu, J. (2010). Real-time activity recognition in wireless body sensor networks: From simple gestures to complex activities. In *16th International Conference on Embedded and Real-Time Computing Systems and Applications (RTCSA)*, 43–52. IEEE.

Wang, L., Gu, T., Tao, X., and Lu, J. (2012). A hierarchical approach to real-time activity recognition in body sensor networks. *Pervasive and Mobile Computing*, *8*(1), 115–130.

Wattenhofer, R., Li, L., Bahl, P., and Wang, Y.-M. (2001). Distributed topology control for power efficient operation in multihop wireless ad hoc networks. In *In Proceedings of Joint Conference of the IEEE INFOCOM and IEEE Computer and Communications Societies*, Volume 3, 1388–1397. IEEE.

Watteyne, T., Augé-Blum, I., Dohler, M., and Barthel, D. (2007). Anybody: a self-organization protocol for body area networks. In *Proceedings of the ICST 2nd International Conference on Body Area Networks*, 6. ICST (Institute for Computer Sciences, Social-Informatics and Telecommunications Engineering).

xsens (2014). MTw Awinda Wireless Motion Tracker.

Yang, C., He, Z., and Yu, W. (2009). Comparison of public peak detection algorithms for MALDI mass spectrometry data analysis. *BMC Bioinformatics*, *10*(1), 13.

Yang, S., Lu, J.-L., Yang, F., Kong, L., Shu, W., and Wu, M.-Y. (2013). Behavior-aware probabilistic routing for wireless body area sensor networks. In *IEEE Global Communications Conference (GLOBECOM)*, 444–449.

Yang, Y., Smith, D. B., and Seneviratne, S. (2019). Deep Learning Channel Prediction for Transmit Power Control in Wireless Body Area Networks. In *IEEE International Conference on Communications (ICC)*, 1–6. IEEE.

Yazdandoost, K. Y. (2007). Channel model for body area network (BAN). *IEEE 802.15-07-0943-00-0*.

Yazdandoost, K. Y. and Sayrafian-Pour, K. (2009). TG6 channel model ID: IEEE 802.15-08-0780-12-0006. *IEEE 802.15 working group document*.

Young, A. D. (2010). Wireless realtime motion tracking system using localised orientation estimation.

Young, A. D., Ling, M. J., and Arvind, D. (2007). Orient-2: A realtime wireless posture tracking system using local orientation estimation. In *Proceedings of the 4th Workshop on Embedded Networked Sensors*, 53–57. ACM.

Yusif, S., Soar, J., and Hafeez-Baig, A. (2016). Older people, assistive technologies, and the barriers to adoption: A systematic review. *International Journal of Medical Informatics*, *94*, 112–116.

Zahid, N., Sodhro, A. H., Zafar, R. F., Zahid, B., Khan, S. A., and Akhter, F. (2019). Regression-based Transmission Power Control for Green Healthcare. In *2nd International Conference on Computing, Mathematics and Engineering Technologies (iCoMET)*, 1–9. IEEE.

Zang, W. and Li, Y. (2015). Motion aware transmission power control scheme in wireless body area network. In *IEEE Workshop on Signal Processing Systems (SiPS)*, 1–5. IEEE.

Zang, W. and Li, Y. (2017). Gait Cycle Driven Transmission Power Control Scheme for Wireless Body Area Network. *IEEE Journal of Biomedical and Health Informatics*, *22*(3), 697–706.

Zhang, H., Safaei, F., *et al.* (2018). Channel autocorrelation-based dynamic slot scheduling for body area networks. *EURASIP Journal on Wireless Communications and Networking*, *1*(1), 246.

Zhang, J., Smith, D., and Chen, Z. (2012). Linear finite state Markov chain predictor for channel prediction. In *IEEE 23rd International Symposium on Personal Indoor and Mobile Radio Communications (PIMRC)*, 2085–2089. IEEE.

Zhang, Y. and Zhang, B. (2017). A relay-aided transmission power control method in wireless body area networks. *IEEE Access*, *5*, 8408–8418.

Zhou, B., Koerger, H., Wirth, M., Zwick, C., Martindale, C., Cruz, H., Eskofier, B., and Lukowicz, P. (2016). Smart soccer shoe: monitoring foot-ball interaction with shoe integrated textile pressure sensor matrix. In *Proceedings of the 2016 ACM International Symposium on Wearable Computers*, 64–71. ACM.

Zhu, H., Zhong, X., Yu, Q., and Wan, Y. (2013). A localization algorithm for mobile wireless sensor networks. In *IEEE International Conference on Intelligent System Design and Engineering Applications (ISDEA)*, 81–85.

Zhu, R. and Zhou, Z. (2004). A real-time articulated human motion tracking using tri-axis inertial/magnetic sensors package. *IEEE Transactions on Neural Systems and Rehabilitation Engineering*, *12*(2), 295–302.